

Triphenylamine and Carbazole-Based Hole Transporting Materials

and their Applications in Organic Field-Effect Transistors

Dissertation

zur Erlangung des Grades

Doktor der Naturwissenschaft

(Dr. rer. nat.)

eingereicht im Fachbereich C – Mathematik und Naturwissenschaften
der Bergischen Universität Wuppertal

von

Benjamin Souharce

aus Bordeaux, Frankreich

Wuppertal, 2008

Die Dissertation kann wie folgt zitiert werden:

urn:nbn:de:hbz:468-20080287

[<http://nbn-resolving.de/urn/resolver.pl?urn=urn%3Anbn%3Ade%3Ahbz%3A468-20080287>]

"Science sans conscience n'est que ruine de l'âme."

François Rabelais, Pantagruel (1532)

"... plutôt la tête bien faite que bien pleine."

Michel Eyquem de Montaignes, Les Essais, Livre I (1580)

Die vorliegende Arbeit wurde in der Zeit von Mai 2004 bis Mai 2007 am Lehrstuhl für Makromolekulare Chemie des Fachbereichs C – Mathematik und Naturwissenschaften der Bergischen Universität Wuppertal unter Anleitung von Prof. Dr. U. Scherf angefertigt.

Mein besonderer Dank gilt Herrn Prof. Dr. Ullrich Scherf für die interessante Themenstellung und zahlreiche Fragestellungen sowie seine vielfältige persönliche Unterstützung und angenehme Handlungsweise.

1. Gutachter: Prof. Dr. U. Scherf (BU Wuppertal)
2. Gutachter: Prof. Dr. A. Grimsdale (NTU Singapore)
eingereicht am: TT.02.2008

Abstract

Hole transporting materials based on π -conjugated organic compounds have already been the focus of intense research and investigation. Nevertheless, the charge transport mechanism occurring in such materials and its relation to the device stability in oxidizing atmosphere remains not fully clear. It has been demonstrated many times that the stability issue for *p*-type organic materials is one of the key features for their application in organic field-effect transistors.

In a conjoint work with the *Evonik Degussa Creavis*, research were lead to develop a series of novel polymeric compounds usable as semiconducting layers of organic field-effect transistors (OFETs) e.g. for printed radio frequency identification tags (RFID Tags) being processed and working under ambient conditions.

In this regard, arylamine-based aromatic materials such as triphenylamine- or carbazole-type polymers constitute ideal candidates for such applications due to their good environmental stability and OFET properties coupled with an easy processability of the polymeric materials.

In chapter 2, a series of six main chain polytriphenylamines (PTPAs) with different alkyl substituents and aromatic systems will be described. Chapter 3 deals with different *N*-aryl substituted 3,6-polycarbazoles and their use as active layer in OFETs. At last, higher condensed aromatic systems based on the phenazine unit comprising model compounds as well as the corresponding polymers are presented in chapter 4. In each chapter, the key reactions are depicted including history, mechanism and the application for our approach. Additionally, a short introduction presents the state-of-the-art for the mentioned classes of compounds.

All the materials synthesized during this work were intensively analysed by spectroscopic methods and most of them tested as semiconducting layer in OFET devices in order to determine the influence of certain structural factors on the intrinsic electronic properties of the compounds. The stability problem has been intensively addressed and discussed with the goal to provide a better understanding of the oxidation/degradation mechanism taking place in OFET devices while operating.

Table of Contents

Abstract	VII
Table of Contents	IX
List of Symbols and Abbreviations	XII
1. General Introduction	1
1.1. Conjugated Polymers and Organic Electronics	1
1.2. Triphenylamines: General Aspects	3
1.3. Triphenylamine-Based Materials	4
1.4. Charge Transport in Organic Semiconductors	14
1.4.1. Charge Carriers: Solitons and Polarons	14
1.4.2. Electrical Conductivity and Charge Carrier Mobility	15
1.4.3. Charge Transport Mechanism in Polymers	15
1.5. Organic Field-Effect Transistors (OFETs)	17
1.5.1. Basic OFET Architectures	17
1.5.2. OFET Principle	18
1.5.3. OFET Characteristics: Output and Transfer	19
1.5.4. OFET Model and Field-Effect Mobility	20
1.5.5. OFET Parameters: On/Off Ratio, Hysteresis and Turn-On Voltage	21
1.6. Aim and Scope	22
2. Polytriphenylamine-Type Materials	24
2.1. Introduction	24
2.2. Synthesis	24
2.2.1. Monomer Synthesis	24
2.2.2. Polymer Synthesis	40
2.3. Material Characterization	45
2.3.1. Spectroscopic Investigation	45
2.3.2. OFET Investigation	51
2.4. Conclusion	59
3. Carbazole-Based Materials	61
3.1. Polycarbazoles	61
3.2. Poly(<i>N</i>-phenylcarbazole)s	66
3.2.1. Poly(<i>N</i> -phenylcarbazole-3,6-diyl) (PNPC)	67
3.2.2. Poly(<i>meta</i> -dicarbazolyl-phenylene) (PdCP)	72
3.3. Conclusion	80
4. Phenazine-Based Materials	82

4.1. Introduction	82
4.2. Model Compound	84
4.2.1. Synthesis	84
4.2.2. Optical Properties and Stability Investigation	85
4.2.3. OFET Characteristics	86
4.3. Phenazine-Containing Polymers	87
4.3.1. Synthesis	88
4.3.2. Optical Properties and OFET Investigation	91
4.3.3. Conclusion	92
5. Summary	94
6. Outlook	95
6.1. New Polymers for OFETs	95
6.2. Triphenylamine-Based Polymers as Bio-Sensor and Dyes	96
7. Experimental Section	98
7.1. General Methods	98
7.2. Synthesis of Triphenylamine-Based Materials	98
7.2.1. General procedure for the synthesis of <i>N,N</i> -bis(4-bromophenyl)-arylanilines (MTPAs)	98
7.2.2. General procedure for the synthesis of triphenylamine-based polymers (PTPAs)	101
7.3. Synthesis of Carbazole-Based Monomers and Polymers	104
7.3.1. Synthesis of 9-(4-octylphenyl)carbazole (<i>NPC8</i>)	104
7.3.2. 3,6-Dibromo-9-(4-octylphenyl)carbazole (<i>MNPC8</i>)	105
7.3.3. Poly[9-(4-octylphenyl)carbazole] (<i>PNPC8</i>)	106
7.3.4. 2,6-Dibromo-4- <i>tert</i> -butylaniline	106
7.3.5. 3,5-Dibromo-1- <i>tert</i> -butylbenzene	107
7.3.6. 3-Methylcarbazole	107
7.3.7. 1,3-Bis(6'-methylcarbazol-9'-yl)-5- <i>tert</i> -butylbenzene (<i>dCP</i>)	108
7.3.8. 1,3-Bis(3'-bromo-6'-methylcarbazole-9'-yl)-5- <i>tert</i> -butylbenzene (<i>MdCP</i>)	109
7.3.9. Poly[1,3-bis(3'-methylcarbazole-9'-yl)-5- <i>tert</i> -butylphenylene-6',6"-diyl] (<i>PdCP</i>)	109
7.4. Synthesis of the Phenazine-Based Materials	110
7.4.1. 5,10-Dihydrophenazine	110
7.4.2. 5,10-Bis(4-octylphenyl)-5,10-dihydrophenazine (<i>d8PPz</i>)	110
7.4.3. 5,10-Bis(4-bromophenyl)-5,10-dihydrophenazine (<i>MdPPz</i>)	111
7.4.4. 9-Decylcarbazole	111

7.4.5. 9,9'-Didecyl-3,3'-bicarbazole	112
7.4.6. 6,6'-Dibromo-9,9'-didecyl-3,3'-bicarbazole	113
7.4.7. 9,9'-Didecyl-6,6'-bis(4,4,5,5-tetramethyl-1,3,2-dioxaborolan-2-yl)-3,3'- bicarbazole	113
7.4.8. Alternating Copolymer <i>dPPz</i> /Bis- <i>N</i> -decylcarbazol (<i>PdPPz1</i>)	114
7.4.9. Random Copolymer <i>dPPz</i> (20%)/ <i>TPA3</i> (<i>PdPPz2</i>)	115
7.4.10. Alternating Copolymer Phenazine <i>TPA3</i> (<i>PdPPz3</i>)	115
References and Notes	117
Acknowledgement	
Curriculum Vitae	

List of Symbols and Abbreviations

aq.	aqueous
BPy	2,2'-bipyridyl
COSY	correlated spectroscopy
d	doublet
DMF	dimethylformamid
DPPF	1,1'-bis(diphenylphosphino)ferrocene
DP	degree of polymerization
DSC	differential scanning calorimetry
EL	electroluminescence
EDTA	ethylenediaminetetraacetic acid
eq.	equivalent(s)
GC-MS	gas chromatography-mass spectrometry
GPC	gel permeation chromatography
HOMO	highest occupied molecular orbital
LUMO	lowest unoccupied molecular orbital
M_n	number average molecular weight [$\text{g}\cdot\text{mol}^{-1}$]
M_w	weight average molecular weight [$\text{g}\cdot\text{mol}^{-1}$]
$\text{Ni}(\text{COD})_2$	<i>bis</i> (1,5-cyclooctadien)nickel(0)
NMR	nuclear magnetic resonance
NOESY	Nuclear Overhauser effect spectroscopy
OFET	organic field-effect transistor
OLED	organic light-emitting diode
$\text{P}(t\text{-Bu})_3$	tri- <i>tert</i> -butylphosphine
PD	polydispersity
$\text{Pd}_2(\text{dba})_3$	tris(dibenzylidenacetone)dipalladium(0)
PL	photoluminescence
ppm	parts per million
PTPA	polytriphenylamine
RT	room temperature
s	singlet
t	triplet
THF	tetrahydrofuran
UV-Vis	ultraviolet-visible
δ	chemical shift [ppm]
λ	wavelength [nm]

1. General Introduction

1.1. Conjugated Polymers and Organic Electronics

Troughout its history, mankind has always used macromolecular materials such as wood, leather or wool in all-day life. In the 19th century, the French pharmacist Henri Braconnot described pioneering work in derivatizing cellulose compounds and thus probably one of the earliest important study in polymer science.^[1] The development of vulcanization procedures in the later 19th century improved the durability of the natural polymer rubber, signifying the first popularized semi-synthetic polymer.^[2] The 20th century saw the emergence of new modified natural polymers and synthetic materials and the arising of polymer science. The first wholly synthetic polymer (or plastic), Bakelite, was introduced in 1909.^[3] Despite the advances in synthesis and characterization of polymers, an understanding of the macromolecular character did not take place before the 1920's. Until this time, scientists thought polymers were clusters of small molecules (colloids) held together by intermolecular forces according to the association theory advanced by the chemist Thomas Graham in 1861.^[4] In 1920 Hermann Staudinger first proposed that polymers consist of long chains of atoms held together by covalent bonds^[5] and was awarded for his work with the Nobel Prize in Chemistry in 1953. Since then the polymer industry grew exponentially developing plastics like Nylon, polyethylene or Teflon. Nowadays, polymers find applications in nearly every industry field with a worldwide production of over 10⁸ tones yearly. Polymers are widely used as adhesives and lubricants, as well as components for products ranging from childrens' toys to aircraft. Most of the plastic materials are known as electric insulator but this vision changed in 1977 with Alan J. Heeger, Alan G. McDiarmid and Ideki Shirakawa.^[6] These pioneers asserted that polyacetylene can become conductive by oxidation or reduction of the unsaturated polymer backbone with halogen vapors (oxidative doping process). In 2000 they were awarded with the Nobel Prize of Chemistry "*for the discovery and development of conductive polymers*". Such conducting (or semiconducting in neutral state) polymers are called π -conjugated polymers due to the presence of π -bonded electrons in each main chain atom (preferably carbon) leading to a backbone of alternating single and double (or triple) bonds. In the following years, a lot of other π -conjugated polymers such as poly(*para*-phenylene) (PPP), poly(*para*-phenylenevinylene) (PPV),^[7] polyfluorene (PF)^[8] or polythiophene (PT)^[9] have been developed and investigated.

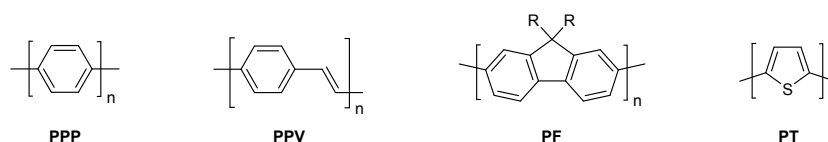


Figure 1.1: Examples of π -conjugated polymers.

Some of these materials found applications in the field of xerography^[10] and optoelectronic devices such as light emitting diodes (OLEDs),^[11] field-effect transistors (OFETs)^[12] or organic solar cells.^[13] In the last few years, new application areas have emerged with their use in biosensors or as implants.^[14]

The industry has already showed a lot of interest in optoelectronic applications. OLEDs have been the first technology field under intense industrial R&D with prototypes developed by companies like CDT, Samsung, Fujitsu Siemens, Toshiba or Sony. Solar cell applications have also come in focus of industrial actors (e.g. Konarka Technologies) which invest in the development of new “low cost” photovoltaic products. One of the most promising markets for organic electronics is the one of intelligent labels, so-called RFID tags. They are considered the next generation of printed identification labels as replacement for the bar code. Such devices are simple passive electronic devices, preferably made of organic semiconducting materials, in which information can be stored and read out by a contactless technique. Compared to silicon, organic semiconducting materials present several advantages. Except the low production costs, the most significant one is the possibility of using printing techniques on large areas and on flexible substrates. Companies like *Evonik Degussa* and *PolyIC* have already heavily invested in the development and the prototype production of so-called printed chips.^[15] The first products based on this technology were announced in 2007 as shown in Figure 1.2.



Figure 1.2: RFID tags (from PolyIC).

Easy processibility and sufficiently high performances are two specifications requested for semiconducting materials used in this kind of applications.^[16] Poly(3-alkylthiophene)s (P3ATs) are one promising candidate which fulfill these requirements with a hole mobility μ_p up to $0.1 \text{ cm}^2 \cdot \text{V}^{-1} \cdot \text{s}^{-1}$, on/off ratios up to 10^6 and a good solubility in common organic solvents. Nevertheless, thiophene-based polymeric materials present several restrictions due to their poor stability under ambient conditions and the necessity of thermal post-treatments to afford the optimal performances.^[17] In this view, triarylamine-based materials presents an alternative to P3AT because of their good performance, amorphous solid state structure and high stability. A wide range of triarylamine-based derivatives and polymers have already been developed and investigated for OLED or solar cell applications.^[18] In 2000, Veres *et al.* from Vecia published the first results about main-chain polytriphenylamines (PTPAs or PTAAs) as semiconducting (hole transporting) layer in OFETs.^[19]

1.2. Triphenylamines: General Aspects

Necessary material properties like sufficient thermal stability, non-crystalline or amorphous morphology of thin films and electrochemical reversibility in addition to high electronic-grade purity constitute some of the requirements for a wide variety of optoelectronic materials for applications in printed electronic devices. Triarylamine derivatives are well known photoconducting materials with high hole mobility which have already been used in xerographic applications.^[20] The structural unit triphenylamine (TPA), responsible for the photoconducting and hole transporting properties, can be incorporated into a broad range of small molecules (e.g. star-shaped, oligomers) and polymers (e.g. dendrimers, homopolymers, copolymers). Many of the resulting aromatic amines are hole transporting materials where the electron donating amine nitrogen atom is responsible for the hole transporting behavior.

The TPA functional moiety possesses two basic properties: an easy oxidizability of the amine nitrogen atom and the ability to transport positive charges. The charge involved in the transport for these materials are radical cations which necessitate two requirements: the electrical or photophysical formation of the radical cation and its sufficient stability to undergo an infinite number of redox cycles. Under oxidative conditions, unsubstituted TPA moieties dimerize to tetraphenylbenzidine, commonly called triphenylamine-dimer (TPD), via formation of an unstable monocationic radical as depicted in Figure 1.3.

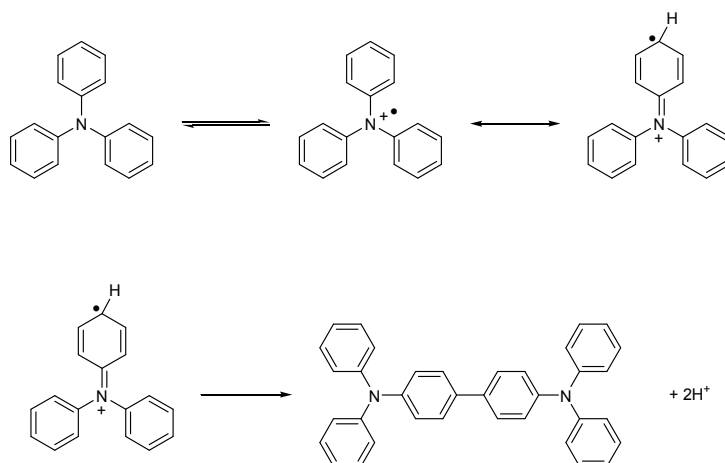


Figure 1.3: Dimerization of the unsubstituted TPA unit by formation of an unstable radical cation.

This dimerization process is accompanied by the loss of two protons per TPD dimer.^[21] The formed TPD dimer can more easily be oxidized than the TPA moiety and undergoes oxidation to give the TPD^{•+} monocation and the TPD²⁺ dication species as proved by cyclic voltammetric studies.^[22] Nevertheless, such dimerization processes can be suppressed in bulky, *p*-substituted TPA derivatives as well as in TPA oligomers. Under application of an electric field, the transport mechanism in such disordered organic systems is assumed to be a hopping process as shown in Figure 1.4 (see chapter 1.4).^[23]

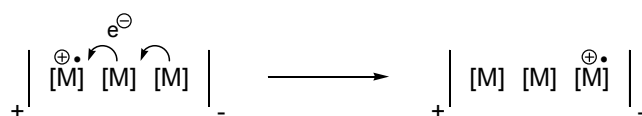


Figure 1.4: Charge transport by a hopping process under electric field for TPA-containing disordered materials.

1.3. Triphenylamine-Based Materials

The amorphous nature of the TPA-containing materials can be enhanced by the attachment of bulky substituents or the generation of more extended TPA oligomers via connection by *para*-linkages. Numerous TPA-based small molecules, oligomers or polymers have already been developed and investigated. Among them, star-shaped triarylamines have been receiving many attentions. The star-shaped structure leads to a decreased crystallization tendency due to the bulky, non-planar geometry. Shirota *et al.*^[24] synthesized numerous low oxidation potential, star-shaped oligotriarylamine compounds with different cores (Figure 1.5).

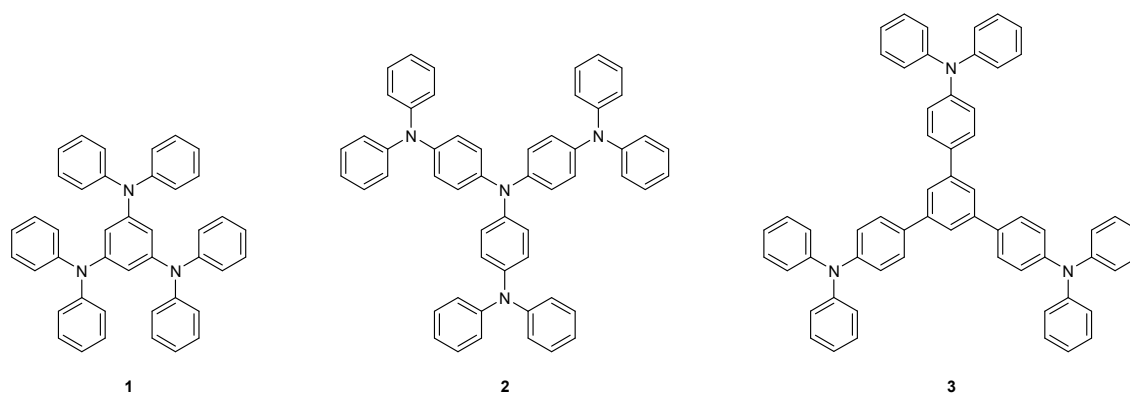


Figure 1.5: Star-shaped triphenylamines: 1,3,5-tris(diphenylamino)benzene TDAB (**1**) with benzene core, 4,4',4''-tris(diphenylamino)triphenylamine TDATA (**2**) with triphenylamine core and 1,3,5-tris(4-diphenylaminophenyl)benzene TDAPB (**3**) with 1,3,5-triphenylbenzene core.

These compounds were generally synthesized by Ullmann couplings starting from the corresponding triiodo core segments with the suitable secondary amine. In order to improve the thermal and optical properties, Thelakkat *et al.* prepared several star-shaped triphenylamines derivatives with a wide range of substituents in *para*-positions.^[25] The size of the π -conjugated system within the TDAB derivatives can be extended by attaching diarylamino substituents in the *para*-positions to obtain extended starbust molecules (Figure 1.6).^[26]

Starbust triarylamines (**4** and **5**) were also synthesized by Ullmann condensation of 1,3,5-tris[(4-phenylaminophenyl)amino]benzene with the corresponding aryl iodide and did not exhibit any crystallinity at all, in contrary to the all-phenyl substituted compounds.^[27] These star-shaped molecules were tested as hole transport layer in electronic devices and presented appreciable properties in OLEDs or solar cells.^[28]

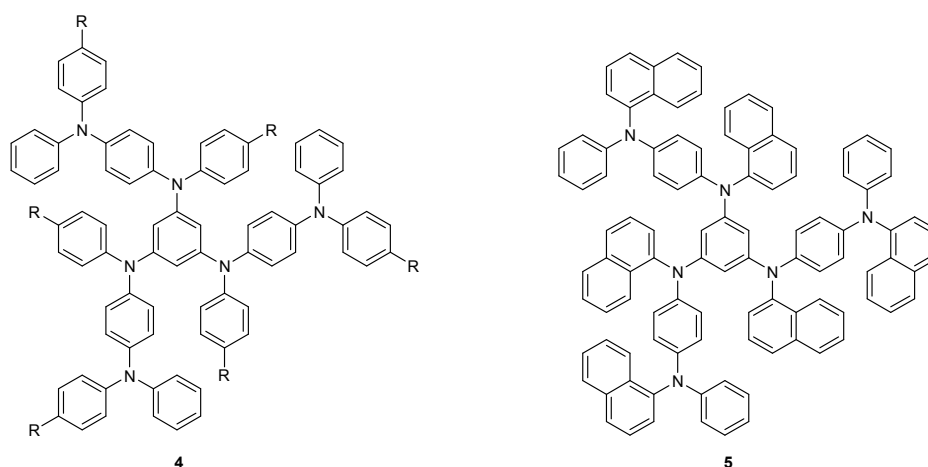


Figure 1.6: Starbust triarylamine derivatives according to Thelakkat *et al.*^[25,26]

Spiro derivatives in which spiro cores are substituted with TPA moieties present an alternative to obtain bulky, amorphous compounds (Figure 1.7).^[29]

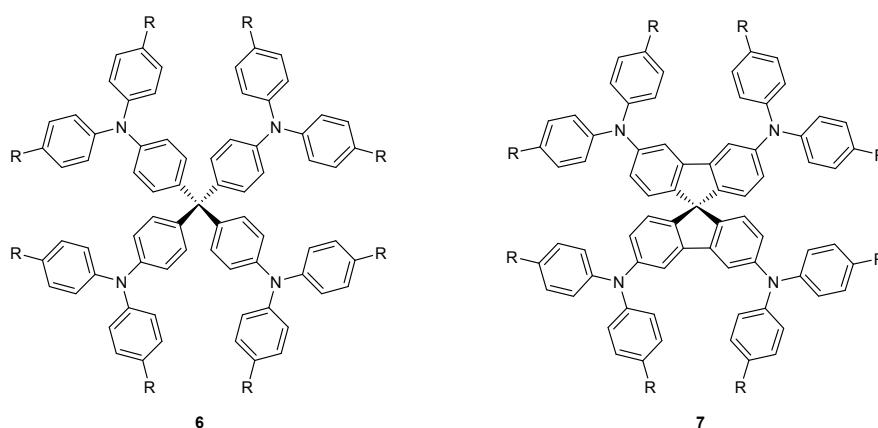


Figure 1.7: Spiro triphenylamine compounds.

Nevertheless, irrespectively to spiro structure, a lot of these derivatives crystallize indicating the possibility of closely packed ensembles. The family of compounds **6** and **7** were prepared from a tetra-halogenated core (e.g. tetrakis(4-iodophenyl)methane for **6** and tetrabromo-9,9'-spirobifluorene for **7**) and the corresponding diphenylamine by palladium-catalyzed Buchwald-Hartwig amination or copper-catalyzed Ullmann condensation depending on the substituents.

In contrast to star-shaped compounds, linear oligomers (**8**) show a very poor solubility in common solvents like THF and chloroform due to their high crystallization tendency. Strohrigel *et al.* reported the synthesis and cyclic voltametric study of oligomeric TPAs up to tetramers (Figure 1.8).^[30]

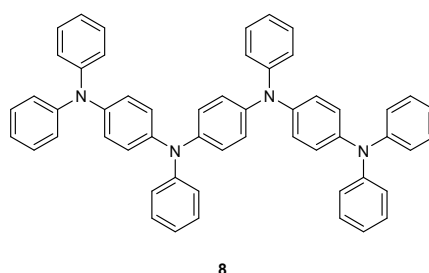


Figure 1.8: Linear triphenylamine tetramer prepared by Strohrigel *et al.*^[30]

The oligomer **8** is prepared by coupling of a lithiated secondary amine (here *N,N'*-diphenyl-1,4-phenylenediamine) with 4-iodotriphenylamine according to a procedure by Neuenhoffer *et al.*^[31] An attempt to prepare PTPA by this method only resulted in an

poorly soluble and non-processable mixture of oligomers and polymers. Later, Tokito *et al.* synthesized well defined soluble oligomers up to pentamers by Ullmann coupling (Figure 1.9).^[32]

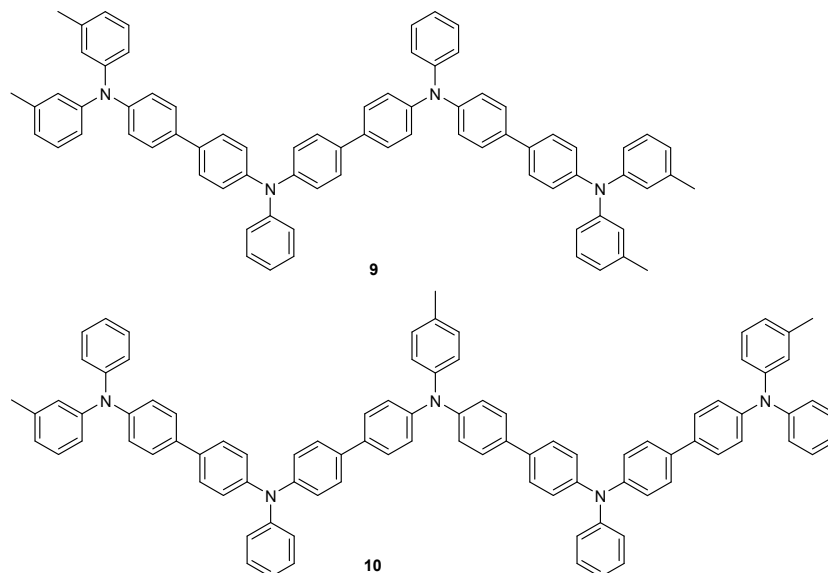
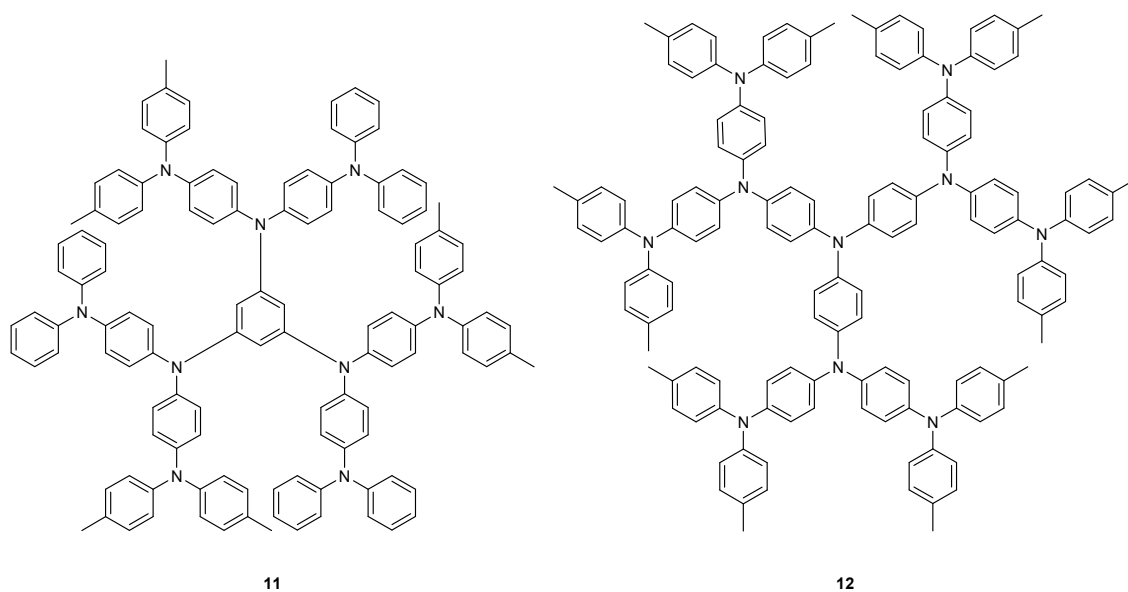


Figure 1.9: Soluble linear triphenylamine oligomers prepared by Tokito *et al.*^[32]

Recent developments to extended oligotriphenylamines led to dendritic structures (dendrimers and hyperbranched polymers) which represent a new class of highly branched compounds with a multitude of end-groups (Figure 1.10).^[33]



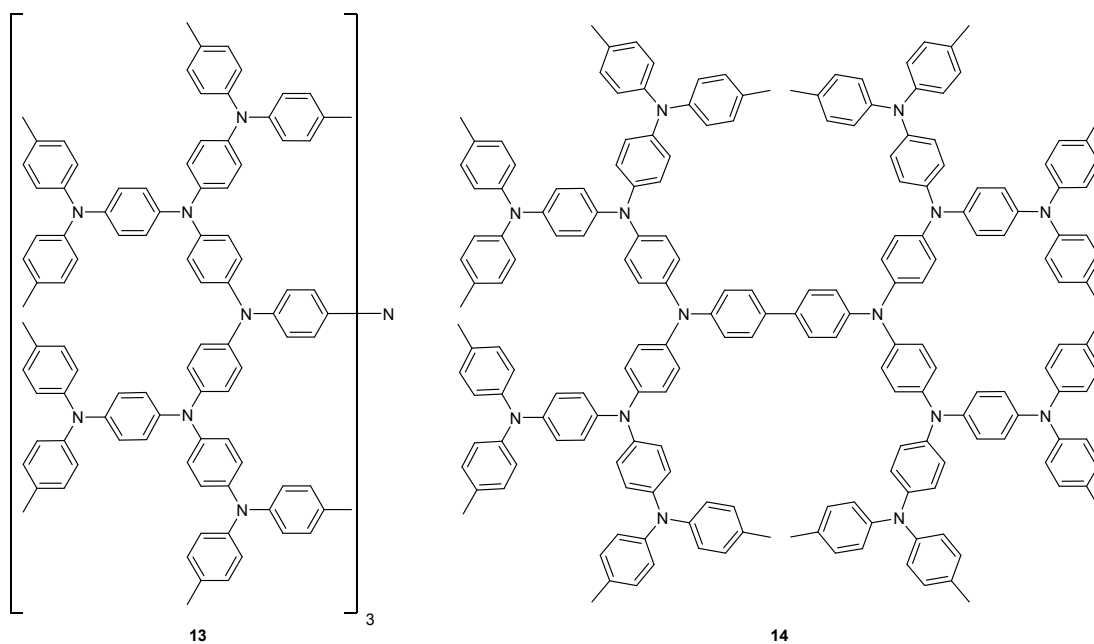


Figure 1.10: Dendritic and hyperbranched oligotriphenylamines.

Tanaka *et al.* reported an hyperbranched polytriphenylamine with triphenylamine units as core synthesized by nickel-catalyzed Grignard coupling of monometalated tribromo monomers to afford a polymer with an assumed degree of polymerization of 16 repeat units.^[34] As the Grignard procedure was not satisfactory due to the generation of large amounts of cross-linked insoluble products, Wang *et al.* used a palladium-catalyzed Negishi coupling of the corresponding chlorozinc derivative to obtain a fully soluble, branched polymer **15** (Figure 1.11).^[35]

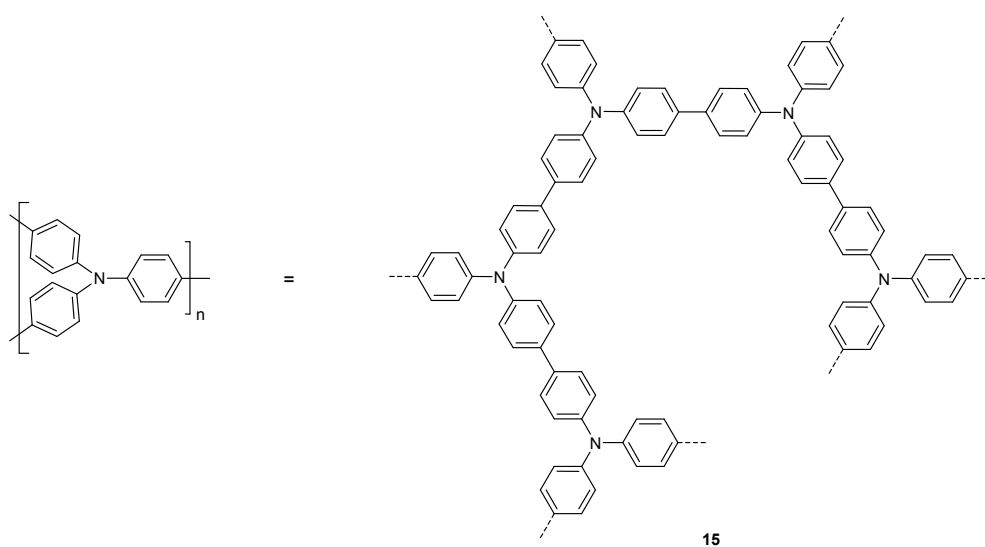


Figure 1.11: Hyperbranched polytriphenylamine according to Wang *et al.*^[35]

Polymers with side-chain TPA moieties have also been widely investigated over the past few years. Stolka *et al.* reported the first synthesis and study of such side chain triphenylamine polymers (**16**) derived from the class of poly(methyl methacrylate)s (PMMA). As shown in Figure 1.12, the polymers carry a substituted aromatic amine in the side chain and were obtained by free radical polymerization.^[36]

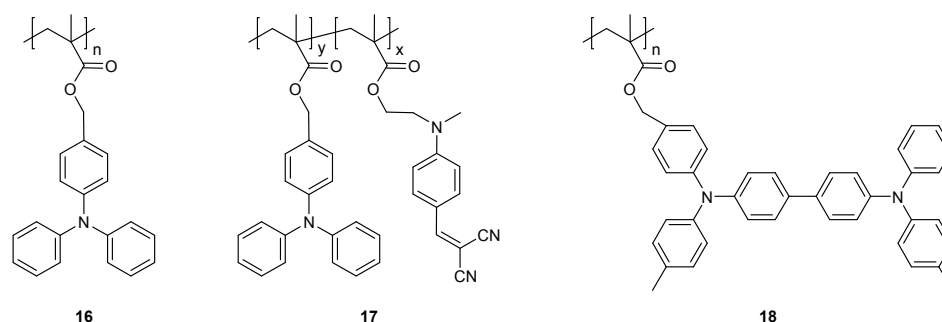


Figure 1.12: PMMA derivatives carrying TPA derivatives pending units or poly(triphenylamine methacrylate).

The materials exhibited a similar to higher hole transport mobility than that of the widely used poly(*N*-vinylcarbazole) (PVK) as well as a high photoconductivity in the UV region. Other polymers, **17** and **18**, have been developed by Sato *et al.* for photorefractive applications.^[37] These materials were also reported as hole transporting layer in OLEDs, in combination with Alq₃ as green triplet emitter.^[38] Bellmann *et al.* described the anionic polymerization to a series of low molecular weight side chain polymers ($M_n < 10^4$ g·mol⁻¹) from vinyl monomers with substituted TPD pending units (Figure 1.13) which were tested as hole transporting and injecting layer in OLEDs.^[39]

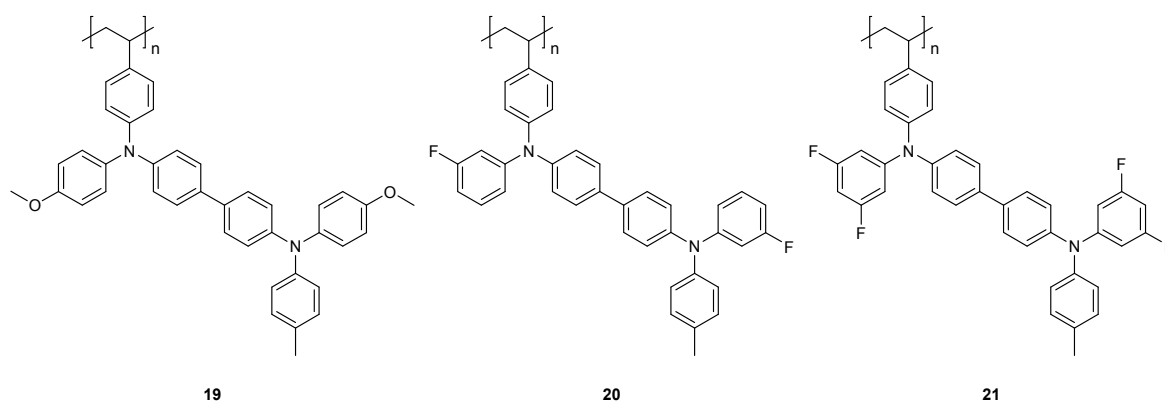


Figure 1.13: Vinyl polymers with substituted TPD side groups.

Bacher *et al.* synthesized and characterized photocrosslinkable hole conducting TPA or TPD substituted polystyrenes.^[40] The monomers were synthesized in standard free radical polymerization protocols with α,α' -azo-bis(isobutyronitrile) (AIBN) as initiator to afford the materials depicted in Figure 1.14.

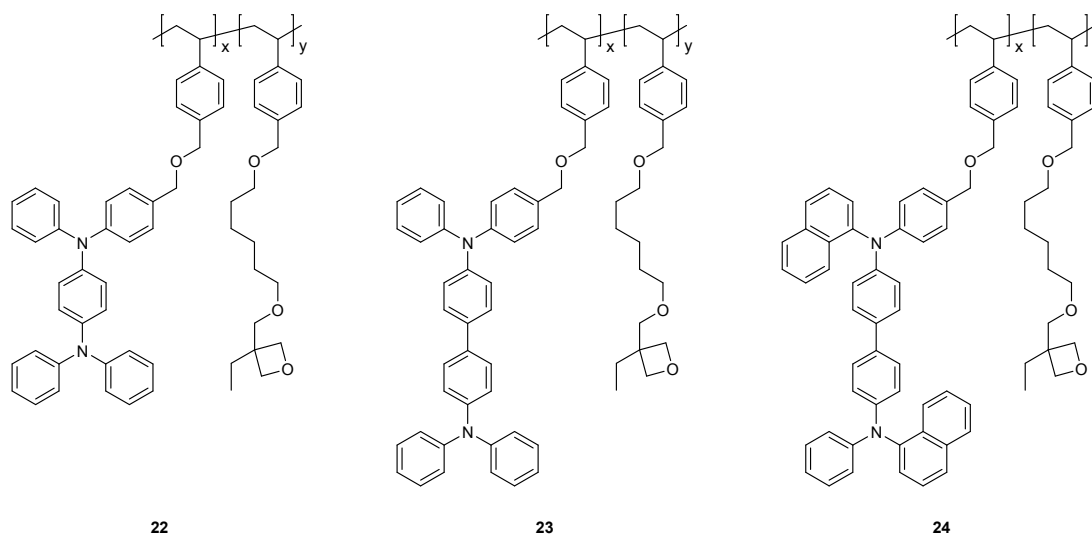


Figure 1.14: Photocrosslinkable polystyrene with TPA or TPD derivatives as pending unit according to Bacher *et al.*^[40]

Many polymers with TPA units in the backbone have been developed for applications in optoelectronic devices. Main chain TPA polymers with ether “spacers” of appreciable molecular weight ($M_n > 10^4$ g·mol⁻¹) could be afforded by Ullmann coupling of bis(secondary amines) and aromatic diiodides involving phase transfer catalysis and dichlorobenzene as solvent (Figure 1.15).^[41]

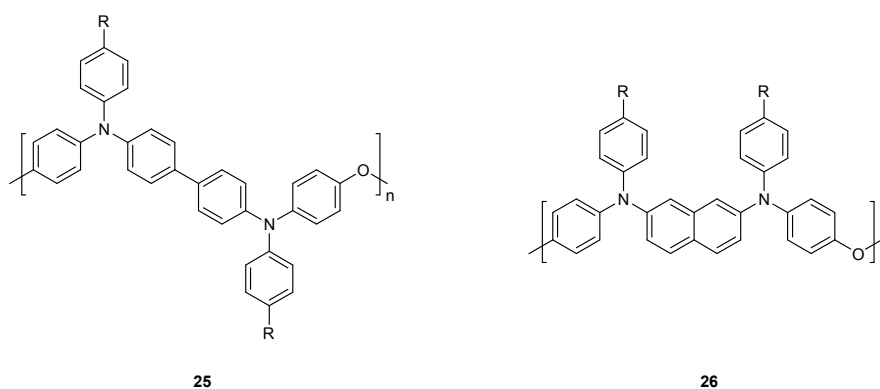


Figure 1.15: Main chain polytriarylamines with ether spacers according to Thelakkat *et al.*^[41]

The polymers **25** and **26** present an interesting amorphous behavior, electrochemical stability as well as solubility in common solvents and can be efficiently applied as hole injecting layer in multilayer OLEDs.^[42] Triarylamine-based polymers can also be prepared by palladium-catalyzed amination of aryl halides. This method was independently developed by Hartwig^[43] and Buchwald^[44] in the early 90's to effectively synthesize tertiary aromatic amines from primary or secondary amines. Problems arising by the transfer of this synthetic procedure to polymerization reactions (phosphorous moieties from the ligands incorporated into the polymer main chain, dehydrohalogenation of the aryl halide, or cyclizations as side reaction) have been overcome by Goodson *et al.*^[45] With the help of more suitable phosphine ligands and starting from "oligomeric" monomers, high molecular weight polymers ($M_n > 10^4 \text{ g}\cdot\text{mol}^{-1}$) as depicted in Figure 1.16 could be obtained.

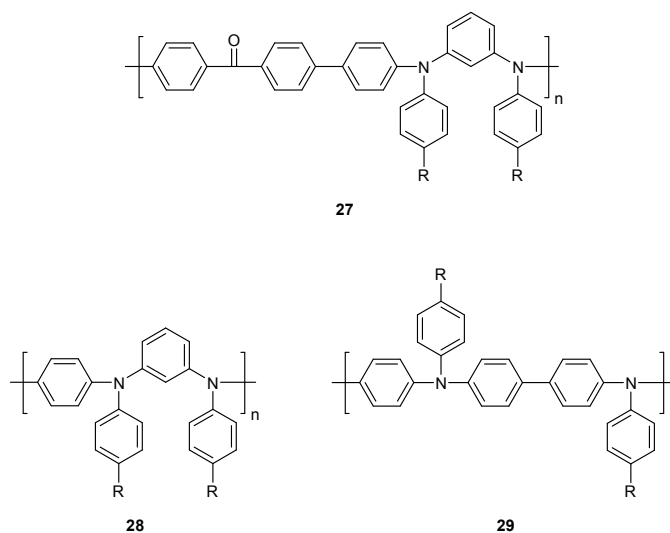


Figure 1.16: Main chain polytriarylamines synthesized by palladium catalyzed Buchwald-Hartwig amination reaction according to Goodson *et al.*^[45]

Triphenylamine units were also incorporated in "classical" emissive polymers like poly(*para*-phenylenevinylene) (**30**, **31**)^[46] or poly(9,9-dialkylfluorene) (**32-34**)^[47] in order to improve their hole injection and transport properties (Figure 1.17).

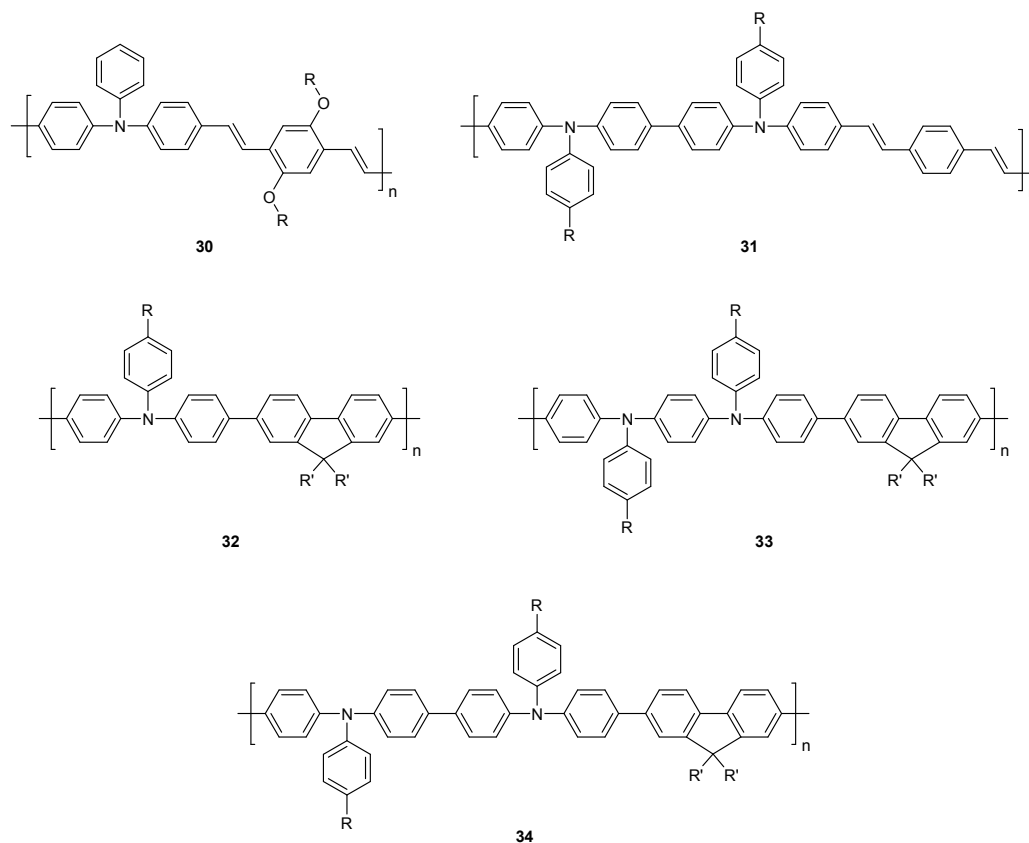


Figure 1.17: Alternating copolymers containing TPA moieties.

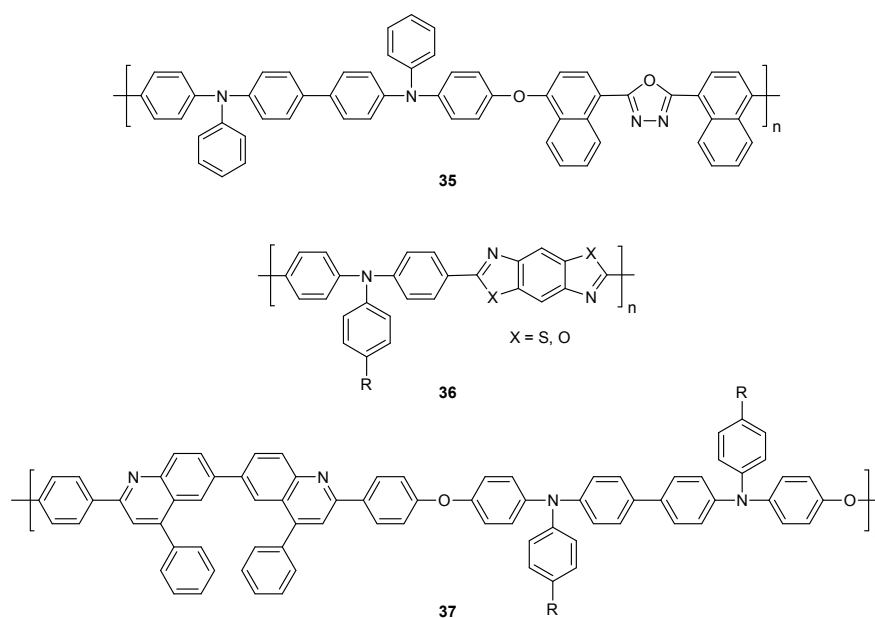


Figure 1.18: Alternating copolymers with TPA and heterocyclic units.

As depicted in Figure 1.18, several alternating copolymers containing heterocyclic functional monomers such as oxadiazole (**35**),^[48] benzoxazole/benzothiazole (**36**)^[49] or

quinoline (**37**)^[50] units have been developed due to their bipolar nature (supporting both hole and electron transport).

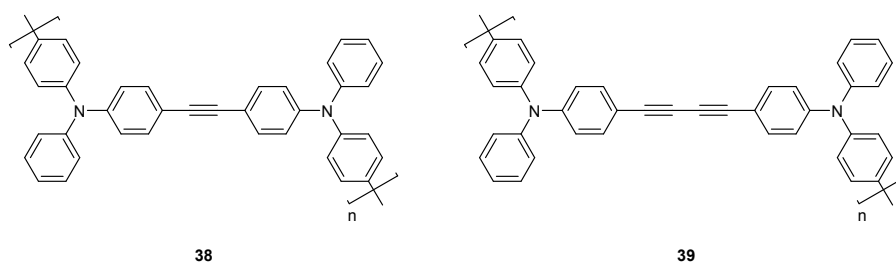


Figure 1.19: Main chain linear polytriarylamines via electrochemical polymerization according to Lambert *et al.*^[52]

The first elaboration of triphenylamine dimers and oligomers resulted from an electrochemical oxidation of suitable triphenylamine monomers.^[21] In 2000 Petr *et al.* developed a procedure for the preparation of polytriarylamines by electrochemical oxidation of triphenylamine with Bu_4NPF_6 as electrolyte in a toluene/acetonitrile mixture resulting in a strongly cross-linked, insoluble polymer.^[51] In 2003, Lambert *et al.* electrochemically synthesized a linear TPA-type main chain polymer from a “dimeric” monomer containing two acetylene or diacetylene bridged TPA units (Figure 1.19).^[52] The polymerization reaction to linear polymers was possible due to the high reactivity of the radical cation at the end of the growing polymer chain.

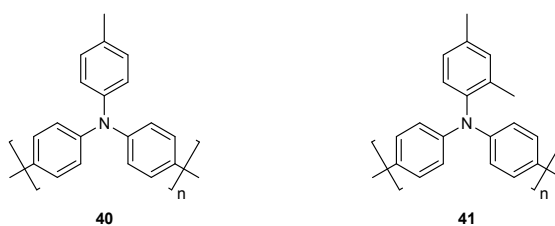


Figure 1.20: Main chain, polymeric triphenylamines PTPA1 (**40**) and PTPA2 (**41**) according to Veres *et al.*^[19]

In 2002 Veres *et al.* reported the first main chain, polymeric triphenylamine (PTPAs) as semiconducting material for solution-processed OFETs.^[19] Their polymers were synthesized by reductive aryl-aryl coupling of dichloro-functionalized monomers in presence of a nickel chloride/zinc catalytic system. The functionalized monomers resulted from a one-pot Ullmann coupling of 1-chloro-4-iodobenzene with the suitable aniline derivative. The PTPAs **40** and **41** prepared according to this procedure exhibited a

molecular weight M_n around $3000 \text{ g}\cdot\text{mol}^{-1}$ with a polydispersity PD between 1.5 and 1.9 after soxhlet extraction to remove low molecular weight oligomers. In this study, it was observed that only the high molecular weight fractions lead to high OFET performance. It was also determined that chlorine atoms remaining at the ends of the polymer chains lead to lower hole mobilities. In order to remove these unwanted chloro-end groups, chlorobenzene was used as an end-capping reagent.

1.4. Charge Transport in Organic Semiconductors

1.4.1. Charge Carriers: Solitons and Polarons

During the charge transport in an organic, semiconducting material, the individual molecules form excited states. Contrary to inorganic semiconductors, the excited states of organic semiconductors are much more localized. The charge carriers involved in the charge transport in conjugated organic materials are polarons, bipolarons, or solitons. These “quasi-particles”^[53] can move along the π -bonds as well as between adjacent macromolecules.^[54] When an electron is added to or removed from a neutral chain, it causes the chain to deform, creating a characteristic pattern of bond deformation. The formed charge plus the deformation pattern constitute a polaron. Along with the chain deformation, there is a characteristic change of the energy level structure: a level is pulled out of the valence band into the gap and another is pulled out of the conduction band (Figure 1.21). Polarons can have a charge $+e$ (hole polaron P^+) or a charge $-e$ (electron polaron P^-) with a spin $\frac{1}{2}$.

A bipolaron is formed by the interaction of two polarons of the same charge. They are spinless, doubly charged carriers ($+2e$ for positive bipolaron BP^{2+} and $-2e$ for negative bipolaron BP^{2-}). If more electrons are put on or removed from a polymer chain, larger energy bands can be generated within the band gap.

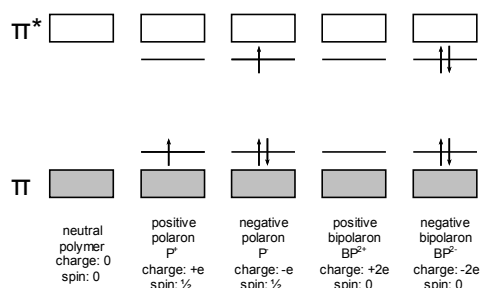


Figure 1.21: Energy levels of non-degenerate conjugated polymers: neutral polymer, a positive and negative polaron, and a positive and negative bipolaron.

Polarons and bipolarons described above can be formed in so-called “non-degenerated ground state” polymers. In the case of “degenerated ground state polymers” such as polyacetylene, the carriers involved are solitons. They can move along the polymer chain with their energy level in the middle of the band gap. Neutral solitons have a spin $\pm\frac{1}{2}$; charged solitons do not have a spin.

1.4.2. Electrical Conductivity and Charge Carrier Mobility

The electrical conductivity σ is determined by the sum of the products of electron/hole carrier mobilities μ_e / μ_p and carrier concentrations (n electron, p hole):

$$\text{Eq. 1.1} \quad \sigma = e n \mu_e + e p \mu_p$$

Electrons or holes injected into a conjugated semiconducting material result either in positively or negatively charged polarons/bipolarons which can move.

Semiconductor	$\mu_e [cm^2 \cdot V^{-1} \cdot s^{-1}]$	$\mu_p [cm^2 \cdot V^{-1} \cdot s^{-1}]$
Single-crystalline silicon	1 500	480
Hydrogenated amorphous silicon	0.11	< 0.1
Tetracene	≈ 2	≈ 2
	10 000 ^[a,c]	100 000 ^[a,c]
Pentacene	1.7	2.7
	10 000 ^[a,c]	100 000 ^[a,c]
α -Sexithiophene	0.7	1.1
	≈ 200 ^[b]	≈ 200 ^[b]
Regioregular poly(3-hexylthiophene)	-	0.1
Perfluorinated copper phthalocyanine	1.7	-
Perylene	5.5	0.4
Fullerene C ₆₀	2.1 ^[c]	1.8 ^[c]

[a] At 1.7 K; [b] At 100 K; [c] Superconductive below a certain critical temperature.

Table 1.1: Mobilities of electrons μ_e and holes μ_p in typical inorganic and organic semiconductors at room temperature unless otherwise indicated.^[55]

The charge carrier mobility μ is one of the central parameters for the charge transport in semiconducting materials. It gives a measure how easy electrons or holes drift through a semiconductor in response to an electric field (Table 1.1). Although charge carrier mobilities in single-crystalline silicon are much larger, for practical applications a mobility of approx. $1 \text{ cm}^2 \cdot \text{V}^{-1} \cdot \text{s}^{-1}$ (as found in amorphous silicon) remains the benchmark.^[55]

1.4.3. Charge Transport Mechanism in Polymers

Many conjugated, organic materials are intrinsically semiconducting materials. They are able to transport charges generated by light, injected by electrodes, or due to chemical

doping. The structure of conjugated, organic materials strongly differs from the three-dimensional crystal structure of most inorganic semiconductors, for example silicon (Si) or germanium (Ge) crystals, which are characterized by a long regular order and strongly bonded atoms. This results in long-range delocalized energy bands (valence band VB and conduction band CB), separated by a "forbidden" energy band gap E_g . Charge carriers added to the semiconductor are strongly delocalized and can move in these energy bands with a relatively large mean free path (depicted as the straight line in Figure 1.22,a). The limiting factor for this band transport is the scattering of the carriers at thermal lattice vibrations, i.e. phonons which disrupt the crystal symmetry (Figure 1.22,a).^[56] The mobility for band transport increases with decreasing temperature.

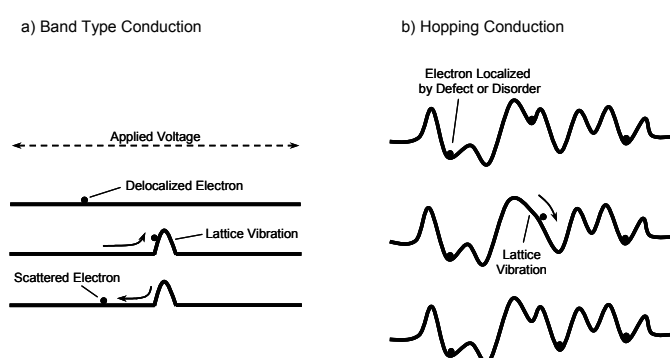


Figure 1.22: Charge transport mechanisms in solids: a) Band transport and b) Hopping transport.^[56]

On the other hand, in most conjugated, organic materials the molecules are bonded by weak van der Waals (or intramolecular) forces resulting e.g. from the hydrogen atom interactions. They typically exhibit narrow energy bands, including the highest occupied molecular orbital (HOMO) and the lowest unoccupied molecular orbital (LUMO), with a wide energy band gap. The charge transport mechanism in such organic semiconductors is connected to the degree of disorder in the material. Due to the complexity of the organic semiconducting materials, it was still not possible to develop a closed theory of charge transport. Several models of charge transport depending on the molecular structure and, hence, on the structural order of the materials have been developed, as the polaron model for organic single crystals^[57] or the multiple trapping and temperature release (MTR) model^[58] and the grain boundary (BG) model^[59] for polycrystalline organic semiconductors. Because of their disorder, semiconducting polymers can not be simply regarded as possessing two delocalized energy bands separated by an energy gap. Bäessler proposed a model based on the Miller-Abraham hopping theory^[60] assuming that the charge transporting sites, which are the segments of the main chain polymer, are subject to a

Gaussian distribution of energies (Figure 1.23), implying that all states are localized.^[61] Due to the observation of a Gaussian shape in the absorption spectra of such polymers, the shape of the density of states (DOS) is suggested to be Gaussian. The charge carriers are believed to move by hopping (phonon-assisted tunneling) on and between the chains. If the carrier is localized due to defects, disorder or selflocalization, e.g. in the case of polarons, the lattice vibrations are essential for a carrier to move from one site to another (Figure 1.22,b). For hopping transport the mobility increases with increasing temperature.

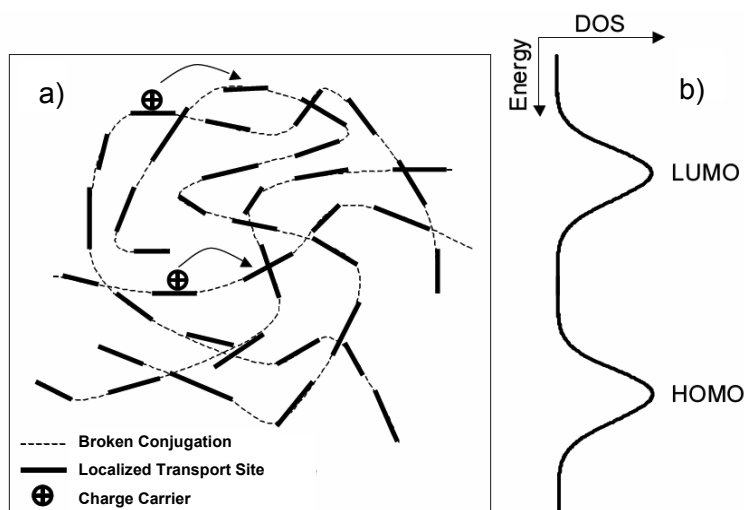


Figure 1.23: (a) Polymer chains broken up in conjugated segments (charge transport sites) between which the charge carriers hop. (b) A representation of the density of states approximated by a Gaussian distribution for the HOMO and LUMO levels.^[61]

For the description of the temperature and gate voltage dependencies of organic field-effect transistors, Vissenberg and Matters^[62] adapted a percolation model based on variable range hopping in an exponential density of states described by Monroe for inorganic semiconductors.^[63]

1.5. Organic Field-Effect Transistors (OFETs)

1.5.1. Basic OFET Architectures

Field-effect transistors based on organic semiconducting materials are in most of the cases thin film transistors (TFTs). They can be built in two main types of device architectures: in top-gate or bottom-gate geometry as depicted in Figure 1.24.^[64] In the top-gate configuration, the source and drain electrodes are deposited on a PET or glass substrate. The semiconducting layer is then generated on the top of the electrodes and separated from the gate electrode by an insulating layer (Figure 1.24,a). In the

bottom-gate configuration, the gate electrode is deposited directly on the gate and separated from the semiconducting film by a dielectric layer. Here, two different configurations are suitable: bottom-gate/bottom-contact where the source and drain electrodes are situated directly on the dielectric with the semiconductor on top, or the bottom-gate/top-contact where the semiconductor is deposited directly on the insulator with the source and drain electrodes on top (Figure 1.24,b).

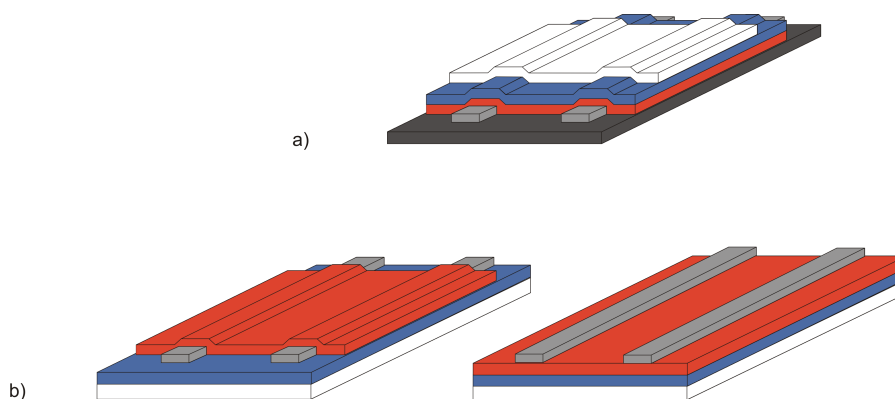


Figure 1.24: Architecture of an OFET in a) top-gate configuration and b) bottom-gate/bottom-contact configuration (left) or bottom-gate/top-contact configuration (right) with: substrate (black), source and drain electrodes (grey), semiconductor (red), insulator (blue) and gate electrode (white).

1.5.2. OFET Principle

The field-effect transistor FET (or thin film transistor TFT) controls the flow of electrons from the source S to drain D by affecting the size and shape of a "conductive channel" created and influenced by the voltage (or lack of voltage) V_G applied across the gate G and source S terminals. (Figure 1.25) This conductive channel is the "stream" through which charge carriers flow from source S to drain D . When a negative gate voltage V_G is applied, positive charges are generated at the semiconductor interface adjacent to the gate dielectric (a p -type conducting channel is formed). Charges carriers can be then extracted by the electrodes by applying a voltage V_D between drain and source. Such organic semiconductors with ability to conduct only positive charge carriers are said to be p -type semiconductors. On the other hand, when a positive voltage is applied to the gate negative charges are generated at the semiconductor interface adjacent to the gate dielectric (a n -type conducting channel is formed). Negative charges (electrons) can then be injected and extracted by the electrodes by applying a voltage V_D between drain D and source S . Such organic semiconductors with ability to conduct only negative charge

carriers are said to be n -type semiconductors. A third type of transistor, called ambipolar, can transport both positive and negative charge carriers (hole and electrons).

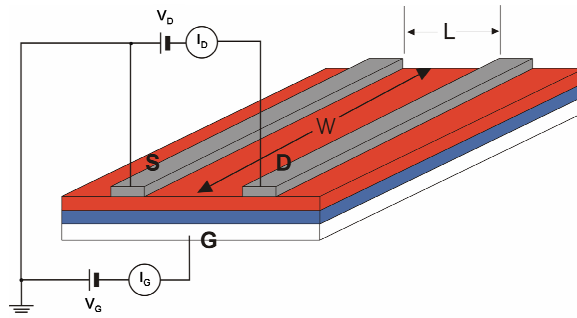


Figure 1.25: OFET principle with I_D drain-to-source current, V_D drain-voltage, I_G gate-to-source current, V_G gate voltage, W channel width, L channel length, S source D drain and G gate.

1.5.3. OFET Characteristics: Output and Transfer

The output and transfer characteristics are the two typical measures used in the characterization of field-effect transistors. They allow to determine the FET parameters of the devices described below. The output characteristic is obtained by measuring the drain-to-source current I_D during drain-voltage V_D sweeps at various constant gate voltages V_G . In the transfer characteristics the drain-to-source current I_D is measured by applying various constant drain-voltages V_D and sweeping the gate-voltage V_G . Figure 1.26 depicts a typical set of output and transfer curves.

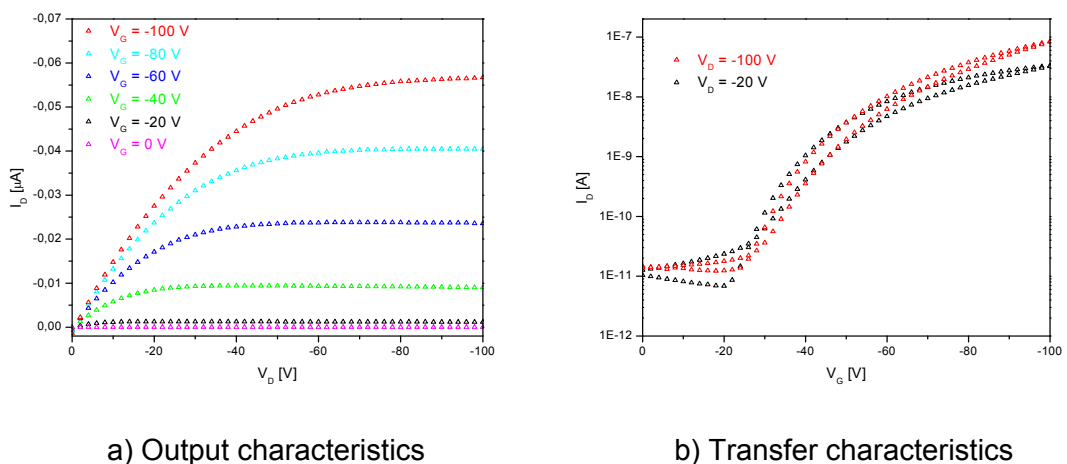


Figure 1.26: Typical set of curves for a) output characteristics and b) transfer characteristics (semilogarithmic plot) of an organic field-effect transistor with drain-to-source current I_D , drain voltage V_D , and gate voltages V_G .

1.5.4. OFET Model and Field-Effect Mobility

In order to describe theoretically the current-voltage characteristics of a field-effect transistor Horowitz *et al.* proposed a model^[65] which will be only roughly described here. From the output characteristics two different regimes can be determined: the linear domain in which the drain-to-source current I_D increases proportionally to the drain-voltage V_D and the saturation domain in which the drain-to-source current I_D stays constant as shown in Figure 1.27.

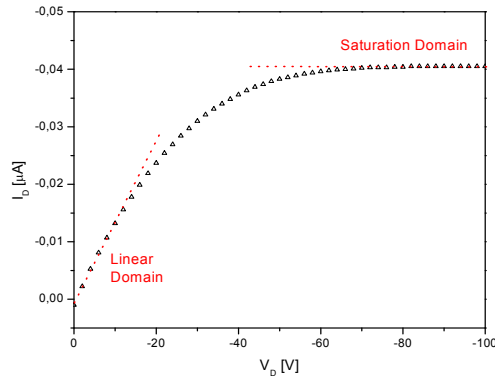


Figure 1.27: Linear and saturation domains in output characteristics.

In the linear regime, the source-to-drain current $I_{D,lin}$ for $V_D < V_G$ can be described according to:

$$\text{Eq. 1.2} \quad I_{D,lin} = \frac{W\mu_{FET,lin}C_i}{L} \left[(V_G - V_0)V_D - \frac{V_D^2}{2} \right]$$

where $I_{D,lin}$ the source-to-drain current in the linear regime, W the channel width, L the channel length, $\mu_{FET,lin}$ the field-effect mobility in the linear regime, C_i the insulator capacitance per unit area, V_G the gate voltage, V_D the drain voltage and V_0 the drain voltage for $V_G = 0$ V.

In the saturation regime, the source-to-drain current $I_{D,sat}$ which stays constant for $V_D > V_G$, can be described by:

$$\text{Eq. 1.3} \quad I_{D,sat} = \frac{W\mu_{FET,sat}C_i}{2L} (V_G - V_0)^2$$

where $I_{D,sat}$ the source-to-drain current in the saturation regime and $\mu_{FET,sat}$ the field-effect mobility in the saturation regime.

The charge carrier density in a FET is distributed non-uniformly and is decreasing from the semiconductor/insulator (S/I) interface to the bulk. Therefore, the field-effect mobility in an OFET has not the same value for all regions and charge carriers. The major part of the

charge carriers is, however, located near the S/I interface and has nearly the same mobility in this region, but the mobility still depends on the applied gate-voltage V_G .

Using the equation 1.4, the field-effect mobility of an OFET in the linear regime ($V_D < V_G$) can be calculated by:

$$\text{Eq. 1.4} \quad \mu_{\text{FET,lin}} = \frac{L}{WC_i V_D} \left(\frac{\partial I_D}{\partial V_G} \right)_{V_D=\text{const}}$$

In the same way, using the equation 1.5, the field-effect mobility of an OFET in the saturation regime ($V_D > V_G$) can be calculated as:

$$\text{Eq. 1.5} \quad \mu_{\text{FET,sat}} = \left(\frac{\partial \sqrt{I_{D,\text{sat}}}}{\partial V_G} \right)_{V_D=\text{const}}^2 \frac{2L}{WC_i}$$

It is to notice that the equations 1.4 and 1.5 have been derived under the assumption of a constant mobility. But in organic semiconductors, due to the significant dependence of the mobility on the gate voltage and the temperature, these equations could only be used to afford an approximate value of the mobility. Moreover, the influence of contact resistance is neglected. For further enhancement of this method, Horowitz *et al.* proposed an improved model for the determination of the field effect mobility considering the influence of the temperature and the gate voltage.^[66]

The mobilities measured within this study were the mobilities $\mu_{\text{FET,sat}}$ from the saturation domain which gave the best results and allowed a direct comparison of different devices made of different semiconducting materials.

1.5.5. OFET Parameters: On/Off Ratio, Hysteresis and Turn-On Voltage

The three parameters on/off ratio, hysteresis and turn-on voltage can be graphically described with the transfer characteristics curve as shown in Figure 1.28.

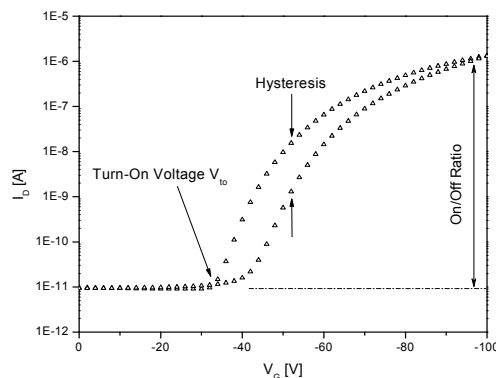


Figure 1.28: Transfer characteristics of an OFET.

The on/off ratio is the ratio of the source-to-drain current in the on-state $I_{D,on}$ (high V_D and high V_G) to the source-to-drain current in the off-state $I_{D,off}$ (high V_D and $V_G = 0$ V). Well performing devices should exhibit on/off-current ratios in the order of 10^6 .

The hysteresis represents the difference of source-to-drain current I_D between forward and backward sweeps. A big hysteresis is a hint for impurities or instability of the material. In this regard, an hysteresis as small as possible is always desired.

The turn-on voltage V_{on} is the gate-voltage, at which no band-bending in the semiconductive layer is observed (flat-band condition). In general, it is the first gate voltage at which the conducting channel is generated and the charge carriers start to flow from the source to the drain electrodes. Below V_{on} no gate-voltage dependence to source-to-drain current I_D is observable, while I_D increases with V_G above V_{on} . In an ideal semiconductor, where no fixed (or trapped) charges are present neither in the semiconductor nor in the dielectric layer, V_{on} should be zero. The turn-on voltage of an OFET is closely related to localised (or trapped) charges at the semiconductor/dielectric interface. Degradation processes, such as doping under ambient conditions, where the number of these charge traps changes, can generate shifts of V_{on} .

1.6. Aim and Scope

Inspired by the work of the Avecia group, a couple of triarylamine-based materials have been synthesized within this study. Different polymers as well as small molecule model compounds were investigated in order to determine the impact of several structural factors on the properties of the materials used as active layers in OFETs. In the second chapter, the synthesis of main-chain triphenylamine-based polymers with different alkyl substituents as well as different aromatic systems within the backbone was described. The influence of the structural modifications on the processability has been investigated as well as the optical properties of the polymers. In the chapter 3, investigations of polytriarylamines with carbazole building block are reported. *N*-aryl substituted polycarbazoles were synthesized and investigated. Chapter 4 introduces small molecules and polymers based on the 5,10-diphenylphenazine unit. The model compounds have been synthesized to optimize the synthetic procedures and to run first device tests. A series of corresponding copolymers have been prepared to determine the influence of an increased number of triarylamine units within the materials.

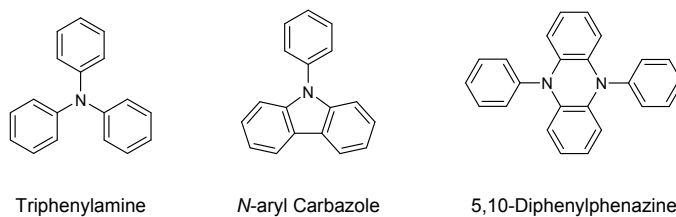


Figure 1.29: Functional moieties of the synthesized materials.

All derivatives synthesized for this study have been characterized by NMR and mass spectroscopy. Additionally, UV-Vis and photoluminescence (PL) as well as OFET investigations have been carried out for the semiconducting materials. All results are discussed in details and summarized at the end of each chapter.

2. Polytriphenylamine-Type Materials

2.1. Introduction

The synthesis of compounds containing *N*-aryl moieties has recently met with a great deal of interest due to their importance in diverse fields including natural products,^[67] photography,^[68] and electronic materials.^[69] Among them, polytriphenylamine-type materials (Figure 2.1) have gained many attention from chemists and physicists. Their properties as organic hole transporting materials made them a research target towards OLED^[70] or solar cell^[71] devices or organic field-effect transistors.^[16,19]

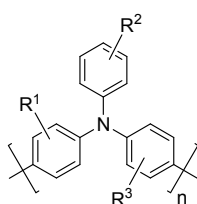


Figure 2.1: General chemical structure of polytriphenylamine-type materials.

The synthesis of such materials commonly occurs in two major steps. First, functionalized monomers are obtained by amination reaction of an aryl halide compound with an amine (Figure 2.2). The functionalized monomer can then polymerize in an aryl-aryl coupling reaction.

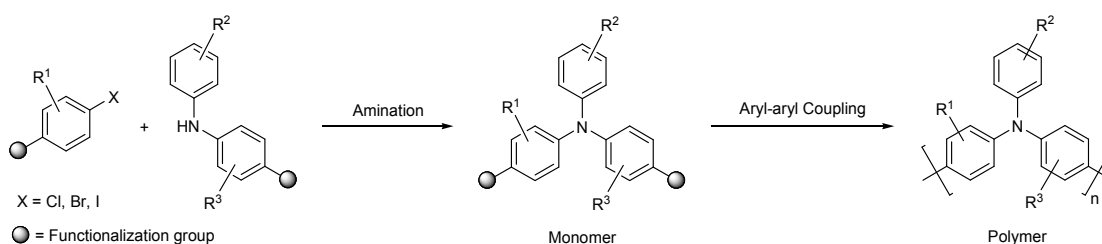


Figure 2.2: Synthesis of polytriphenylamine-type materials.

2.2. Synthesis

2.2.1. Monomer Synthesis

The amination reaction of aryl-halides according to Buchwald and Hartwig will be now presented in detail as well as the advantages (and disadvantages) of this amination reaction compared to other procedures. The reaction mechanism and the role of the

catalytic system will also be described. Afterwards, the synthesis and structure investigation of our triphenylamine-based monomeric species will be outlined.

2.2.1.1. The Buchwald-Hartwig Amination Reaction

Despite the “simplicity” of the triarylamine moiety, the synthesis of these compounds is often difficult. Synthetic procedures involving nitration and reduction steps are incompatible with many functional groups and often require protection and deprotection steps. Reductive aminations, which involve formation of an imine from an arylamine and subsequent reduction of the imine, are often multiplestep procedures and require a preformed carbon-nitrogen (C-N) bond, an excess of the amine, and sluggish reductions.^[72]

One of the most widely used methods for the synthesis of triarylamines is the Ullmann-type condensation, in which a diarylamine is condensed with an aryl halide in the presence of a base and a copper catalyst (Figure 2.3).^[73]

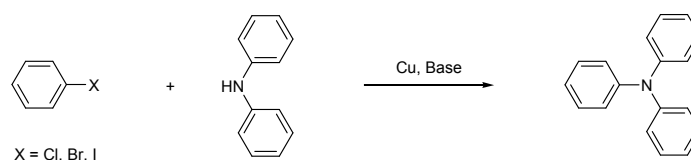


Figure 2.3: Amination of aryl halides according to Ullman.^[73]

Traditionally, this method has been plagued by the requirement of stoichiometric amounts of copper compounds and harsh reaction conditions (e.g. high temperatures) while often giving diarylation side products, providing poor yields and being substrate-specific. Improved reaction conditions have been developed to circumvent some of these problems. For example, it has been determined that the addition of crown ethers as phase-transfer catalyst allows milder reaction conditions. Recently, 1,10-phenanthroline has been employed to coordinate the copper, enabling lower temperatures and shorter reaction times. These catalytic systems also allow the twofold coupling of anilines with two equivalents of an aryl halide to form a symmetric triarylamine, a process which is difficult under traditional Ullmann conditions. Copper-mediated reactions derived from the Ullman reaction for C-O, C-S or C-N bond formations are now also subject of increasing interest.^[74]

In the early 1980's, Kosugi *et al.* reported the coupling of electron-neutral aryl bromides with tin amides in presence of a palladium catalyst containing a sterically hindered aromatic phosphine ligand as depicted in Figure 2.4.^[75]

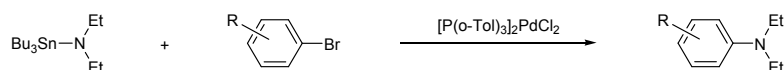


Figure 2.4: C-N bond formation according to Kosugi *et al.*^[75]

The scope of this reaction appeared to be limited to dialkylamides and electron-neutral aryl halides. The use of aryl halides with additional nitro, acyl, methoxy, and dimethylamino substituents gave poor yields upon palladium-catalyzed reaction with tributyltin diethylamide. Furthermore, aryl bromides were the only aryl halides that provided any reaction product. However, this prior work demonstrated that the carbon-nitrogen bond formation could also be catalyzed by palladium complexes.

Palladium-catalyzed coupling chemistry has proven to be a powerful method for the formation of new carbon-carbon (C-C) bonds at aryl halides or triflates by replacement of the aryl halogen or pseudo-halogen with a carbon nucleophile.^[76] A variety of main group and transition metal reagents such as tin and boron compounds but also aluminum, zinc, magnesium, and silicon reagents, are used as carbon nucleophiles. Nickel and palladium complexes are now the preferred catalysts in these cross-coupling reactions.

In the late 1990's, the groups of Buchwald^[44] and Hartwig^[43] inspired by the work of Kosugi *et al.* developed a new tin-free method to produce a carbon-nitrogen bond under mild conditions by reaction of an amine and a aryl halide in presence of a palladium catalyst, phosphine ligands and a strong base in an aromatic solvent (Figure 2.5).

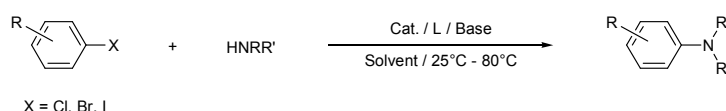


Figure 2.5: General Buchwald-Hartwig amination reaction with catalyst (e.g. $\text{Pd}_2(\text{dba})_3$, $\text{Pd}(\text{dba})_2$ or $\text{Pd}(\text{OAc})_2$), ligand (e.g. $\text{P}(o\text{-tolyl})_3$, PPh_3 , $\text{P}(t\text{-Bu})_3$, $\pm\text{BINAP}$, DPPF or JohnPhos), base ($\text{NaO}-t\text{-Bu}$ or $\text{LiN}(\text{SiMe}_3)_2$) and aromatic solvent (e.g. benzene, toluene or xylene).

The first synthetic attempt published concurrently by Buchwald and Hartwig in 1995 showed that amines could react with an aryl bromide in the presence of an alkoxide or silylamide base (e.g. $\text{NaO}-t\text{-Bu}$ or $\text{LiN}(\text{SiMe}_3)_2$) with the catalyst used by Kosugi *et al.* Many catalytic systems (Figure 2.5) have now been efficiently applied and allow the reaction of various amine species (cyclic secondary, acyclic secondary, aliphatic primary, aromatic amine) and aryl "halide" compounds (bromides, iodides, chlorides, triflates and sulfonates). The mechanism of the Buchwald-Hartwig amination is very similar to aryl-aryl coupling reactions such as Miyaura-Suzuki, Stille or Negishi-type reaction (Figure 2.6).

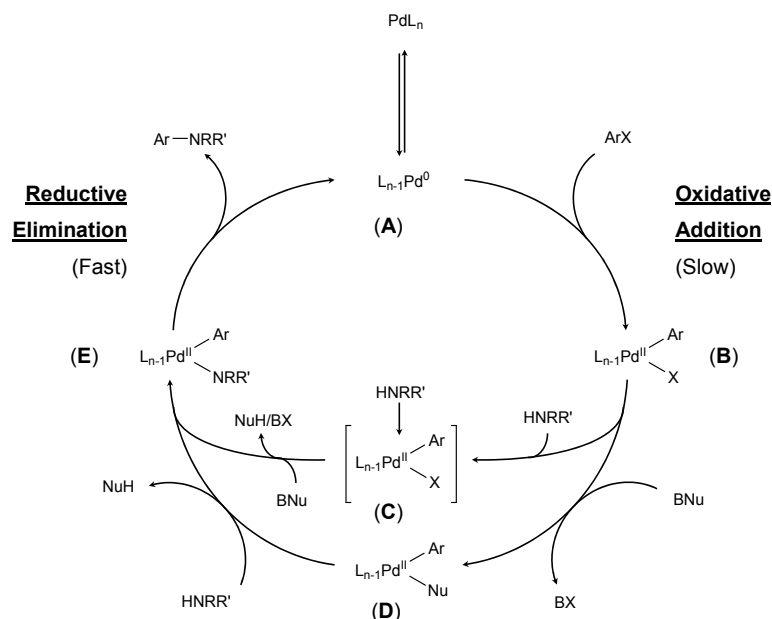


Figure 2.6: General mechanism of the Buchwald-Hartwig amination.

At first, the formation of the palladium(II) species **B** takes place by oxidative addition of the aryl halide (or triflates) on the palladium(0) complex **A**. The palladium(II) complex **B** can further react in two pathways: coordination of the amine to the intermediate **C** followed by deprotonation to afford the palladium(II) complex **E** or formation of **E** via the nucleophile complex **D**.^[77] At least, reductive elimination of the C-N coupled compound leads to the regeneration of the catalyst.

However, the palladium(II) complex **E** can undergo a side reaction where a reduction of the aryl halide to the corresponding aromatic hydrocarbon is observed (Figure 2.7).^[78]

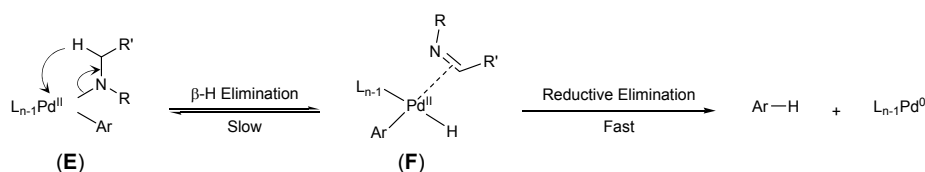


Figure 2.7: Reductive elimination reaction mechanism as side reaction in the catalytic cycle of the Buchwald-Hartwig reaction.

Hereby, in a first step, a slow reversible β -H elimination at the palladium(II) complex **E** takes place and leads to the palladium(II)-imino complex **F**. Through a fast reductive elimination, the dehalogenated arene is formed and the catalyst regenerated. Other side reactions, such as epimerization of α -chiral amine (Figure 2.8) lead to a reduction of the stereospecificity and the enantiomeric excess. However, this side reaction can be avoided by an appropriate ligand design.^[79]

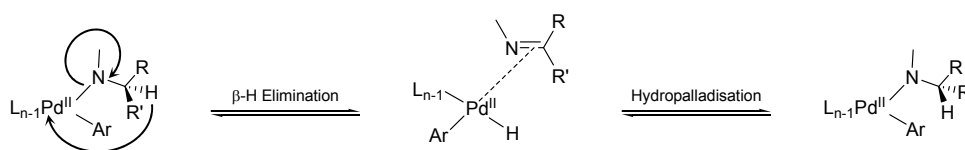


Figure 2.8: Epimerisation of α -chiral amine substrates.

As already mentioned, the ligand at the metal center and the amine substrate play a crucial role regarding the scope, the selectivity and the yield of the amination reaction. The groups of Buchwald^[44] and Hartwig^[43] reported in 1995 a very efficient catalytic system based on tris(dibenzylideneacetone)dipalladium(0) ($\text{Pd}_2(\text{dba})_3$) and tri(*ortho*-tolyl)phosphine ($\text{P}(\text{o-tolyl})_3$). This catalytic system revealed to be efficient for intermolecular aminations of a large range of aryl halides with secondary amines, and also for electron-poor aryl halides with primary amines. However, for primary amines and electron-neutral aryl halides, only poor yield of the expected products were obtained from the reaction. Arene reduction as side reaction is favored here. The catalytic system can be also applied to an intramolecular amination of aryl halides towards nitrogen-containing heterocycles (Figure 2.9). For this kind of reactions, $\text{Pd}(\text{PPh}_3)_4$ in presence of a mixture $\text{NaO-}t\text{-Bu}/\text{K}_2\text{CO}_3$ appeared to be an even more efficient catalyst system.^[80]

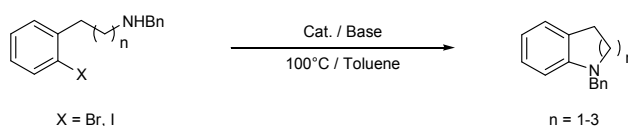


Figure 2.9: Intramolecular Buchwald-Hartwig amination with $\text{Pd}(\text{PPh}_3)_4$ as catalyst and $\text{NaO-}t\text{-Bu}/\text{K}_2\text{CO}_3$ as base in toluene.^[80]

In order to broaden the scope of the amination reactions aryl halides and amines, more effective, bidentate chelate ligands like 1,1'-bis(diphenylphosphino)ferrocene (DPPF) and 2,2'-bis(diphenylphosphino)-1,1'-binaphthyl (\pm BINAP) were developed. This kind of ligands appeared to be more efficient than $\text{P}(\text{o-tolyl})_3$ for primary alkylamines, cyclic secondary amines or anilines due to the low amount of arene byproducts formed during the reaction. For these bidentate chelate ligands, the regeneration to the palladium(II) complex **E** is faster than the reductive elimination towards the palladium(0) complex **A** during the β -H elimination (Figure 2.10). For the coupling of electron-neutral, hindered aryl halides with primary amines in presence of DPPF, the formation of diarylation products

couplings of aryl halides and aryl boronic esters.^[84] These catalysts couple a wide range of aryl chlorides, including electron-rich ones, with secondary and primary alkyl amines and anilines.

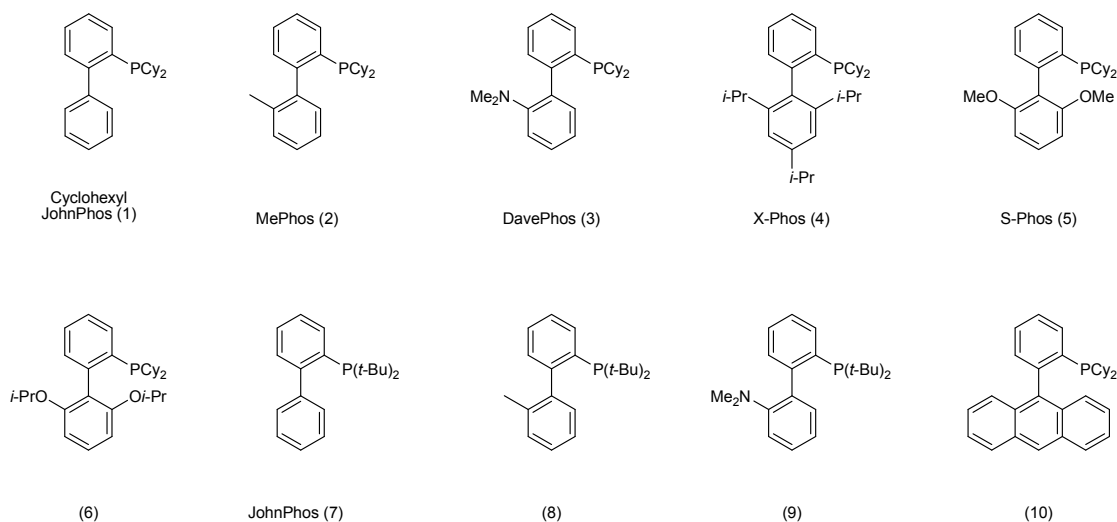


Figure 2.12: Bulky, electron-rich biarylphosphine ligands

As shown in Figure 2.14, the mechanism of the oxidative addition step can differ depending on the ligands involved and the geometry of the primary palladium(II) complex. In the case of triphenylphosphine ligands (PPh_3), Fauvarque and Amatore^[85] independently showed that oxidative addition of aryl halides to $\text{Pd}(\text{PPh}_3)_3$ occurs after dissociation of one ligand to generate a linear $\text{Pd}(\text{PPh}_3)_2$ intermediate which then inserts into the carbon-halogen bond to generate the complex $(\text{PPh}_3)_2\text{Pd}(\text{Ar})(\text{X})$ (Figure 2.13,a). Hartwig *et al.*^[86] showed that palladium complexes with hindered phosphine ligands such as $\text{P}(o\text{-tolyl})_3$, which are stable in their disubstituted form, also undergo the oxidative addition of aryl halides after dissociation of one phosphine ligand. This trisubstituted intermediate then dimerizes to form a stable, dimeric palladium(II) complex (Figure 2.13,b). Hartwig and co-workers also showed that oxidative addition to palladium(0) complexes with bidental bisphosphine ligands, such as \pm BINAP or DPPF, occurs after dissociation of one chelating ligand under generation of a bent monoligand complex (Figure 2.13,c).^[87]

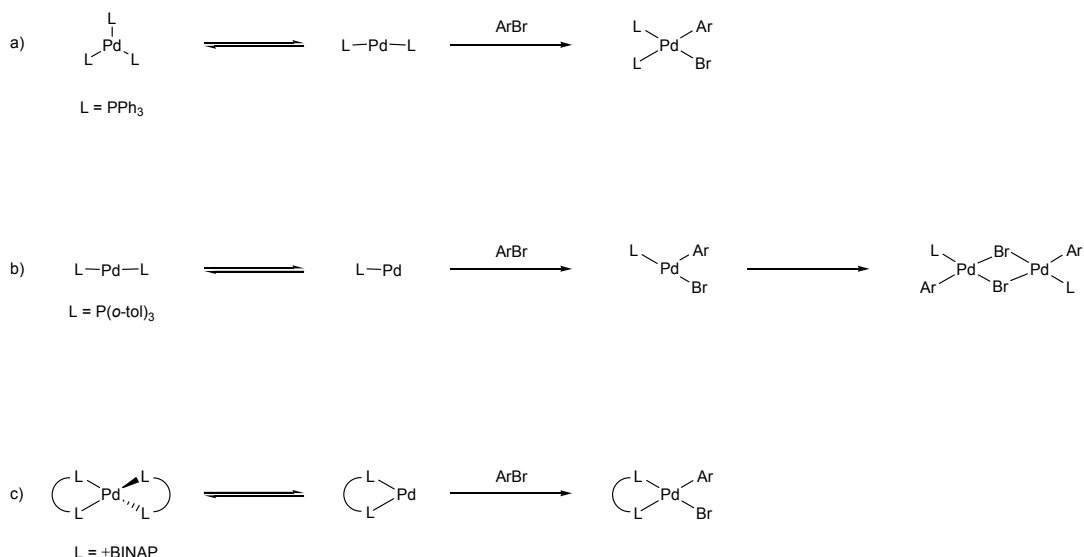


Figure 2.13: Oxidative addition mechanisms for a) PPh₃, b) P(*o*-tolyl)₃ and c) ±BINAP as ligand.^[88]

The use of the sterically, hindered monodentate ligand P(*t*-Bu)₃ instead of P(*o*-tolyl)₃ leads to a dramatic acceleration of the rate of the oxidative addition.^[89] In this case, in contrary to the P(*o*-tolyl)₃ complex, the reactive, T-shaped P(*t*-Bu)₃ complex does not undergo any dimerization (Figure 2.14).

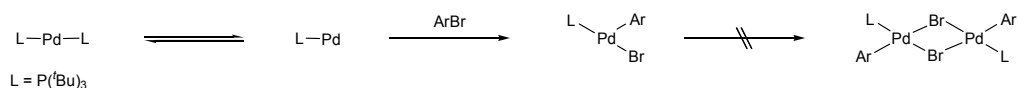


Figure 2.14: Oxidative addition mechanisms for the ligand P(*t*-Bu)₃.^[88]

The reductive elimination step plays a determining role concerning the yield and the scope of the Buchwald-Hartwig amination reaction.^[90] Kinetic studies showed that the reductive elimination can follow two concurrent pathways: a fast reductive elimination from a trisubstituted complex in the case of hindered monodentate phosphine ligands such as P(*t*-Bu)₃ (Figure 2.15,a) or a slower reductive elimination from a *cis*-tetrasubstituted complex in the case of bidentate chelating ligands such as DPPF (Figure 2.15,b).

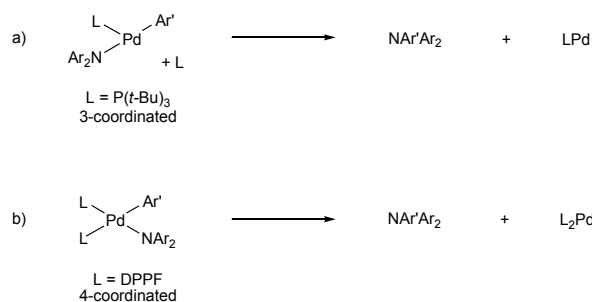


Figure 2.15: Possible mechanisms for the reductive elimination of a) trisubstituted or b) tetrasubstituted palladium complex.^[88]

Wolfe *et al.* investigated the reductive elimination occurring from a tetrasubstituted palladium(II) complex bearing a chelating ligand (DPPF). The study revealed that the combining of an electron-rich ligand and an electron-poor aryl halide leads to the fastest reductive elimination.^[91] Moreover in aryl palladium(II) amido complexes with chelating ligands the reductive elimination is faster than the β -H elimination as side reaction.^[92] It was demonstrated that β -H elimination from square-planar amido complexes occurs after generation of trisubstituted complexes.^[93] Thus, catalyst complexes tetrasubstituted with bidentate chelate ligands exhibit slow β -H elimination but facile reductive elimination. As a consequence, the suppression of the β -H elimination leads to a better selectivity in the formation of aryl amines over the formation of arene by-products.

Sterically hindered ligands like P(*t*-Bu)₃ also enhance the relative rate of the reductive elimination over the β -H elimination.^[94] Reductive elimination reduces the coordination number of the metal where the β -H elimination either increases it or leaves it unchanged. Sterically hindered ligands therefore accelerate the reductive elimination but suppress the β -H elimination and thus favor the formation of the amine versus the formation of arene side product. Hereby, a strong influence of the sterically hindered phosphine ligands on the rate of reductive elimination can be observed. For example, aryl palladium(II) amido complex with the P(*t*-Bu)₃ ligand allow the reductive elimination at $-10\text{ }^{\circ}\text{C}$ while for analogous the complex with DPPF or PPh₃ as ligand a reaction temperature of $70\text{ }^{\circ}\text{C}$ is necessary. However, the low coordination number of such palladium complexes can cause a problem in the case of primary amine substrate which can displace one ligand molecule. The tetrasubstituted complex that is generated in this case revealed to be inactive for the coupling of aryl chlorides.^[88]

In summary, the effectivity of the catalytic system for the Buchwald-Hartwig amination reaction is strongly influenced by different factors: the electronic nature of the aryl halide (electron-poor or electron-rich), the leaving group (e.g. chloride, bromide, triflate) the steric hindrance (both of the ligand or the amine), or the amine component involved (e.g.

primary, secondary or heterocyclic amine). For example, mild coupling reactions of less active aryl chlorides occur with catalysts containing phosphines with sterically hindered alkyl substituents (e.g. $P(t\text{-Bu})_3$), but reactions of aryl bromides occur with catalysts containing triarylphosphines (e.g. $P(o\text{-tolyl})_3$ or PPh_3). In the case of secondary amines, a greater steric hindrance at the aryl halide improves the rate of the reductive elimination versus the $\beta\text{-H}$ elimination. Moreover, the use of sterically hindered, monodentate ligands accelerates the coupling of secondary amines with aryl halides. Nevertheless, the reductive elimination proceeds slower with palladium amido complexes generated from primary amines in relation to those generated from secondary amines. Thus the $\beta\text{-H}$ elimination side reaction more often competes with the reductive elimination in the coupling of primary amines with aryl halides. Primary amines are more tightly bound to the palladium cores than secondary amines and can lead to ligand displacements in the complex. Considering this, catalytic systems with bidentate chelate ligands are more reactive in the coupling of secondary amines with aryl halides than catalysts containing monodentate ligands.

2.2.1.2. Functionalized Monomers

Different triphenylamine-based, functional monomers were synthesized for our study. These monomers were synthesized by an amination of an aryl halide with an aniline compound according to Buchwald and Hartwig. As mentioned previously, catalytic systems containing bidentate chelate ligands are most effective for the coupling of primary amine with aryl halides. Thus, the catalytic system used here, composed of $Pd_2(dba)_3$ (catalyst) and DPPF (ligand), allowed a direct, “double arylation” of the aniline in a one-pot synthesis in a modified procedure after Louie *et al.* (Figure 2.16).^[95]

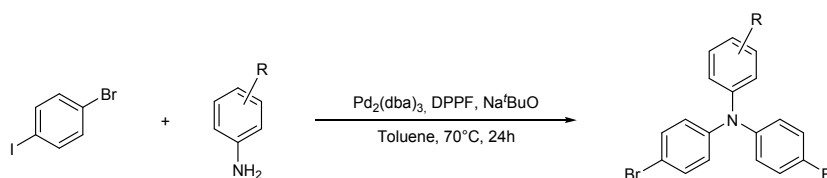


Figure 2.16: Synthesis of the functionalized triphenylamine-based monomer.

In this case, 1-bromo-4-iodobenzene was used as aryl halide. The lower dissociation energy of the C-I bond compared to the C-Br bond permits to obtain bromine functionalized monomers in one step without further manipulation. The other components utilized for this reaction are the commonly used sodium-*tert*-butoxide NaO-*t*-Bu as base and toluene as solvent.

Two modification strategies were investigated for this kind of monomers. The first one involves a variation for the substituent of the “side chain” aryl group; the second was based on the increase of the aromatic system of the polymeric target by increasing the number of phenylene units between two nitrogen atoms.

First, a range of five functionalized monomers with different substituents on the “side chain” phenyl group were synthesized (Figure 2.17) in order to determine the influence of these different substituents on the processability and field effect transistor properties.

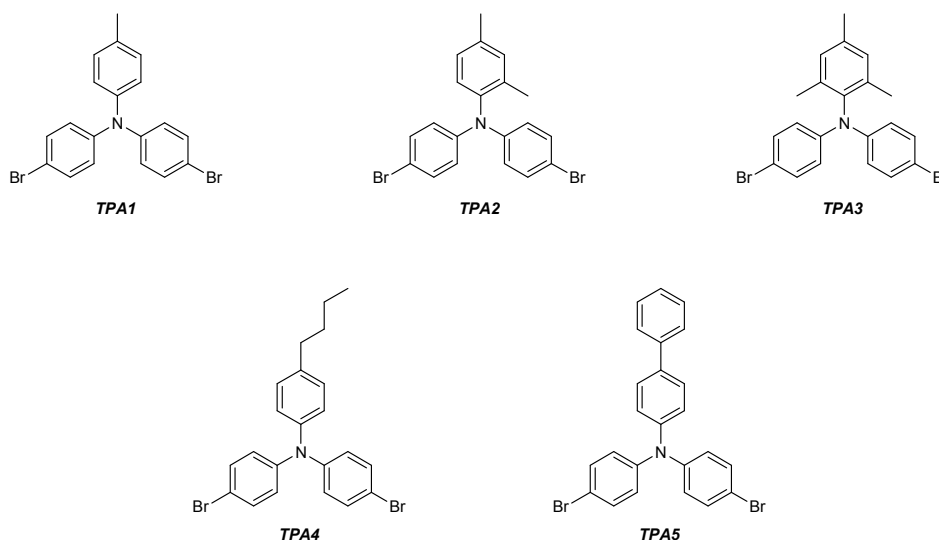


Figure 2.17: Synthesized monomers with variations of substituents along the side-chains.

The yields of the coupling reactions vary from 40 to 70 % depending on the aniline derivative involved. The molecular structures of the monomeric compounds were investigated by mass spectrometry and NMR spectroscopy. The ^1H NMR spectra of the five compounds all show similar doublets for the proton (a) between $\delta = 7.20$ and 7.30 ppm as well as the doublet for the proton (b) between $\delta = 6.80$ and 6.95 ppm with a coupling constant of $^3J = 8.8 \pm 0.2$ Hz. Hereby, (a) is more downfield shifted due to the influence of the neighboring halogen functional group (Figures 2.18–2.22).

The **TPA1** monomer is commercially available from *Sensient Imaging Technologies GmbH - Syntec Division*. Therefore, no analytical data for this compound will be provided here.

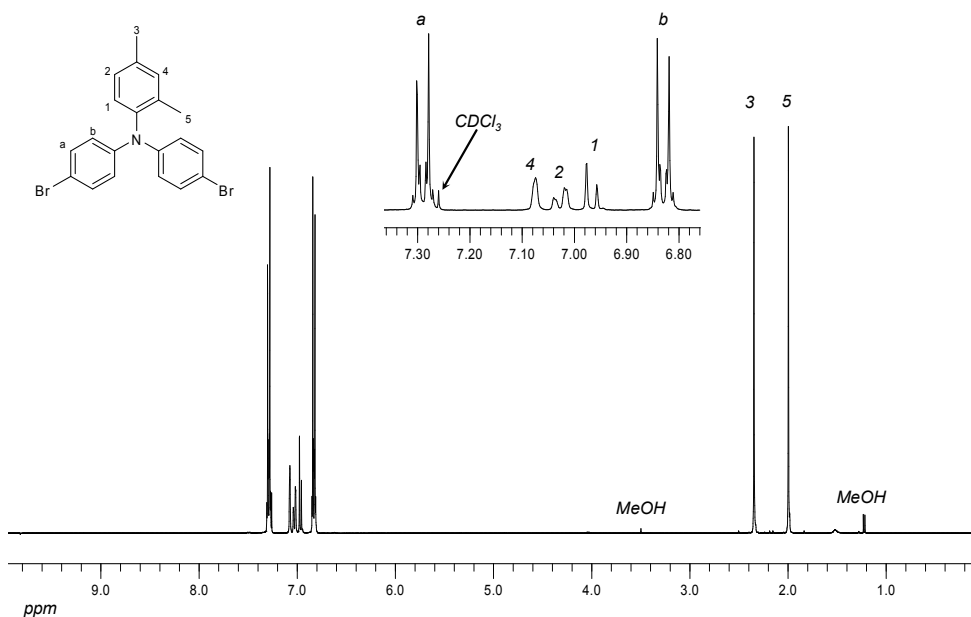


Figure 2.18: ^1H NMR of **TPA2** monomer in CDCl_3 .

Figure 2.18 shows the ^1H NMR spectrum of the **TPA2** monomer in CDCl_3 . For the protons (a) and (b), two doublets at $\delta = 6.83$ and 7.29 ppm respectively can clearly be observed. Beside (a) and (b), the proton (4) can be determined as the sole singlet ($\delta = 6.99$ ppm) in the aromatic region. The methyl group (5) shows a lucid through space ^1H - ^1H NOESY signal connected with (b) and can then be assigned to the singlet at $\delta = 1.90$ ppm. The second methyl group (3) exhibits a singlet at $\delta = 2.26$ ppm and couples with (4) and (2) in the ^1H - ^1H ROESY spectrum. Thus, the proton (2) can be associated to the doublet at $\delta = 6.95$ ppm ($^3J = 8.1$ Hz) in the aromatic region of the ^1H NMR spectra. Finally, the proton (1) can be identified as a doublet at $\delta = 6.89$ ppm which couples with (2) with a constant $^3J = 8.0$ Hz. Moreover, ten aromatic signals beside the two peaks for the two methyl carbon atoms ($\delta = 21.0$ ppm and $\delta = 18.3$ ppm) can be observed on the ^{13}C NMR spectrum. The ^{13}C NMR (dept135) analysis reveals five tertiary as well as five quaternary carbon atoms as expected. Among them, a typical signal at $\delta = 113.9$ ppm which is characteristic for a C-Br group can be observed. The molecular integrity of **TPA2** is also verified by mass spectrometric investigation with a molar peak at 430.6 g $\cdot\text{mol}^{-1}$.

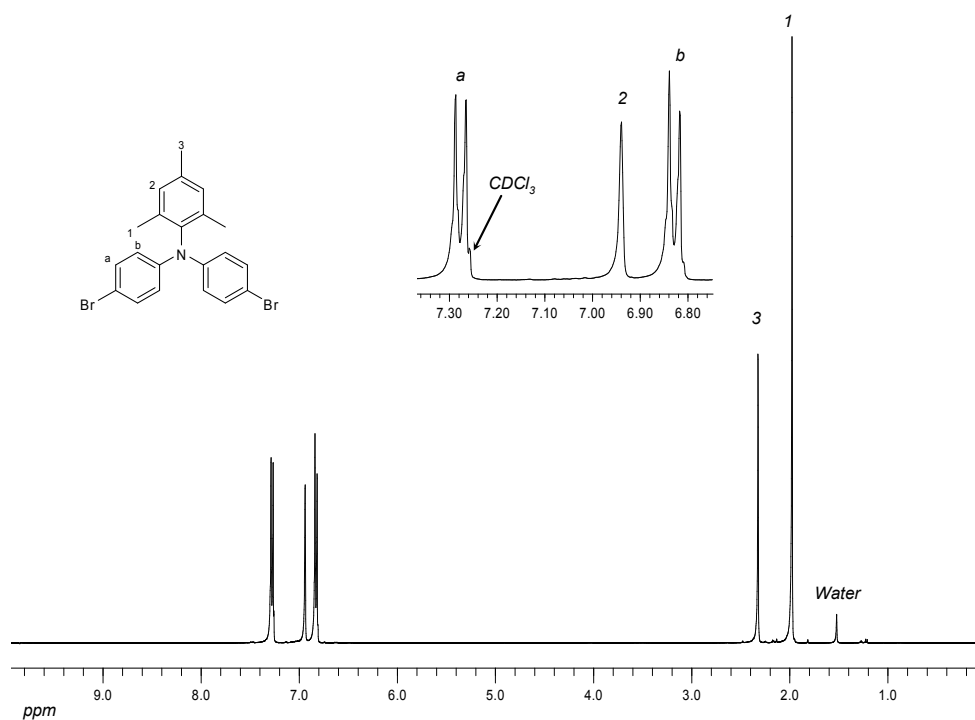


Figure 2.19: ^1H NMR of **TPA3** monomer in CDCl_3 .

In the aromatic region of the ^1H NMR spectrum of the **TPA3** monomer in CDCl_3 (Figure 2.19), one singlet at $\delta = 1.98$ ppm for the protons of the methyl groups (1) and one at $\delta = 2.32$ ppm for the protons of the methyl group (3) can be observed. In the aromatic region, beside (a) and (b), the singlet at $\delta = 6.94$ ppm refers to the proton (2). In the ^{13}C NMR spectrum, beside the two methyl carbon peaks in the aliphatic region ($\delta = 21.0$ and 18.4 ppm), eight peaks can be observed in the aromatic region. The ^{13}C NMR (dept135) analysis allows to recognize three non-equivalent tertiary carbon atoms and five non-equivalent quaternary carbon atoms as expected. Moreover, one peak for a quaternary carbons arises at approx. 115 ppm ($\delta = 113.1$ ppm) which is typical for a C-Br carbon. The molecular structure is confirmed by mass spectrometry study with a molar peak at 444.6 $\text{g}\cdot\text{mol}^{-1}$.

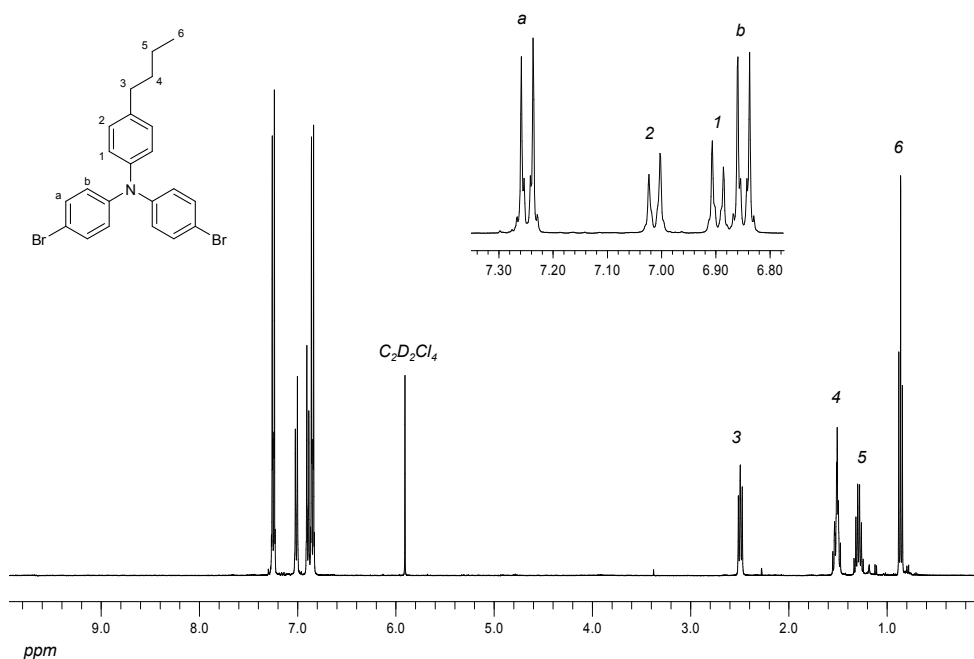


Figure 2.20: ^1H NMR of **TPA4** monomer in $\text{C}_2\text{D}_2\text{Cl}_4$.

In the ^1H NMR spectrum of **TPA4** in $\text{C}_2\text{D}_2\text{Cl}_4$ (Figure 2.20), the protons of the *n*-butyl side chain can be assigned to the four signals in the aliphatic region with a triplet at $\delta = 0.86$ ppm for (6), a sextet at $\delta = 1.29$ ppm for (5), a multiplet at $\delta = 1.51$ ppm for (4) and a triplet at $\delta = 2.50$ ppm for (3) with a common coupling constant $^3J = 7.5$ Hz. As for **TPA2**, the two signals for the protons (a) and (b), respectively at $\delta = 6.85$ and 7.25 ppm, present the typical coupling pattern. The proton (2) shows a clear through space coupling with (3) (^1H - ^1H NOESY spectra) and can be therefore associated with the doublet at $\delta = 7.01$ ppm ($^3J = 8.4$ Hz) in the ^1H NMR spectra. The remaining doublet at $\delta = 6.89$ ppm can finally be associated to the proton (1) coupling with (2) with a constant $^3J = 8.3$ Hz. Hereby, (2) is logically downfield shifted due to the inductive effect induced by *n*-butyl group. In the ^{13}C NMR spectrum (dept135), one primary and three secondary carbon atoms can be observed in the aliphatic region as well as four tertiary and four quaternary carbon atoms in the aromatic region, with a typical C-Br signal at $\delta = 115.1$ ppm. The molecular structure was also proved by the mass spectrometry with a molar peak at 459.6 g·mol $^{-1}$.

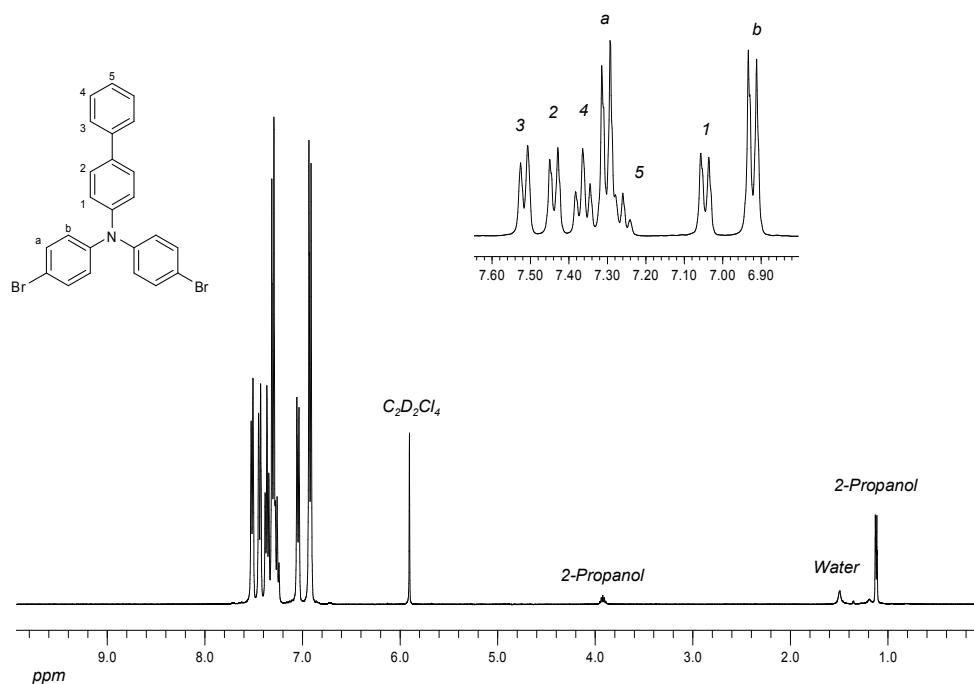


Figure 2.21: ^1H NMR of **TPA5** monomer in $\text{C}_2\text{D}_2\text{Cl}_4$.

As shown in Figure 2.21, every proton of the biphenyl side chain of the **TPA5** monomer can be attributed to a peak in the aromatic region of the ^1H NMR spectrum. The protons (1) and (2) can be associated to the two doublets respectively at $\delta = 7.04$ and 7.44 ppm, respectively through the common coupling constant $^3J = 8.4$ Hz and the clear ^1H - ^1H COSY coupling signal. The signal for the proton (2) is deshielded due to the steric effect induced by the neighboring phenyl group. The only doublet left at $\delta = 7.51$ ppm ($^3J = 7.5$ Hz) can then be assigned to the proton (3). The protons (4) and (5) can be attributed to the two triplets at $\delta = 7.36$ and 7.26 ppm respectively due to the common coupling constant $^3J = 7.5$ Hz and the two clear signals for the coupling of (4) with (3) and (5) in the ^1H - ^1H COSY spectrum. Finally, the molecular integrity was confirmed by mass spectrometry with a molar peak at $479.6 \text{ g}\cdot\text{mol}^{-1}$.

Other monomers leading to structurally modified PTPA polymers were also synthesized in this study (Figure 2.22). However, only **PTPA6** could be obtained in suitable yield. The polymers **PTPA7** and **PTPA8** could not be prepared in satisfactory yields. Therefore, only the monomer **TPA6** leading to **PTPA6** will be described.

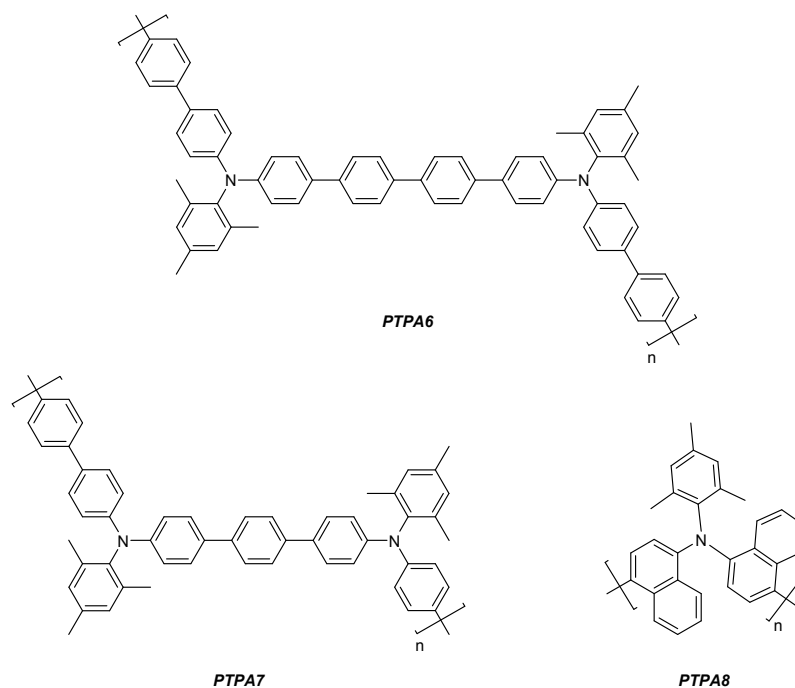


Figure 2.22: Polymers representing structural modification of PTPAs.

The monomer **TPA6** was synthesized according to the same Buchwald-Hartwig amination method introduced before. In this case, 4-bromo-4'-iodobiphenyl was used as aryl halide in order to directly afford the target monomer as depicted in Figure 2.23. This reaction yielded about 50 % of the **TPA6** monomer as pale yellow crystals after purification. As previously described, the structural integrity of **TPA6** was checked by NMR spectroscopy and mass spectrometry.

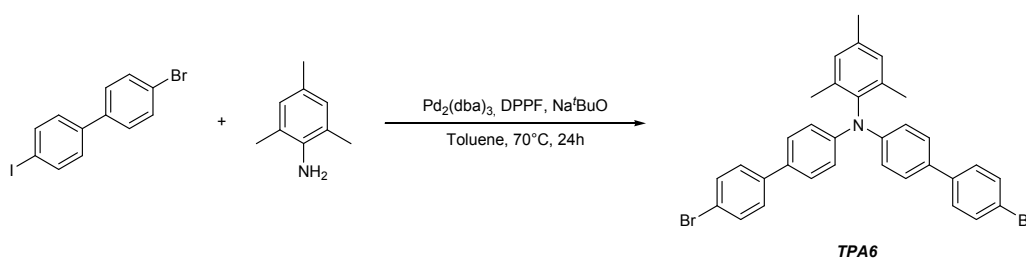


Figure 2.23: Synthesis of the functionalized monomer **TPA6**.

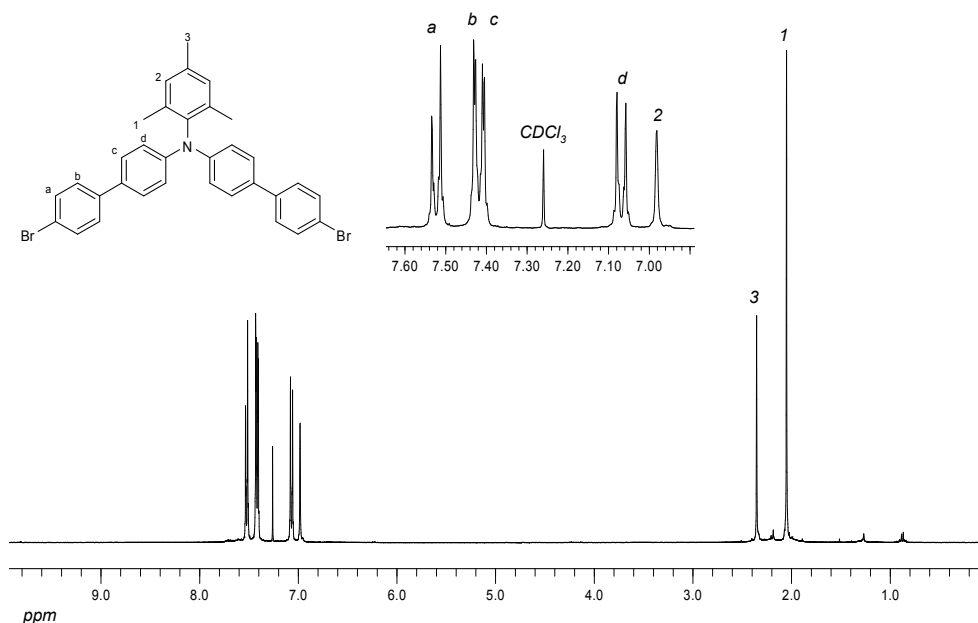


Figure 2.24: ^1H NMR of **TPA6** monomer in CDCl_3 .

In the aliphatic region of the ^1H NMR spectrum of **TPA6** in CDCl_3 (Figure 2.24) two singlets at $\delta = 2.05$ and 2.35 ppm can be respectively assigned to the protons of the methyl groups (1) and (3). In the aromatic region, the only singlet at $\delta = 6.98$ ppm can be logically attributed to the proton (2). The proton (d) can be identified by a clear coupling signal with (1) in the ^1H - ^1H NOESY spectrum and associated to the doublet at $\delta = 7.07$ ppm ($^3J = 8.7$ Hz) in the ^1H NMR spectrum. By ^1H - ^1H COSY NMR investigation, the protons (c) and (b) could be assigned to the multiplet at $\delta = 7.42$ ppm and the proton (a) to the doublet at $\delta = 7.52$ ppm ($^3J = 8.7$ Hz). Hereby, the doublet for (a) is downfielded due to the influence of the neighboring electronegative bromine atom. The structural integrity of **TPA6** was also confirmed by the mass spectrometry with a molar peak at $597.6 \text{ g}\cdot\text{mol}^{-1}$.

2.2.2. Polymer Synthesis

In this chapter, the synthetic methods involved in the generation of the TPA-based polymers (PTPAs) will be exposed. As for the precedent part, the metal-catalyzed aryl-aryl coupling reactions involved, from mechanism to the optimization of the reaction conditions, will be outlined as well as the characterization of the different PTPAs prepared.

2.2.2.1. Metal-Catalyzed Aryl-Aryl Coupling Reactions

Within the last twenty years, transition metal-catalyzed reactions have revolutionized the area of organic synthesis. Aryl-aryl coupling reactions are generally known as reactions

between an activated R-X compound (R = aryl, alkyl and X = Cl, Br, I, OTos, OTf) with an appropriate leaving group and a carbanion or carbanion equivalent counterpart under transition metal catalysis in order to form a new carbon-carbon bond. While halogen or triflate leaving groups are widely and most commonly used, the choice concerning the metal M of the carbanion equivalent is much more multiple.^[96] Popular examples utilize boron (Suzuki-Miyaura), tin (Stille), zinc (Negeshi), magnesium (Kumada-Tamao), silicon (Hiyama), lithium (Murahashi) or copper (Normand) organyls. A wide range of transition metals as catalysts for these reactions has been investigated but particular attention has been paid to palladium, copper and nickel complexes.^[97] The extensive research in the past decades have lead to an huge variety of reaction conditions and even to new types of coupling reactions as the heteroatom-carbon bond formation of which the Buchwald-Hartwig reaction as outlined before is a prominent example.^[83]

Nevertheless, common to all these reactions is their mechanism described as a catalytic cycle. The different steps have been widely and intensively investigated to achieve a broader and deeper understanding of these reactions and resulted in a lot of mechanistic details.

One of the very useful transition metal-mediated reactions is the nickel(0) mediated homo-coupling reaction according to Yamamoto, which undergoes a somewhat different reaction cycle. Semmelhack *et al.* were the first to observe the coupling of two aryl halides towards biaryls under use of stoichiometric amounts of (1,5-dicyclooctadiene)nickel(0) (Ni(COD)₂).^[98]



Figure 2.25: Coupling of aryl halides to biaryl according to Semmelhack *et al.*^[98]

Due to the mild reaction conditions, this reaction has been proposed as an alternative to the copper catalyzed Ullmann-type coupling reaction which requires very harsh conditions.^[73] During their studies toward conjugated polymers, the group of Yamamoto extended the scope of this coupling reaction to polymerization reactions by use of 2,2'-bipyridine (BPy) as a supporting ligand leading to increased yields at mild conditions.^[99] Detailed studies concerning the mechanism of this reaction (Figure 2.26) have been carried out by Semmelhack, Yamamoto and Knoch. After the ligand exchange between COD and BPy, the nickel(0) complex **A** undergoes an oxidative addition of the aryl halide under the formation of the nickel(II) aryl complex **B**. The use of BPy as ligand accelerates the reaction drastically as the bipyridine complex **A** undergoes the oxidative

addition much faster. Complex **B** disproportionates within the following step into complexes **C** and **D**. While the complex **C** leaves the reaction cycle, the aryl-aryl coupling product is liberated in a reductive elimination step of the complex **D**.

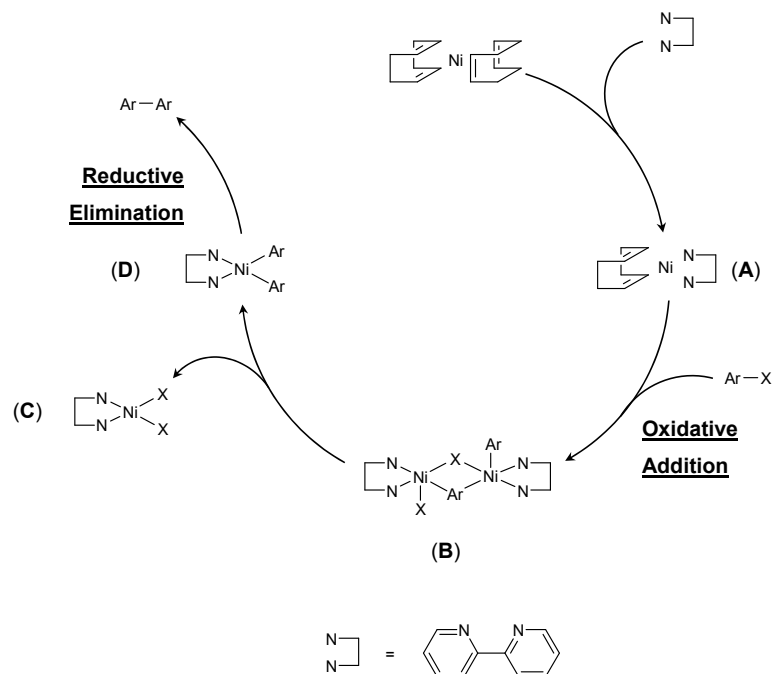


Figure 2.26: Mechanism of the aryl-aryl Yamamoto homo-coupling reaction.

Most Yamamoto-type coupling reactions carried out within this thesis are a variation of the initial synthetic protocol according to Pei and Yang.^[100] Furthermore, it should be noticed that a multitude of related, catalytic nickel(0) mediated reactions have been developed which utilize catalytic amounts of metal complexes together with reducing agents such as zinc, manganese^[101] or electrochemical support.^[102] However, applied to the herein presented monomers, lower yields and molecular weights are obtained.

2.2.2.2. Triphenylamine-Based Polymers

The general synthesis of the triphenylamine-based polymers (PTPAs) elaborated for this study is outlined in Figure 2.27. All the polymers were polymerized by aryl-aryl homo-coupling according to Yamamoto. These nickel-mediated polycondensation reactions were carried on with BPy as supporting ligand and the $\text{Ni}(\text{COD})_2$ catalyst in a toluene/DMF mixture at 70 °C for 3 days.

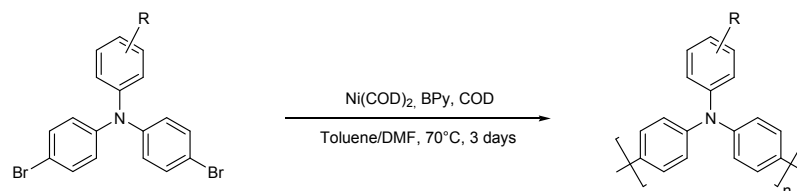


Figure 2.27: Polymerization reaction towards polytriphenylamine.

As for the functionalized monomers, a series of polymers with different substituents at the side chain aromatic group were generated as shown in Figure 2.28.

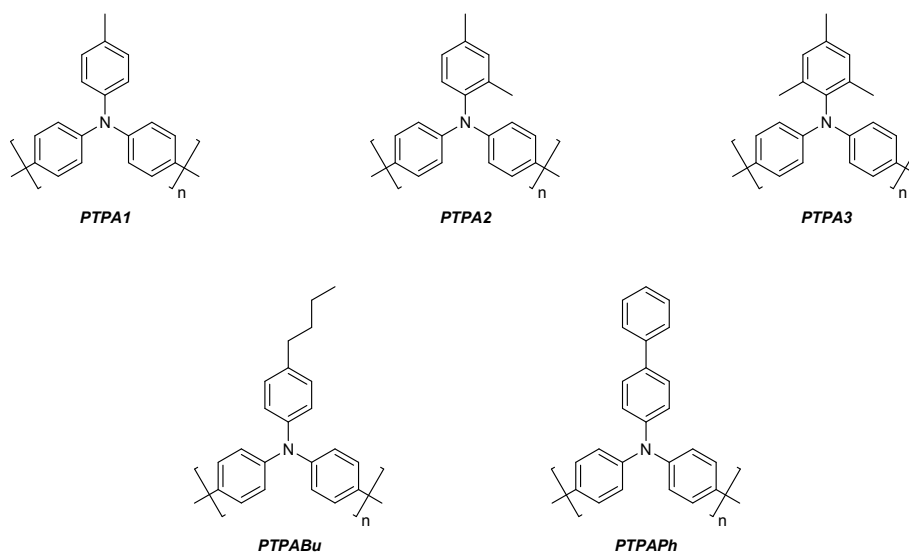


Figure 2.28: Triphenylamine-based polymers (PTPAs).

After polymerization and filtration the polymers were precipitated into a methanol/acetone/hydrochloric acid mixture in order to remove the remaining catalyst. The obtained greenish polymers were then stirred with hydrazine hydrate over eight hours in order to reduce radical cations build up during the purification process as shown in Figure 2.29.

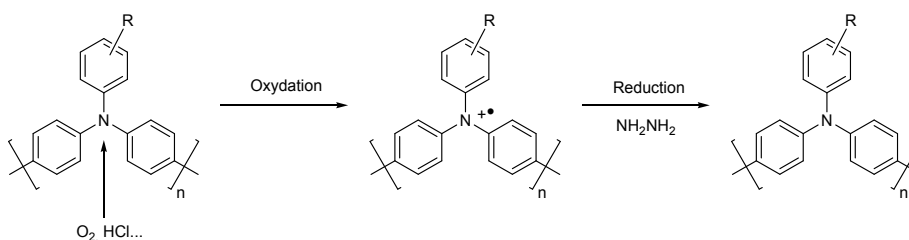


Figure 2.29: Formation and reduction of PTPA radical cations.

A polymeric compound comprising two more phenylene units in the backbone (Figure 2.30) was also synthesized according to a similar procedure.

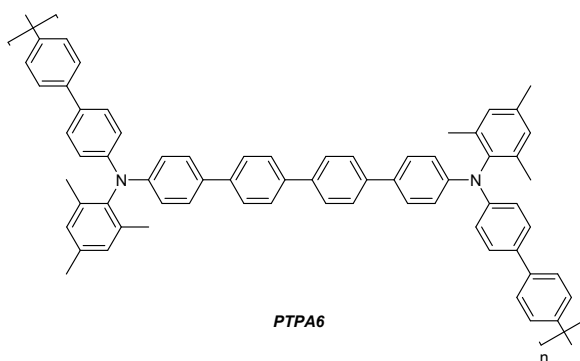


Figure 2.30: Triphenylamine-based polymer **PTPA6** with four interconnected phenylene units between two nitrogen atoms of the backbone.

The raw polymers obtained were then extracted with ethyl acetate over 24 hours and characterized by ^1H and ^{13}C NMR spectroscopy, DSC, GPC, as well as UV-Vis and fluorescence spectroscopy. The results of the NMR analysis are in accordance with the proposed structure (see Experimental Section). The DSC curves did not show any endo- or exothermic peak (e.g. crystallization or melting) and in most cases not even a glass transition proving thus that the polymers prepared are completely amorphous. Only the polymers **PTPA4** and **PTPA5** exhibited a slender glass transition around 140–150 °C.

The molecular weight afforded for the different polymers after extraction are resumed in the Table 2.1. The quite low molecular weight and high polydispersities for some of the polymers are noticeable. These kinds of problems are known for metal-mediated polycondensation reactions of electron-rich monomers.^[103] The substitution of the aromatic side group plays a determining role in the solubilization of the growing polymer chain in the reaction medium used and therefore in the possibility to achieve high molecular weights. Especially the 2,4,6-trimethylphenyl-substituted monomer **TPA3** allows the synthesis of high molecular weight **PTPA3**.

	PTPA1	PTPA2	PTPA3	PTPA4	PTPA5	PTPA6
M_n	2 500	4 600	37 600	8 700	3 200	11 200
M_w	5 100	16 600	68 700	21 400	4 700	19 100
PD	2.0	3.6	1.8	2.5	1.4	1.7

Table 2.1: GPC analysis of the PTPAs.

One other possibility to reduce the polydispersity of the polymers is the use of end-capping reagents like chloro- or bromobenzene during the polymerization reaction. It was asserted that the addition of monofunctional reagents in order to remove the unfavorable halogen atoms remaining as end-groups allows to afford much better semiconducting properties.^[104] However, our study showed that for the two polymers **PTPA1** and **PTPA2** such an end-capping strategy leads, despite a lower polydispersity, to poorer molecular weights and semiconducting properties. Therefore, the end-cap reagents were added at the end of the polymerization period in order to remove remaining bromine atoms. A proper polydispersity control of the polymers is possible by soxhlet extraction (solvent fractionation).

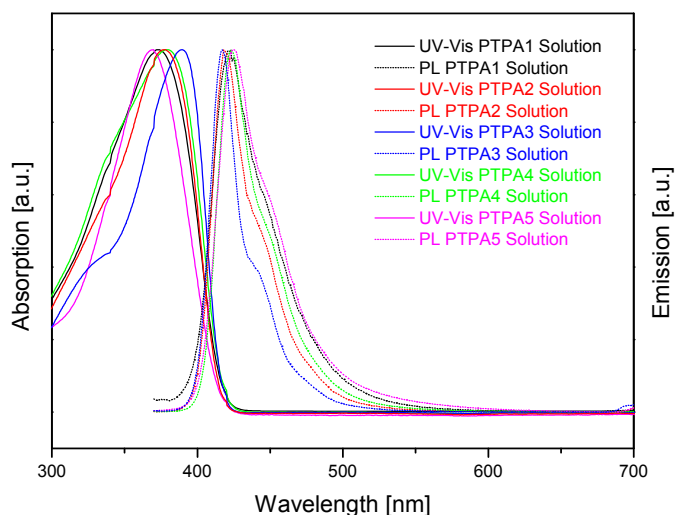
2.3. Material Characterization

2.3.1. Spectroscopic Investigation

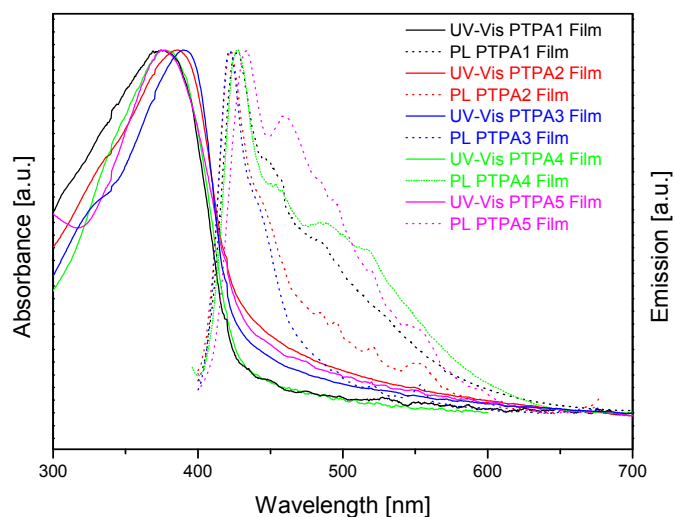
Different spectroscopic methods were used to characterize the PTPAs. Absorption and emission spectra were recorded by UV-Vis and photoluminescence (PL) spectroscopy, both in chloroform solution and in solid state (thin film). These studies allowed to investigate the influence of the side chains on the optical properties as well as the band-gap energies of the materials. On the other hand, the HOMO energy levels of the different polymers were determined by UV photoelectron spectroscopy (UPS).

2.3.1.1. UV-Vis and PL spectroscopic Investigation

The optical properties were investigated both in chloroform and in thin films. All polymers show unstructured UV-Vis spectra with broad absorption bands and almost identical absorption maxima (Figure 2.31).



a) UV-Vis and PL spectra for **PTPA1**, **PTPA2**, **PTPA3**, **PTPA4** and **PTPA5** in chloroform solution.



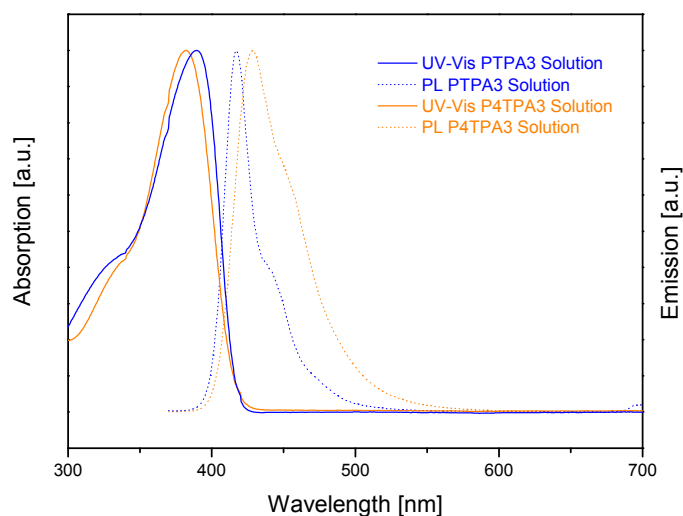
b) UV-Vis and PL spectra for **PTPA1**, **PTPA2**, **PTPA3**, **PTPA4** and **PTPA5** in solid state (thin films).

Figure 2.31: UV-Vis and PL spectra for **PTPA1**, **PTPA2**, **PTPA3**, **PTPA4** and **PTPA5** a) in solution and b) in solid state.

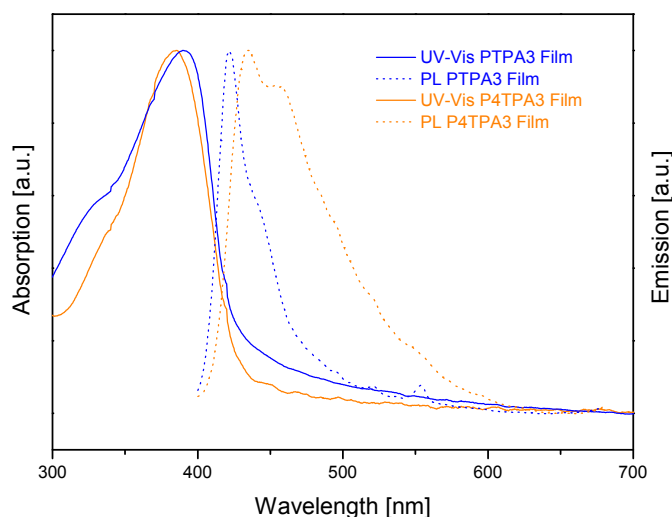
The influence of the substituents at the side chain aromatic group on the optical properties seems to be negligible in regard to shifts of the absorption maxima in solution as well as in the solid state (Table 2.2). The polymer **PTPA3** presents a slight red shift if compared to the other polymers probably related to the higher molecular weight than to any side group influence. It is interesting to notice that the absorption maxima for solutions and films are almost identical for each polymer. This can be explained by the fact that the polymers are completely amorphous and that no formation of ordered phases occurs, e.g. involving π - π

stacking. The polymers show a dark blue luminescence with very close emission maxima around 420 nm. The spectra in chloroform solution are narrow with the appearance of a lower energy shoulder. In the solid state, broader PL bands are observed especially for **PTPA4** and **PTPA5** where vibrational side band appears.

In the same way, increasing the number of phenylene groups between two main chain nitrogen atoms of the backbone (**PTPA3** → **PTAP6**) did not cause significant changes concerning the optical properties in solution. A slight bathochromic shift of 12 nm was observed for the PL maxima (Figure 2.32,a). As for **PTPA5**, a vibrational band at 454 nm appears in the solid state PL spectrum of **PTAP6** (Figure 2.32,b).



a) UV-Vis and PL spectra for **PTPA3** and **PTPA6** in chloroform solution.



b) UV-Vis and PL spectra for **PTPA3** and **PTPA6** in solid state.

Figure 2.32: UV-Vis and PL spectra for **PTPA3** and **PTPA6**, a) in solution and b) in solid state.

		PTPA1	PTPA2	PTPA3	PTPA4	PTPA5	PTPA6
Solution	Absorption [nm]	373	377	389	379	370	382
	Emission [nm]	423	418	417	423	425	429
Film	Absorption [nm]	375	385	390	378	378	385
	Emission [nm]	428	422	422	428	434, 460	435, 454

Table 2.2: Absorption and emission maxima for the PTPAs in solution and in solid state.

The optical band-gap energies of the PTPA materials were determined from the onset position of their absorption bands in the solid state by fitting a tangent to the UV curve with subsequent conversion of the intersection with the wavelength axis from nm to eV as depicted in Figure 2.33.

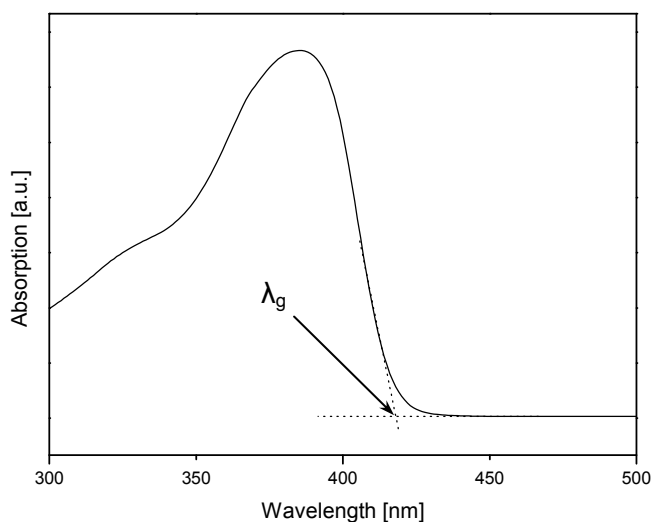


Figure 2.33: Determination of the band-gap from the UV-Vis spectra.

According to Louis de Broglie, the energy (in Joules) is directly related to the wavelength as:

$$\text{Eq. 2.1: } E (\text{J}) = \frac{hc}{\lambda}$$

Considering that $1 \text{ eV} = 1.602176487 \times 10^{-19} \text{ J}$, $h = 6.62606896 \times 10^{-34} \text{ J.s}$ the Plank constant and $c = 299792458 \text{ m.s}^{-1}$ the speed of light, the previous equation can be simplified as:

$$\text{Eq. 2.2: } E (\text{eV}) = \frac{1243.125}{\lambda (\text{nm})}$$

To afford the band-gap energy E_g , a correction of $\Delta E = 300 \text{ meV}$, corresponding to the exciton binding energy involved in the absorption process, must be done on the measured

optical band gap value. The equation for the determination of the band-gap energy by UV-Vis spectroscopy can be then written as follows:

$$\text{Eq. 2.3: } E_g \text{ (eV)} = \frac{1243.125}{\lambda_g \text{ (nm)}} + 0.3$$

It is noticeable that the band-gap energies for the different polymers are almost identical with values around 3.2 eV (Table 2.3). The band-gap energy for **PTPA6** appears very similar despite the presence of a more extended aromatic system between two main chain nitrogens.

	PTPA1	PTPA2	PTPA3	PTPA4	PTPA5	PTPA6
λ_g [nm]	426	433	427	428	439	428
Band Gap [eV]	3.22	3.17	3.21	3.20	3.13	3.20

Table 2.3: Optical band-gap energy E_g for the PTPAs.

2.3.1.2. UV Photoelectron Spectroscopy (UPS)

For this study, the HOMO levels of the different polymers were measured with help of an AC-2 surface analyzer from *Riken Keiki Co.* based on the UV photoelectron spectroscopy principle. UV photoelectron spectroscopy (UPS) or photoemission spectroscopy (PES) refers to the measurement of kinetic energy spectra of photoelectrons emitted by ultraviolet photons, to determine molecular energy levels in the valence region. This method based on the Einstein's photoelectric effect was originally developed for gas-phase molecules by David W. Turner, physical chemist at the Oxford University. The material (usually gases or liquids) to be analyzed is exposed to a beam of UV or X-UV light inducing photoelectric ionization of the sample atoms. The UV light penetrates several micrometers (1–3 μm) into the sample producing photoelectrons throughout the penetration depth of the X-rays.^[105]

The Riken AC-2 photoelectron spectrometer (Figure 2.34) presents the considerable advantage to allow measurements under ambient conditions (air and atmospheric pressure) when a high vacuum environment is needed for classical UPS measurements. This method is commonly presented as "photoelectron spectrometer in the atmosphere" or PESA. However, this spectrometer presents also other non-negligible advantages such as easy sample preparation (spin-coated polymer films on ITO substrates) and short measuring times, as well as the parallel identification of work function, ionization potential and density of states (DOS) for solids.

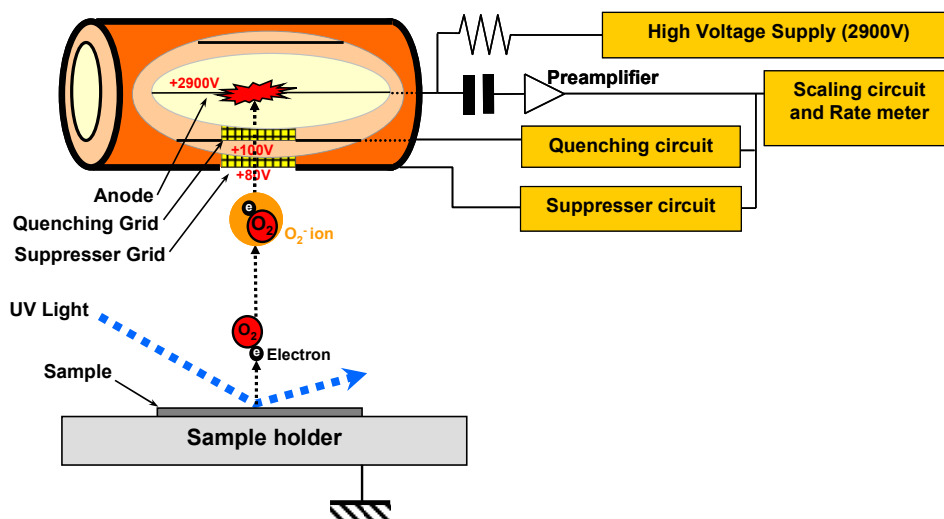


Figure 2.34: AC-2 Riken photoelectron spectrometer.

Here, the photoelectron signal is amplified by electron multiplication as a result of a so-called electron avalanche process or avalanche breakdown. In principle, the ultraviolet ray is applied to the sample and if the energy is sufficient, the photoelectron is discharged. The discharged photoelectrons in the atmosphere come then into contact with the oxygen molecule forming the O_2^- ionic species. These O_2^- ionic species are lead to the counter by the electric field produced by the suppresser grid, pass this grid and finally reach the anode neighborhood. At this stage, the electron avalanche occurs, the O_2^- ion acting as a trigger.

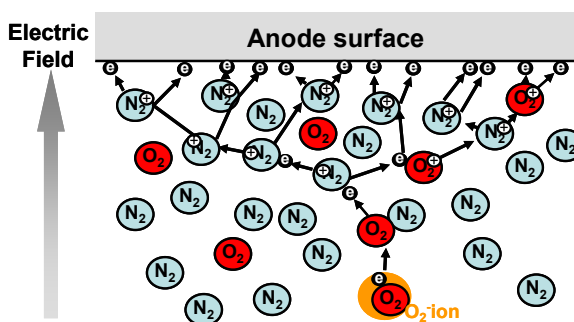
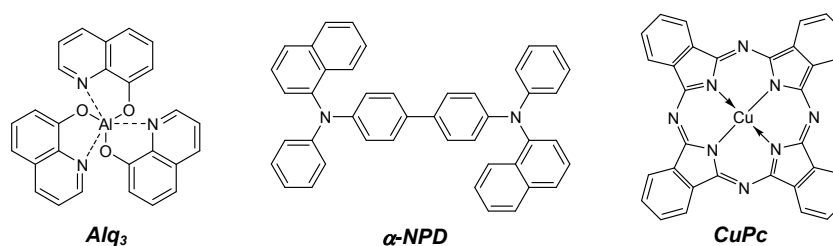


Figure 2.35: Electron avalanche process with air as a medium.

Due to the energy obtained from the high electric field between the grid and the anode, the O_2^- ion is separated into an electron and an oxygen molecule again. The free electrons in the medium (here the air) are subjected to strong acceleration by the electric field, ionizing the mediums' atoms by collision, thereby forming "new" electrons to undergo the same process in successive cycles as shown in Figure 2.35.

This kind of measurements proved to be very reliable for triphenylamine-based material as compared to UPS standard measurements as shown in Table 2.4.



	AC-2 [eV]	UPS [eV] ^[106]
Alq₃	5.84	5.8
α-NPD	5.50	5.4
CuPc	4.99	5.2
ITO	4.7	-

Table 2.4: Ionization potential or work function of some semiconducting materials (Source: *Riken Keiki Co., Ltd*).

It is clear that this kind of measurement is not suitable for materials which are highly sensitive to oxygen and moisture. For some metals or semiconducting materials, the work function or ionization potential measured are shifted as a result of the oxidation of the sample.

The HOMO levels measured for the different PTPA-type polymers are summarized in Table 2.5.

	PTPA1	PTPA2	PTPA3	PTPA4	PTPA5	PTPA6
<i>Band Gap [eV]</i>	3.22	3.17	3.21	3.20	3.13	3.20
<i>HOMO [eV]</i>	5.13	5.10	5.06	5.12	5.16	5.28

Table 2.5: Energetic structure of the PTPAs polymers.

All HOMO levels (ionization potentials) measured for PTPAs polymers are lower than 5 eV considered as an empirical energetic limit of the HOMO level for good stability against oxidation by oxygen (or air).

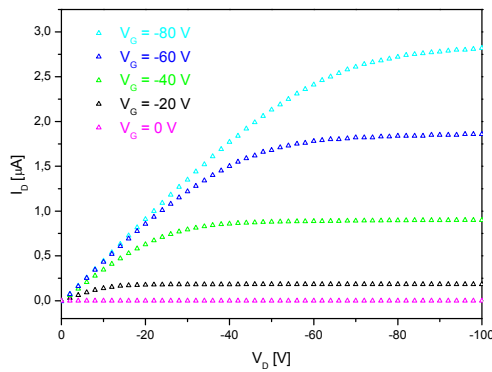
2.3.2. OFET Investigation

All polymers have been investigated as active layers in OFETs in cooperation with the *Evonik Degussa Creavis-S2B Nanotronics* (Marl, Germany) and the Prof. E.J.W. List (TU Graz, Austria). All measurements were done in the glove box on

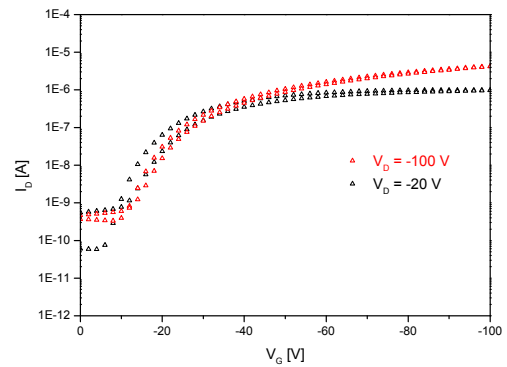
bottom-gate/bottom-contact configured OFETs devices. Highly *n*-doped silicon (Si) wafer pieces with a thermally grown SiO₂ dielectric layer have been used as substrates on which source and drain gold electrodes have been evaporated. All materials have been spin coated from chloroform solution onto the devices.

2.3.2.1. OFET Characteristics

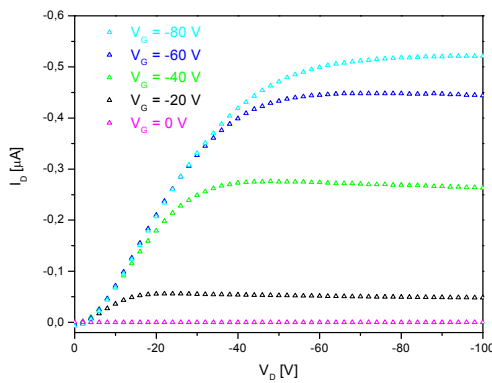
The OFET characteristics of the different triphenylamine-based polymers are shown in Figure 2.36 and the measured mobilities, on/off ratios and turn-on voltages in Table 2.6.



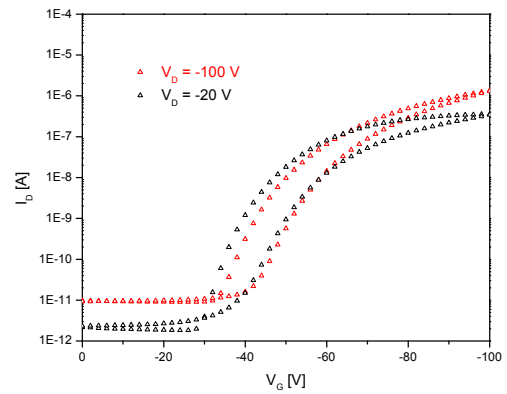
a) Output characteristics **PTPA1**.



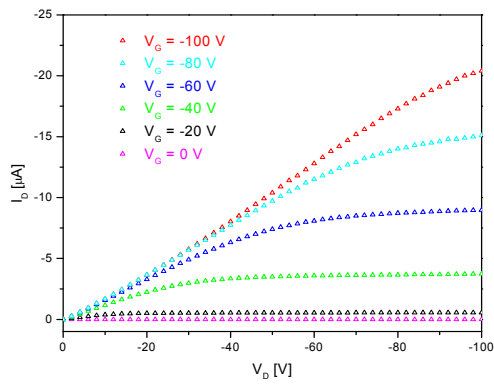
b) Transfer characteristics **PTPA1**.



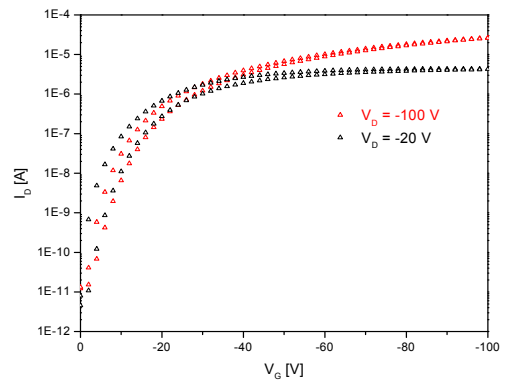
c) Output characteristics **PTPA2**.



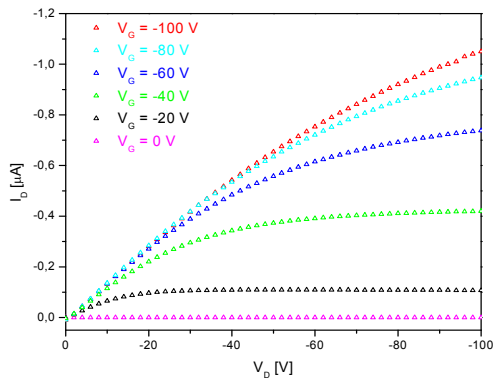
d) Transfer characteristics **PTPA2**.



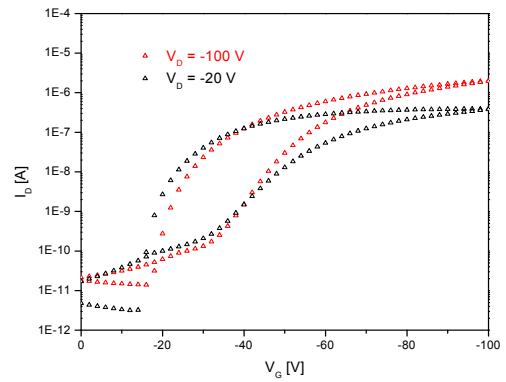
e) Output characteristics **PTPA3**.



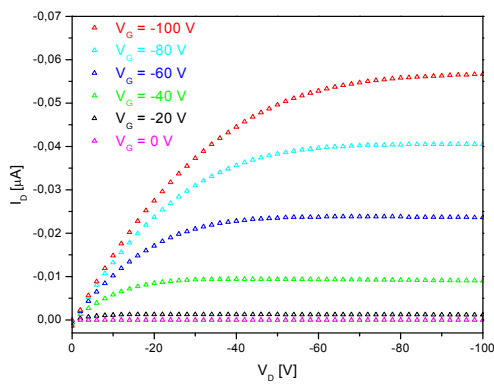
f) Transfer characteristics **PTPA3**.



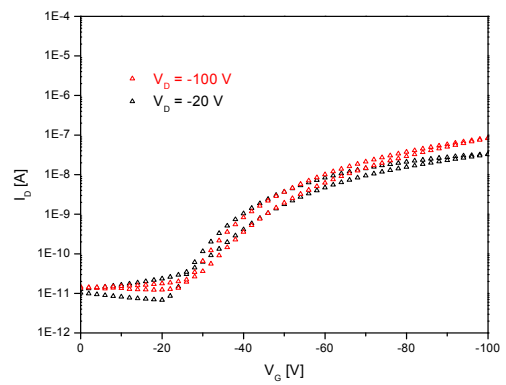
g) Output characteristics **PTPA4**.



h) Transfer characteristics **PTPA4**.



i) Output characteristics **PTPA5**.



j) Transfer characteristics **PTPA5**.

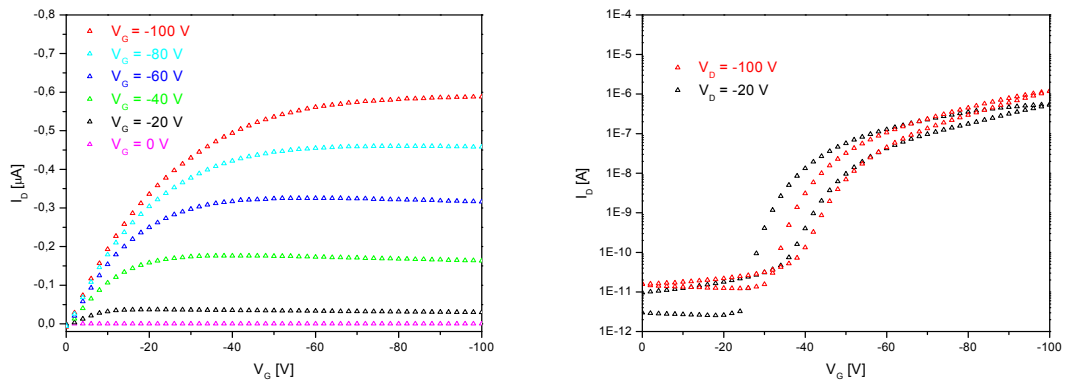
k) Output characteristics **PTPA6**.l) Transfer characteristics **PTPA6**.

Figure 2.36: Output and transfer characteristics for OFETs based on **PTPA1** (a, b), **PTPA2** (c, d), **PTPA3** (e, f), **PTPA4** (g, h), **PTPA5** (i, j) and **PTPA6** (k, l) in bottom-gate/bottom-contact configuration measured in argon under ambient light.

The mobilities of the different polymers were measured from the saturation regime of the output characteristics for high gate voltages ($V_G = -100$ V) and the on/off ratios from the transfer characteristics for high drain voltages ($V_D = -100$ V).

	PTPA1	PTPA2	PTPA3	PTPA4	PTPA5	PTPA6
Mobility [$\text{cm}^2\text{V}^{-1}\text{s}^{-1}$]	5×10^{-4}	1×10^{-4}	9×10^{-4}	1×10^{-4}	1×10^{-5}	1×10^{-4}
On/Off Ratio	10^4	10^4	10^5	10^4	10^4	10^5
Turn-on Voltage [V]	-10	-30	-1	-20	-20	-30

Table 2.6: Mobility and on/off ratio for the triphenylamine-based polymers.

All PTPA based devices investigated showed a typical field-effect transistor behavior with clear saturation regime on the output characteristics for small as for high gate voltages V_G . Of all the OFETs scanned, the one based on **PTPA3** presents the best characteristics with high mobility ($\mu_{\text{FET}} = 9 \times 10^{-4} \text{ cm}^2 \cdot \text{V}^{-1} \cdot \text{s}^{-1}$) and on/off ratio (10^6), as well as small turn-on voltage ($V_{\text{on}} > -1$ V) and hysteresis of the transfer characteristic.

Moderate ($V_{\text{on}} = -10$ V for **PTPA1**, $V_{\text{on}} = -20$ V for **PTPA4** and **PTPA5**) until high ($V_{\text{on}} = -30$ V for **PTPA2** and **PTPA6**) turn-on voltages appear for all other devices. The OFET based on **PTPA4** also exhibits a rather large hysteresis in the transfer characteristics proving the presence of impurities probably due to a previous partial oxidation of the material. On the other hand, devices based on **PTPA1**, **PTPA2**, **PTPA5** and **PTPA6** display slender hysteresis.

Concerning the mobility, **PTPA1** appears to be the best one after **PTPA3** ($\mu_{FET} = 5 \times 10^{-4} \text{ cm}^2 \cdot \text{V}^{-1} \cdot \text{s}^{-1}$) despite a slender on/off ratio around 10^4 . As expected from the OFET characteristics, **PTPA2** and **PTPA4** showed only moderate mobilities ($\mu_{FET} = 1 \times 10^{-4} \text{ cm}^2 \cdot \text{V}^{-1} \cdot \text{s}^{-1}$) with on/off ratios around 10^4 .

PTPA5 and **PTPA6** can be considered as exceptions because of their poor solubility in common solvent. Under these two polymers, no homogenous films could be obtained for device applications. In these conditions **PTPA5** revealed a rather good OFET behavior with a good saturation regime, a poor hysteresis and a fair turn-on voltage but low mobility ($\mu_{FET} = 1 \times 10^{-5} \text{ cm}^2 \cdot \text{V}^{-1} \cdot \text{s}^{-1}$) and on/off ratio (10^4). On the contrary, despite of a weak FET behavior with high turn-on voltage and hysteresis, **PTPA6** revealed better mobility ($\mu_{FET} = 1 \times 10^{-4} \text{ cm}^2 \cdot \text{V}^{-1} \cdot \text{s}^{-1}$) and good on/off ratio (10^5).

2.3.2.2. Molar Mass-OFET Characteristics Relationship

As already described in the case of poly-3-hexylthiophene, the molecular weight of the polymers can have a significant influence on the OFET characteristics.^[107] For such experiments, several polymeric fraction of **P3HT** with increasing molecular weight have been investigated. It allowed to determine that mobility of the **P3HT**-based devices with increased molecular weight of the polymer fractions used as semiconducting layer (as shown in Table 2.7).

P3HT Fractions	M_n [$\text{g} \cdot \text{mol}^{-1}$]	M_w [$\text{g} \cdot \text{mol}^{-1}$]	PD ^[a]	DP ^[b]	Mobility [$\text{cm}^2 \cdot \text{V}^{-1} \cdot \text{s}^{-1}$]	On/Off Ratio
1	1.9×10^4	2.6×10^4	1.35	114	2.6×10^{-3}	3.8×10^4
					4.2×10^{-3} ^[c]	8×10^5 ^[c]
2	1.4×10^4	2.0×10^4	1.48	83	1.3×10^{-3}	1.9×10^4
					4.7×10^{-4} ^[c]	8.1×10^3 ^[c]
3	5.6×10^3	6.6×10^3	1.18	33	1.6×10^{-5}	270
					4.3×10^{-5} ^[c]	1.1×10^3 ^[c]
4	2.2×10^3	3.1×10^3	1.43	13	5.5×10^{-7}	12
					2.5×10^{-6} ^[c]	35 ^[c]

[a] Polydispersity; [b] Degree of Polymerisation; [c] Annealed at 150°C for 5 min

Table 2.7: Relationship between the molecular weight of the **P3HT** polymers and their OFET characteristics (mobility in saturation regime and on/off ratio).^[107]

Similar investigation have been conducted for the PTPAs: the raw polymer was extracted with different solvents (ethyl acetate, dichloromethane then chloroform) in order to become fractions of increasing molecular weight. The results are summarized for **PTPA3** in Table 2.8. Similar results have been observed for the other PTPAs but will not be outlined here.

PTPA3 Fractions	M_n [$g \cdot mol^{-1}$]	M_w [$g \cdot mol^{-1}$]	PD ^[a]	DP ^[b]	Mobility [$cm^2 \cdot V^{-1} \cdot s^{-1}$]	On/Off Ratio
1	3.7×10^4	6.4×10^4	1.7	157	9×10^{-4}	1×10^6
2	5.2×10^3	1.9×10^4	3.6	18	2×10^{-4}	3×10^5
3	650	900	1.4	2-3	5×10^{-5}	1×10^5

[a] Polydispersity; [b] Degree of Polymerisation

Table 2.8: Relationship between the molecular weight of the **PTPA3** polymers and their OFET characteristics (mobility in saturation regime and on/off ratio).

As for the **P3HT**, the fractions with the higher molecular weight provide better OFET properties in the devices. On the transfer characteristics linear and semilogarithmic plots, this tendency is also visible (Figure 2.37). However, the tendency is much weaker for the amorphous **PTPA3** in relation to the semicrystalline **P3HT**.

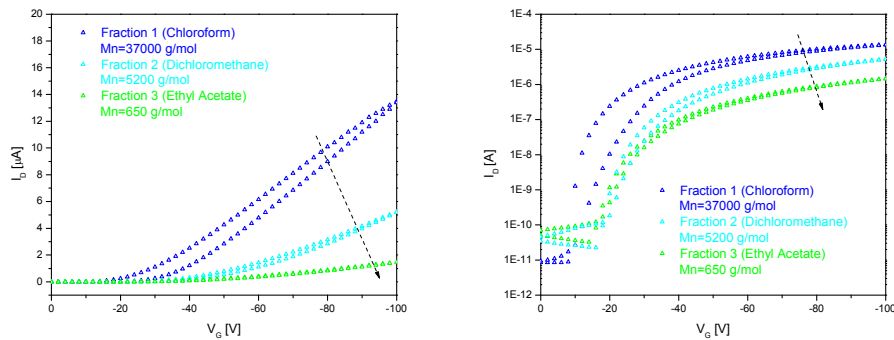


Figure 2.37: Transfer characteristics of the different **PTPA3** fractions with increasing molecular weights in linear and semilogarithmic plots.

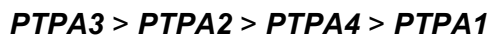
2.3.2.3. Stability Investigation

The OFET characteristics of the different triphenylamine-based polymers has been further investigated in the group of Prof. E.J.W. List in the *University of Technology Graz*, Austria. Time dependant transfer characteristic measurements have been done for **PTPA1**, **PTPA2**, **PTPA3** and **PTPA4** under ambient conditions after five minutes, ten minutes and every ten minutes until one hour exposition.

For all polymers, a shift of the onset voltage of the device under operation could be observed. This could be explained by an increasing amount of traps in the semiconducting materials during the measurements. However, this shift, related to the amount of traps involved, is different for different polymers. The shift of the onset voltage increases in the series:

$$\mathbf{PTPA1} > \mathbf{PTPA4} > \mathbf{PTPA2} > \mathbf{PTPA3}$$

indicating decreasing stabilities of the PTPAs under OFET operation:



The charge carriers in triphenylamine-based materials are radical cations formed by the injection of holes through the anode. Nevertheless, radical cations are also formed due to chemical oxidation, in our case by oxygen of the atmosphere, and act as traps for the mobile charges. Regarding the molecular structures of the polymers, the difference in the stability of the different polymers could be explained by a shielding effect of the *ortho*-substituents. This assumption needs further investigation such as EPR measurement of the polymers in operation. Another possibility could be the use of larger, more bulk substituents such as *tert*-butyl or *iso*-propyl to verify this hypothesis. However, the corresponding monomers could, until now, not be synthesized according to the Buchwald-Hartwig or Ullmann-type amination reaction as depicted in Figure 2.38.

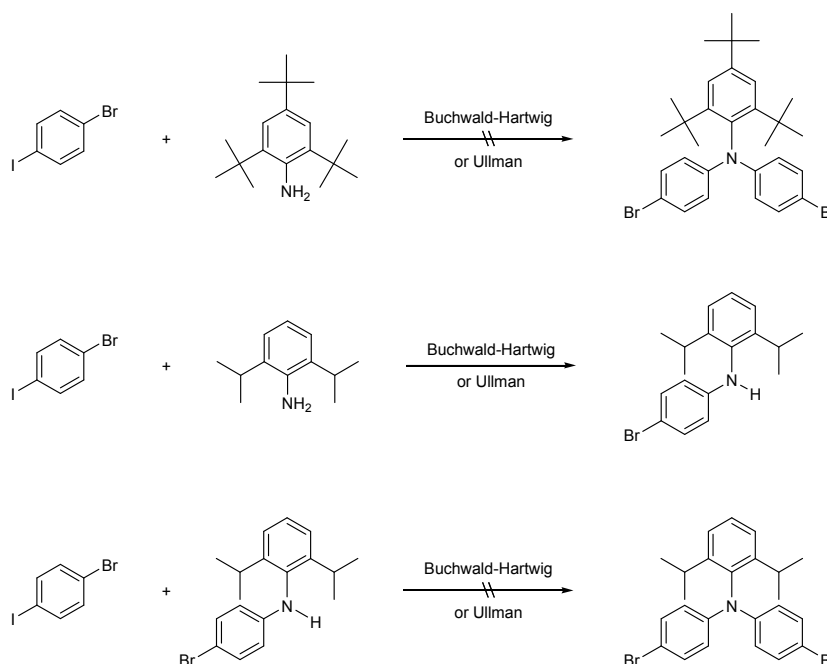
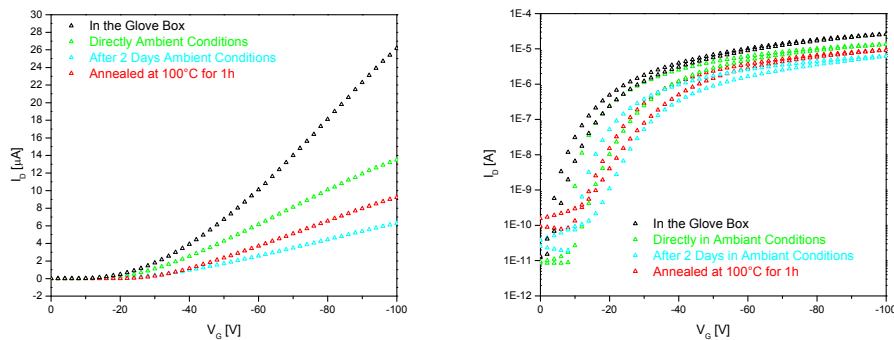


Figure 2.38: Synthesis of monomeric compounds with bigger substituent groups, a) *tert*-butyl and b) *iso*-propyl.

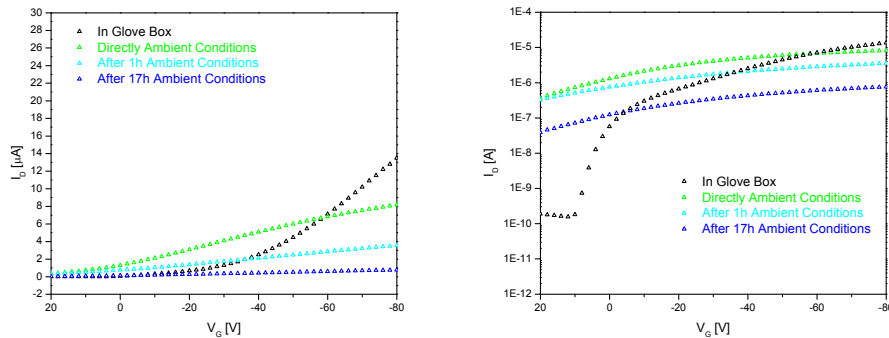
In the case of *tert*-butyl groups in 2,4,6-positions of the side chain aromatic groups, no TPA-product could be found. For *iso*-propyl groups in 2,6-positions, only the monosubstituted product could be isolated. Further arylation of the monosubstituted compound through Buchwald-Hartwig or Ullmann-type reactions did not provide any

monomer either well. This can be explained by the steric hindrance of the *tert*-butyl or, in a slender way, *iso*-propyl groups.

PTPA3 being the polymer with the best OFET characteristics and highest stability was used in further stability tests. Changes of the OFET characteristics after exposure to ambient conditions have been recorded and compared to poly(3-hexylthiophene)-based devices under similar conditions. **P3HT** represents one of the most widely used polymers for OFET applications, regarding to its very good properties, but shows a very poor OFET stability against oxygen (and air).



a) Transfer characteristics of **PTPA3** in linear and semilogarithmic plots under argon atmosphere (black curve), under ambient conditions directly after storage in the glove box (green curve), 2 days storage under ambient conditions (light blue curve) and after one hour annealation at 100 °C (red curve).



b) Transfer characteristics of **P3HT** in linear and semilogarithmic plots under argon atmosphere (black curve), under ambient conditions directly after storage in the glove box (green curve), after 1 hour (light blue curve) and 17 hours exposure (blue curve).

Figure 2.39: Evolution of the transfer characteristics of a) **PTPA3** and b) **P3HT** under exposure to ambient conditions.

The transfer characteristics of both polymers display similar OFET properties under inert atmosphere (Figure 2.39,b, black curves) such as good mobility ($\mu_{FET} \approx 10^{-3} \text{ cm}^2 \cdot \text{V}^{-1} \cdot \text{s}^{-1}$)

and good saturation of the source-to-drain current I_D even if **PTPA3** shows a higher saturation source-to-drain current $I_{D,sat}$. Nevertheless, both polymers show very different behavior after their exposure to an oxidative atmosphere (Figure 2.39,b, green curves). The **PTPA3**-based device exhibits a similar mobility as under glove box conditions and always a good field-effect behavior with a clear saturation regime even if shifted to a smaller saturation source-to-drain current $I_{D,sat}$. On the other hand, the mobility of the **P3HT**-based device decreases dramatically and a very poor field-effect behavior can be observed. Even after two days exposure to air, the **PTPA3**-based device shows a satisfying field-effect behavior with good saturation of the source-to-drain current I_D on the transfer characteristics plots and a mobility $\mu_{FET} = 4 \times 10^{-4} \text{ cm}^2 \cdot \text{V}^{-1} \cdot \text{s}^{-1}$ while **P3HT** does not show any significant field-effect behavior already after one hour storage (Figure 2.39,b, light blue curves). It is interesting to notice that, after annealing to 100 °C for one hour, the **PTPA3**-based device recovers its best mobility ($\mu_{FET} = 9 \times 10^{-4} \text{ cm}^2 \cdot \text{V}^{-1} \cdot \text{s}^{-1}$) under glove-box conditions (Figure 2.39,a, red curves). It can be then concluded that the deterioration of the OFET characteristics of the **PTPA3**-based device is based on fully reversible processes (e.g. aging). The traps formed under ambient conditions can be destroyed by thermal annealing. The results summarized here are in accordance with those of other similar studies.^[108]

2.4. Conclusion

A series of triphenylamine-based polymers have been synthesized and characterized. It has been determined that the side chains have no significant influence on the intrinsic optical and electronic properties but on the processability of the materials. Increasing the number of phenylene groups between two nitrogen atoms of the main chain did not lead to significant decrease of the band-gap energy. Despite a somewhat better stability against air, such a modification induced a dramatic decrease of the processability and the device performance.

A relation between the molecular weight of the PTPA-polymers and the OFET performances could also be deduced by investigating polymer fractions of increasing molecular weight. As for **P3HT**, it was established that the polymer fractions with the highest molecular weight provide the best OFET performances.

Of the polymers studied, **PTPA3**-based devices showed the best field-effect characteristics with a mobility μ_{FET} of approx. $10^{-3} \text{ cm}^2 \cdot \text{V}^{-1} \cdot \text{s}^{-1}$, an on/off ratio up to 10^6 , a turn-on voltage V_{to} above -1 V and almost no hysteresis as well as the best stability under operation. In comparison to the widely used **P3HT**, **PTPA3**-based devices exhibit a far

better stability against air and moisture. All the results presented here are in accordance with a study published by Hübler *et al.* for all-printed PTPA-based transistors.^[108]

This stability was assumed to be a consequence of a shielding effect towards induced by the *ortho*-substituent of the side chain phenyl the nitrogen atom. Initial experiments towards an enhancement of the shielding effect by increasing the size of the *ortho*-substituents (e.g. from methyl group to *iso*-propyl or *tert*-butyl) were carried on. Unfortunately, the monomeric compound could not be isolated in Buchwald-Hartwig or Ullmann amination reactions most probably due to the high steric hindrance at the nitrogen center.

3. Carbazole-Based Materials

3.1. Polycarbazoles

Hole-transporting materials based on the carbazole moiety have been subject of an increasing number of investigations over the last decade. This could be explained by the very interesting features such as low cost of the starting material (*9H*-carbazole), good chemical and environmental stability provided by the fully aromatic unit, easy substitution of the nitrogen atom with a wide range of functional groups permitting a better solubility and a fine tuning of the electronic and optical properties. Moreover, as shown in Figure 3.1, carbazole units can be linked at the 3- and 6-positions to afford poly(3,6-carbazole)s as well as the 2- and 7-positions to afford poly(2,7-carbazole)s. This two isomers exhibit different properties and potential applications.^[109]

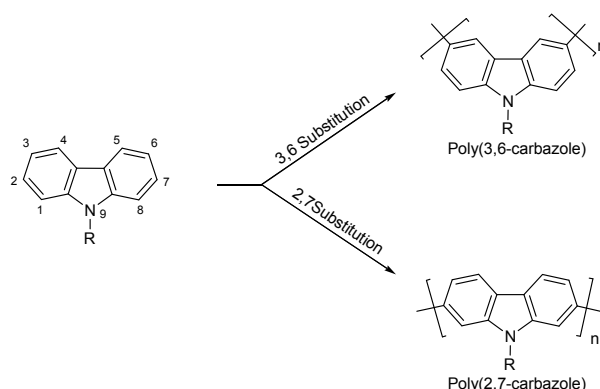


Figure 3.1: Possible substitutions of the carbazole unit: a) poly(3,6-carbazole) and b) poly(2,7-carbazole).

A lot of side chain polymers with pendant carbazolyl groups such as poly(*N*-vinylcarbazole) (PVK) have also been investigated over the last few years.^[110] These materials found applications in the xerographic process, e.g. of photocopy machines or laser printers but will not be described here in detail.

The aromatic backbone of covalently connected carbazole moieties is expected to improve the mobility of the charge carriers (holes), in this case radical cations and dicationic species formed upon oxidation (*p*-doping). The first soluble main-chain oligomers (mainly dimers) based on carbazole units have been synthesized by electrochemical oxidation.^[111] These oligomers were composed of *N*-substituted carbazoles linked in their 3,6-positions (Figure 3.2) or coupled via the 9-positions (nitrogen) of unsubstituted carbazole monomers. Generally, it was found out that the 3-, 6- and 9-positions are the most reactive ones.

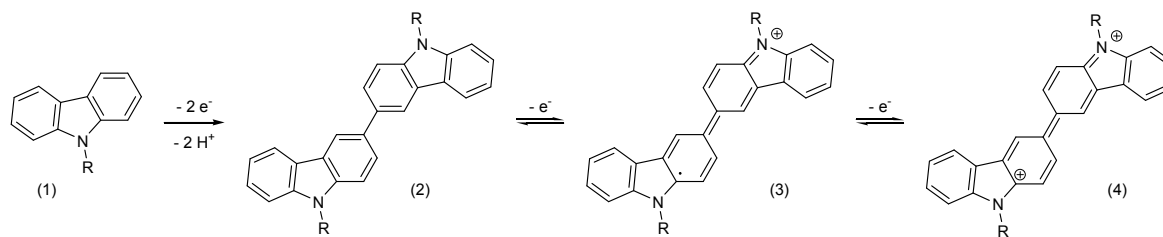


Figure 3.2: Electrochemical oxidation of *N*-alkylcarbazoles (1) into 3,3'-bicarbazyl (2), and further oxidation of (2) into bicarbazylum radical-cation (3) and dication (4).

Due to the high stability of the oxidized states (bicarbazylum cations), only dimers were obtained by electrochemical oxidation of *N*-substituted carbazole units. In 1997, Marrec *et al.* described carbazole-based polymers synthesized by electrochemical polymerization starting from *N,N'*-substituted carbazole dimers. The obtained polymers showed a redox characteristics similar to bicarbazyls (Figure 3.3).^[112]

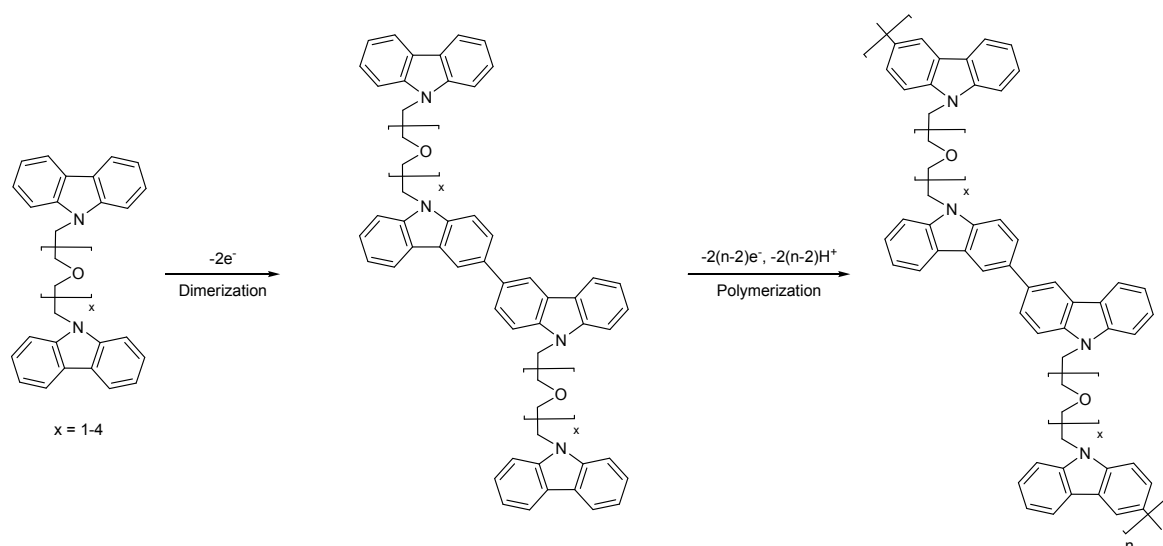


Figure 3.3: Electrochemical polymerization of *N,N'*-substituted carbazole dimers according to Marrec *et al.*^[112]

In the case of a chemical oxidation of *N*-substituted carbazoles with iron(III) trichloride ($FeCl_3$), the resulting product is the 3,3'-bicarbazyl dimer. Obviously, this reaction is often used to produce 3,3'-bicarbazyl dimers (Figure 3.4).^[113]

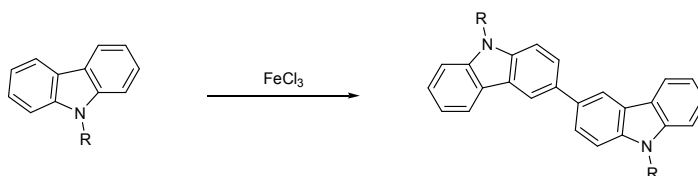


Figure 3.4: Chemical oxidation of *N*-substituted carbazoles with iron(III) trichloride.

Finally, in both cases (electrochemical and chemical oxidation), the stabilization of the oxidized states (bicarbazylum cations), due to the delocalization of the positive charges through the extended π -conjugated system between the two nitrogen atoms, hinders any follow-up coupling reaction and thus polymerization. Siove *et al.* showed that oxidation polymerization by FeCl_3 is possible in the case of sterically hindered carbazole derivatives (e.g. 1,4,5,8,9-pentamethylcarbazole, Figure 3.5). The twisting of the dimeric unit due to the steric hindrance leads to a reduced conjugation between two consecutive carbazole units (non-planar dimers) and then a destabilization of the oxidized 3,3'-bicarbazyls dimer.^[114]

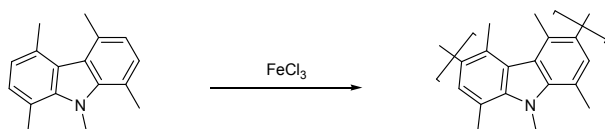


Figure 3.5: Chemical (oxidative) polymerization of 1,4,5,8,9-pentamethylcarbazole according to Siove *et al.*^[114]

Concurrently to the polymerization routes presented previously, the reductive polymerization of 3,6-dihalocarbazoles have been developed for the preparation of poly(3,6-carbazole)s (Figure 3.6). These include electrochemical,^[115] Grignard,^[116] and palladium- or nickel-catalyzed coupling reactions.^[117] All these methods lead to more or less soluble polymers with a molecular weight around $10^4 \text{ g}\cdot\text{mol}^{-1}$, depending on the side chain substitution at the nitrogen atom.

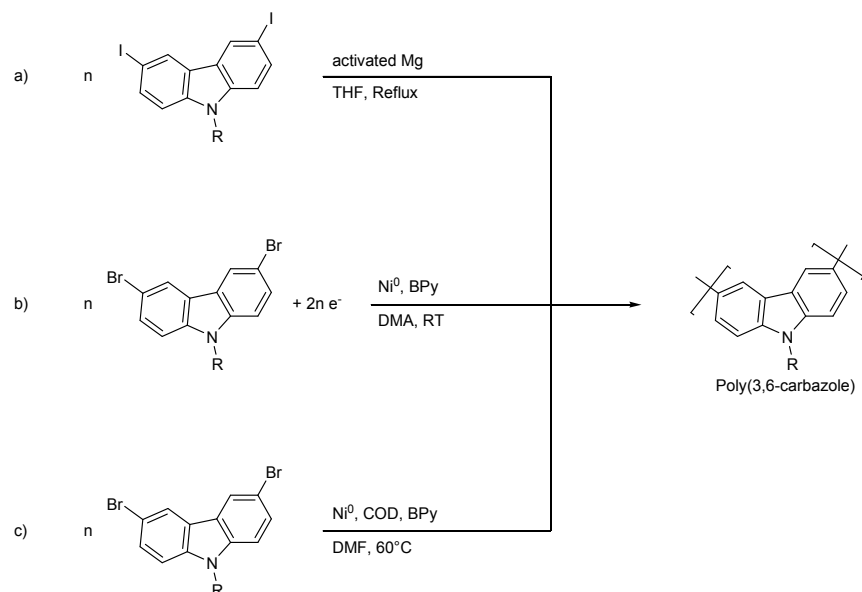


Figure 3.6: Syntheses of poly(3,6-carbazole)s by a) Grignard, b) electroreductive and c) Yamamoto-type coupling reactions.

In 2002, Zhang *et al.* obtained the first high molecular weight poly(*N*-alkyl-3,6-carbazole) ($M_w > 10^5 \text{ g}\cdot\text{mol}^{-1}$) by applying a reverse order during addition of the reagents (nickel catalyst added into the monomer solution) in a coupling procedure according to Yamamoto.^[118]

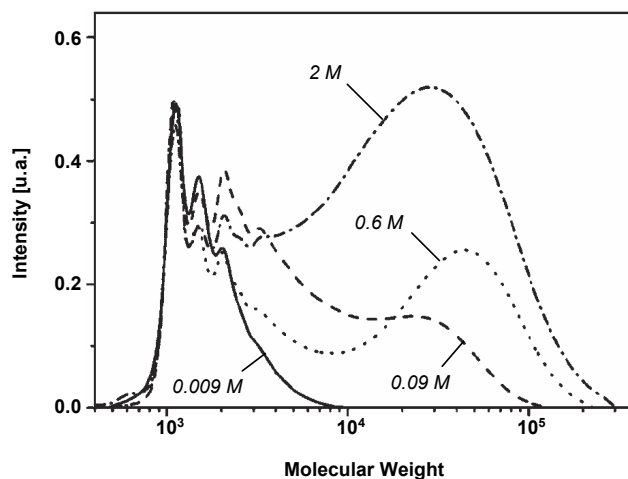


Figure 3.7: GPC curves of poly(*N*-alkyl-3,6-carbazole)s obtained from polymerizations with different monomer concentration.^[119]

Ostrauskaite *et al.* also discovered that, the molecular weight of poly(*N*-alkyl-3,6-carbazole)s under Yamamoto standard conditions strongly depends on

the monomer concentration during the polymerization reaction (Figure 3.7). According to a MALDI-TOF mass spectrometry investigation and analysis of the isotope distribution (for linear and cyclic species) in the MALDI spectrum, the formation of cyclic oligomers (4 to 12 carbazole units) could be illustrated and assessed as the limiting factor for the molecular weight.^[119]

Beside via the 3- and 6-positions, the carbazole units can also be linked in the 2- and 7-positions to afford poly(2,7-carbazole)s (Figure 3.1). Such fully π -conjugated materials are of interest for optoelectronic applications because of the extended conjugation induced by the linkage in 2,7-positions.^[120] These polymers were tested as light emitting layer in blue, polymer light emitting diodes (PLEDs) and as donor material in solar cells.^[121] However, the synthesis of 2,7-carbazole-based materials is much more complicated as compared to 3,6-carbazole-based materials. The 2,7-positions are located in *meta*-position relative to the amino group, not allowing any direct functionalisation by standard electrophilic, aromatic substitutions. On that account, several strategies starting from biphenyl precursors have been developed to produce 2,7-carbazolebased monomers as depicted in Figure 3.8.^[122]

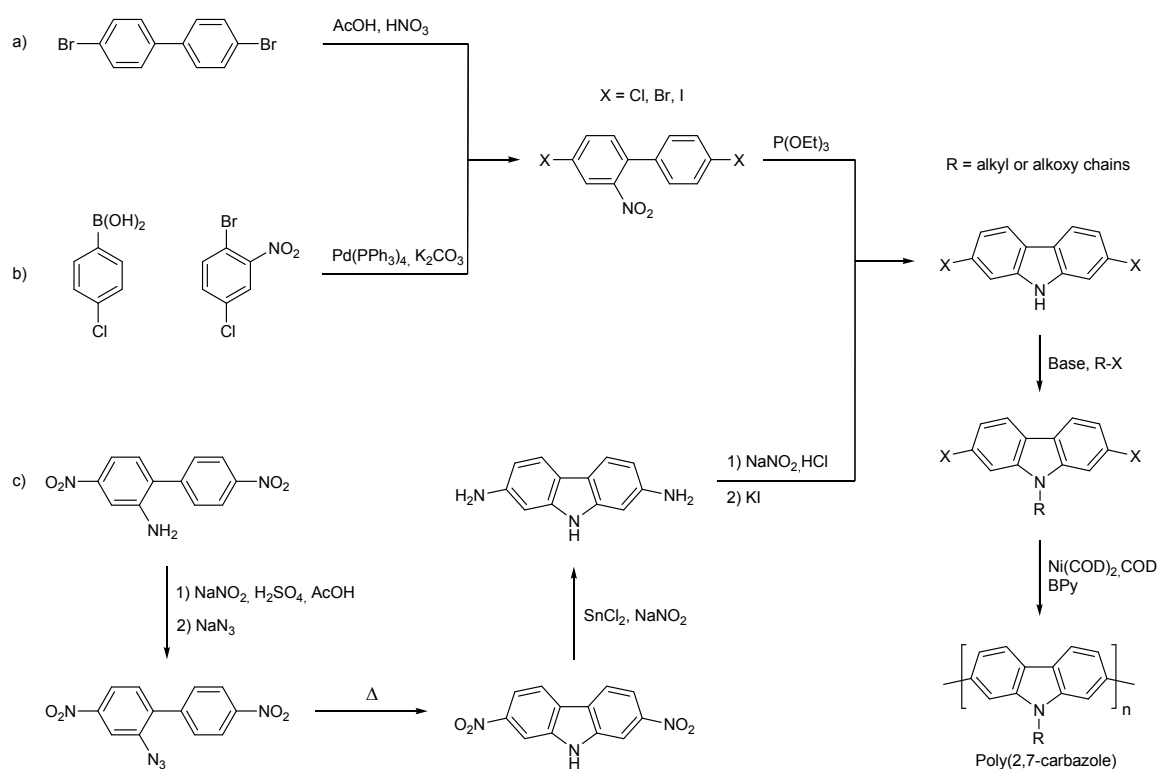


Figure 3.8: Possible synthetic routes for poly(2,7-carbazole).^[109]

More complex carbazole derivatives such as indolocarbazole^[123] or ladder-type carbazole^[124] (Figure 3.9) have been generated and tested for OFET or PLED applications, but will not be further discussed here.

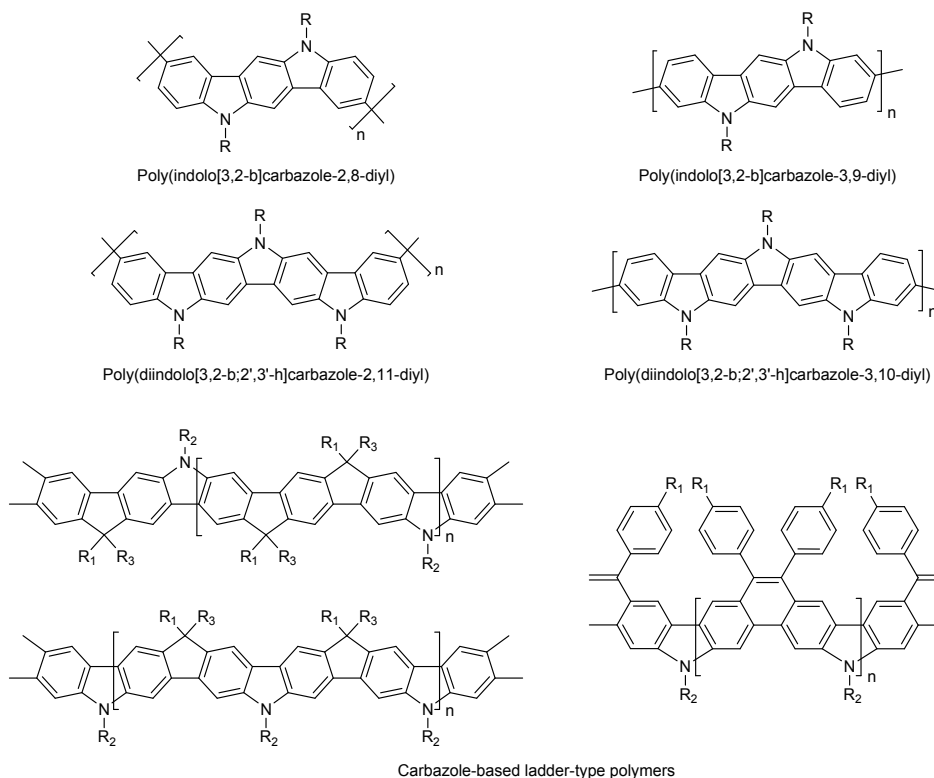


Figure 3.9: Poly(indolocarbazole)s and carbazole-based ladder-type polymers.

3.2. Poly(*N*-phenylcarbazole)s

In this work, we have focused on a special carbazole containing polymers: poly(*N*-phenylcarbazole-3,6-diyl)s. In these derivatives, the nitrogen atom is substituted with an aromatic group. The molecular structure could be described as a “bridged triphenylamine”. The carbon atoms in the 2,2'-position of the amine group are linked (Figure 3.10) allowing a planarization of the monomeric units along the backbone.

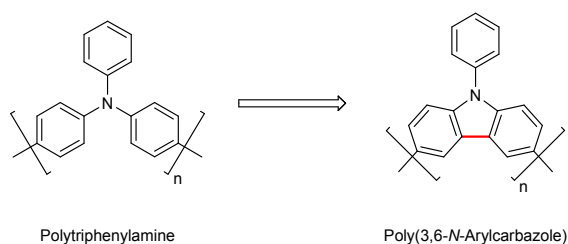


Figure 3.10: Molecular structures of triphenylamine- and *N*-arylcarbazole-based polymers.

Two kinds of *N*-arylcarbazole polymeric materials have been synthesized and investigated. The first one is a poly(*N*-phenylcarbazole-3,6-diyl)s with a long alkyl side chain in the *para*-position of the aromatic side chain phenyl group (PNPC, Figure 3.11,a). The long alkyl chain should allow a better solubility of the polymer in common organic solvents, e.g. toluene, chloroform or THF. The second one was a novel polymer based on *meta*-dicarbazolyl-phenylene units (PdCP, Figure 3.11,b). For PdCPs, the 3,3'-positions of the carbazole units as well as the 5-position of the phenyl group were blocked by an alkyl substituent in order to avoid any unwanted side reactions.

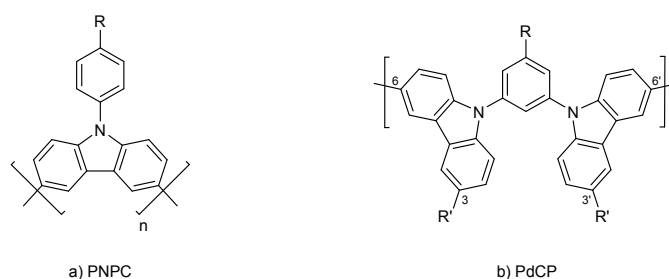


Figure 3.11: Molecular structure of a) poly[9-(4-alkylphenyl)carbazole-3,6-diyl] (PNPC) and b) poly[1,3-bis(3'-alkylcarbazole-9'-yl)-5-alkylphenylene-6',6''-diyl] (PdCP).

3.2.1. Poly(*N*-phenylcarbazole-3,6-diyl) (PNPC)

The polymer described here (**PNPC8**, Figure 3.12) contains an octyl chain as *para*-substituent of the side aromatic group, due to the commercial availability of the starting reagents.

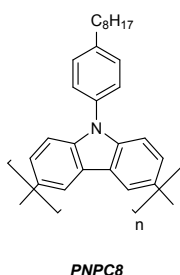


Figure 3.12: Molecular structure of poly[9-(4-octylphenyl)carbazole-3,6-diyl] (**PNPC8**).

3.2.1.1. Synthesis

The non functionalized 9-(4-octylphenyl)carbazole moiety **NPC8** was first synthesized according to Chen *et al.*^[125] as shown in Figure 3.13. Carbazole and the

1-bromo-4-octylbenzene were coupled by a nickel catalyzed reaction derived from the Kumada coupling reaction. The N-MgBr species was generated by in-situ addition of a Grignard reagent to the carbazole in dry THF. The dry THF was then removed under vacuum and replaced by dry toluene under argon. The use of only one solvent (THF or toluene) or a THF/toluene mixture led to a lower yield of the product. The N-C coupling reaction was then performed in toluene under addition of nickel catalyst, triphenylphosphine ligand and aryl halide in a similar way as for a classical Kumada coupling reaction. This reaction yielded about 60 % of the desired product after purification. The NMR spectroscopic investigation was in accordance with the expected spectra and will not be commented here in details. The molecular as structure deduced from NMR spectroscopy was further confirmed by mass spectrometry with the molar peak at $354.8 \text{ g}\cdot\text{mol}^{-1}$.

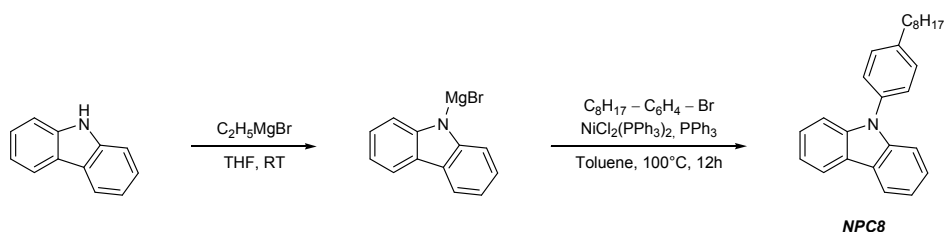


Figure 3.13: Synthesis a 9-(4-octylphenyl)carbazol monomer unit **NPC8** via formation of the N-MgBr compound and N-C coupling reaction.

The carbazole monomer was then brominated in the 3,6-positions with *N*-bromosuccinimide (NBS) (Figure 3.14) in DMF to afford ca 90 % of the monomer as yellow crystals.

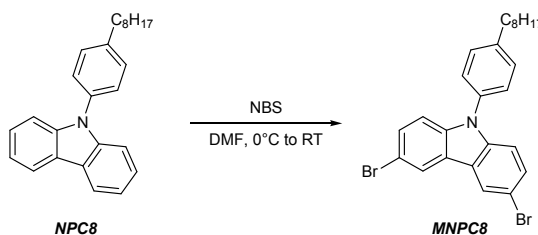


Figure 3.14: Synthesis of the 3,6-dibromocarbazole monomer (**MNPC8**)

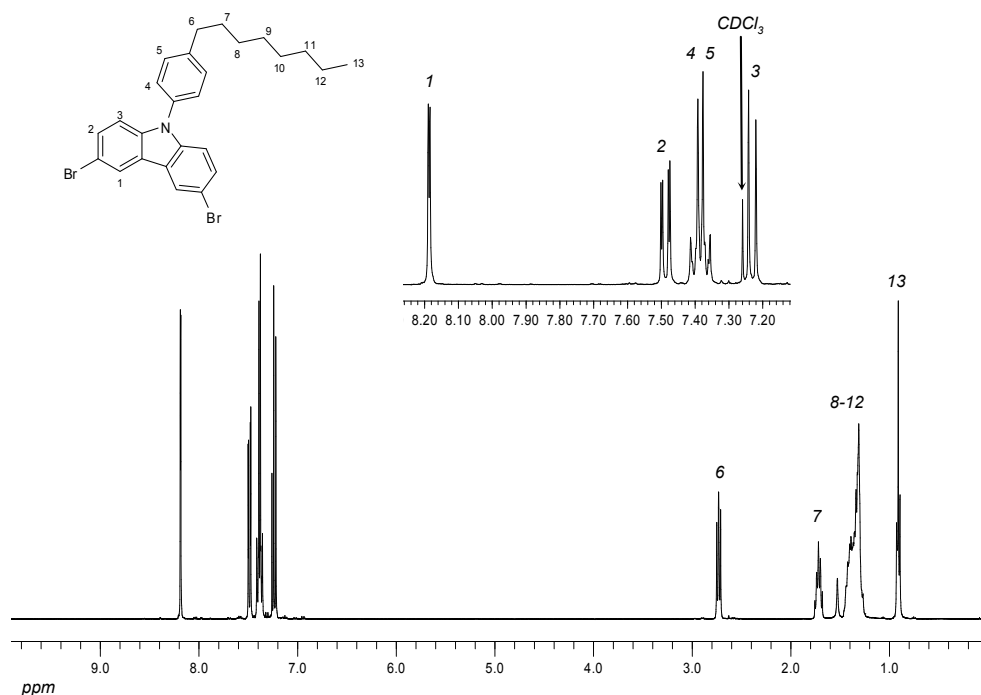


Figure 3.15: ^1H NMR of **MNPC8** in CDCl_3 .

The molecular integrity of the **MNPC8** monomer was investigated by NMR spectroscopy and mass spectrometry. Figure 3.15 shows the ^1H NMR spectrum of **MNPC8** in CDCl_3 . The protons of the octyl side chain can be assigned to the signals in the aliphatic region. The proton (13) can be associated to the triplet at $\delta = 0.91$ ppm ($^3J = 7.0$ Hz). The broad multiplet at $\delta = 1.36$ ppm can be assigned to the protons (12) to (8). The quintuplet at $\delta = 1.72$ ppm and the triplet at $\delta = 2.73$ ppm refer respectively to the protons (7) and (6) with a common coupling constant $^3J = 7.7$ Hz. In the aromatic region, the proton (1) can be associated to the doublet at $\delta = 8.19$ ppm with a coupling constant $^4J = 1.9$ Hz for the long range coupling with the proton (2). Therefore, the proton (2) can be assigned to the doublet of doublets at $\delta = 7.49$ ppm with a coupling constant $^3J = 8.7$ Hz for the coupling with (3) and a long range coupling constant $^4J = 1.9$ Hz due to the coupling with the proton (1). The proton (3) couples with (2) and can be associated to a doublet of doublets at $\delta = 7.23$ ppm ($^3J = 8.7$ Hz). This assumption is confirmed by the ^1H - ^1H COSY investigation with a clear signal for the coupling of (2) with (3). The two remaining protons (4) and (5) can be assigned to the multiplet centered at $\delta = 7.38$ ppm. Moreover, a signal for the through space coupling of (5) with (6) can be identified in the ^1H - ^1H NOESY spectrum. The molecular structure was confirmed by mass spectrometry with a molar peak at $512.5 \text{ g}\cdot\text{mol}^{-1}$.

The monomer **MNPC8** was then polymerized in a microwave-assisted Yamamoto-type aryl-aryl coupling reaction.^[126] The reaction under classical conditions leads to the

formation of oligomeric (and macrocyclic) compounds. Microwave-assisted coupling protocols have already been the subject of a lot of publications.^[127] The reaction has been carried out in a highly concentrated solution of the monomer in THF in presence of Ni(COD)₂ as catalyst and COD and BPy as ligands during twelve minutes at 120 °C (Figure 3.16). At the end of the reaction a solution of bromobenzene was added under argon in order to end-cap the bromine atoms present at the terminals of the polymer chains. After purification, the reaction yielded about 65–70 % of the **PNPC8** polymer as a grey solid.

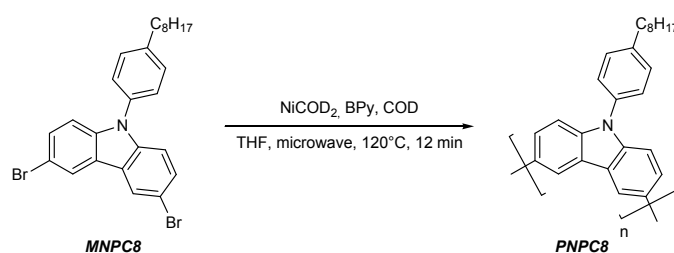


Figure 3.16: Microwave-assisted polymerisation of **PNPC8** according to Yamamoto.

The polymer was extracted with ethyl acetate to remove small molecules and oligomers to afford a polymer with a molecular weight of $M_n = 4.7 \times 10^3 \text{ g} \cdot \text{mol}^{-1}$ and a polydispersity $PD = 1.3$. In the aliphatic region of the ¹H NMR spectrum of the **PNPC8** polymer, four peaks at $\delta = 0.89 \text{ ppm}$, $\delta = 1.27 \text{ ppm}$, $\delta = 1.70 \text{ ppm}$ and $\delta = 2.69 \text{ ppm}$ can be observed for the protons of the octyl side chain. In the aromatic region, one multiplet at $\delta = 7.35 \text{ ppm}$, one doublet at $\delta = 7.71 \text{ ppm}$ and one singlet at $\delta = 8.55 \text{ ppm}$ can be assigned to the protons of the aromatic system by comparison with the ¹H NMR spectrum of the **MNPC8** monomeric compound. For this polymer no thermal transitions could be observed in the DSC curves reflecting an amorphous behavior.

3.2.1.2. Optical Properties and Energy Levels

The polymer **PNPC8** in chloroform solution absorbs light in a range up to 380 nm with two peaks at 259 and 313 nm (maximum absorption λ_{max} , Figure 3.17, Table 3.1). The observed values are similar to the absorption maxima of other 3,6-carbazole-based polymers^[128] as well as dimeric species.^[129] It reflects the restriction of the electronic conjugation along the polymer chain to two carbazole units, regardless of the average molecular weights. Measurement of the solid state absorption (film) for this polymer displays similar values compared to the measurement in solution, with a λ_{max} value at 322 nm (Table 3.1) and indicates that no significant electronic interaction takes place in

the solid state. However the large Stokes shift (119 nm in solution and 129 nm in solid state) implies large structural differences between the ground and excited states for this polymer. **PNPC8** shows a blue emission similar to other 3,6-carbazole-based polymers with a maximum centred at 432 nm in solution and 450 nm in the solid state.

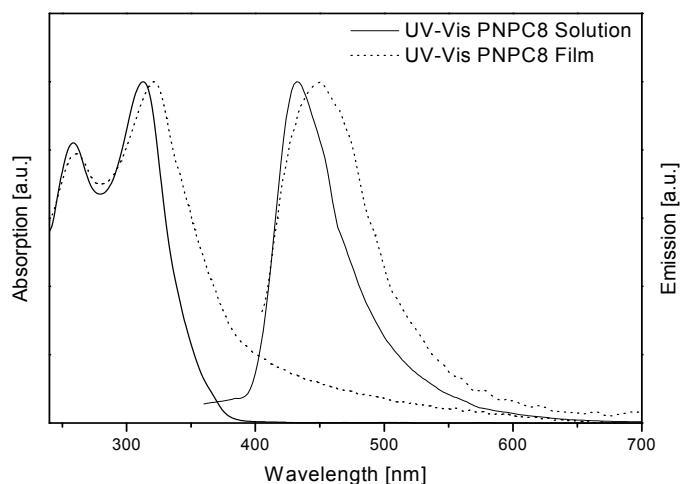


Figure 3.17: UV-Vis and PL spectra of **PNPC8** in chloroform solution and in solid state.

PNPC8		
<i>Solution</i>	<i>Absorption [nm]</i>	259, 313
	<i>Emission [nm]</i>	432
<i>Film</i>	<i>Absorption [nm]</i>	259, 322
	<i>Emission [nm]</i>	451

Table 3.1: Absorption and emission data of **PNPC8** in chloroform solution and in solid state.

The band gap of this polymer, as determined by the onset position of its absorption bands in the solid state ($\lambda_g = 396$ nm), is about 3.4 eV. The ionization energy of this polymer, pointing to the HOMO level of the material, was measured at 5.2 eV by UPS.

3.2.1.3. OFET Properties

For the OFET investigation, devices were built in bottom-gate/bottom-contact configuration. Highly *n*-doped silicon wafers (gate) with a thermally grown SiO₂ dielectric layer on which source and drain gold electrodes have been evaporated were used as substrates. The polymer has been spin coated from chloroform solution onto the devices. The mobility were measured in the saturation regime from the transfer characteristics at $V_D = -100$ V.

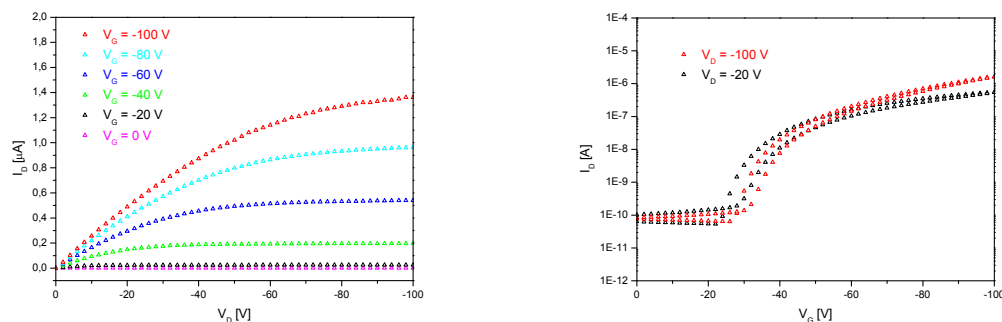


Figure 3.18: Output and transfer characteristics for OFETs based on **PNPC8**.

The transistor based on **PNPC8** showed a field-effect behavior with a clear saturation regime in the output characteristics as plotted in Figure 3.18. A moderate turn-on voltage V_{on} around -20 V with a slight hysteresis can be derived from the transfer curves. Nevertheless, only a quite low mobility with $\mu_{FET} = 6 \times 10^{-5} \text{ cm}^2 \cdot \text{V}^{-1} \cdot \text{s}^{-1}$ in the saturation regime for $V_G = -100$ V has been measured for this device. The on/off ratio was up to 10^5 .

3.2.2. Poly(*meta*-dicarbazolyl-phenylene) (PdCP)

Furthermore, we concentrated on a second class of 3,6-carbazole-based polymers. Due to the commercial availability of the starting reagents, the poly(*meta*-dicarbazolyl-phenylene) synthesized (**PdCP1**, Figure 3.19) contains methyl groups in the 6,6'-positions of the carbazole groups and a *tert*-butyl group at the 5-position of the central *meta*-phenylene moiety.

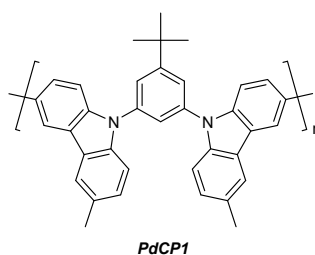


Figure 3.19: Molecular structure of poly[1,3-bis(3'-methylcarbazole-9'-yl)-5-*tert*-butylphenylene-6',6''-diyl] (**PdCP1**).

3.2.2.1. Synthesis

For the synthesis of the monomer **dCP1**, 1,3-dibromo-5-*tert*-butylbenzene has been first produced from 4-*tert*-butylaniline. The 4-*tert*-butylaniline was brominated in the 2,6-positions by bromine in cold dichloromethane (Figure 3.20) to afford 79 % of

2,6-dibromo-4-*tert*-butylaniline as white crystals. The chemical structures of the compounds were determined by mass and NMR investigation. In the ^1H NMR spectrum of 2,6-dibromo-4-*tert*-butylaniline, one singlet at $\delta = 7.37$ ppm for the protons of the benzene core in the aromatic region, one singlet at $\delta = 5.37$ ppm for the proton of the amino group and one singlet at $\delta = 1.20$ ppm for the protons of the *tert*-butyl group could be observed. Moreover, a peak for a quaternary carbon at $\delta = 108$ ppm typical for a C-Br group was observed in the ^{13}C NMR spectrum. The MS analysis displays a molar peak at $306.2 \text{ g}\cdot\text{mol}^{-1}$. Afterwards, the amino group was removed by diazotation and subsequent protonation (Figure 3.20) in order to yield (after purification) 52 % of 1,3-dibromo-5-*tert*-butylbenzene as a colorless oil.

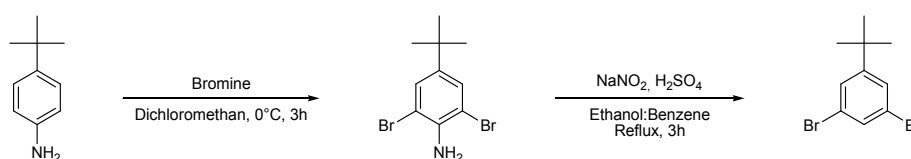


Figure 3.20: Synthesis of 1,3-dibromo-5-*tert*-butylbenzene.

Beside a singlet at $\delta = 1.22$ ppm for the protons of the *tert*-butyl group, the ^1H NMR spectrum did not show any peak for proton of an amine group but one doublet at $\delta = 7.42$ ppm for the two protons in the 4,6-position and one triplet at $\delta = 7.37$ ppm for the proton in the 2-position of the benzene core. These two peaks present a coupling constant of $^4J = 1.6$ Hz typical for a long range coupling in a benzene ring. The molecular integrity was confirmed by mass spectrometric analysis with a molar peak at $293.0 \text{ g}\cdot\text{mol}^{-1}$.

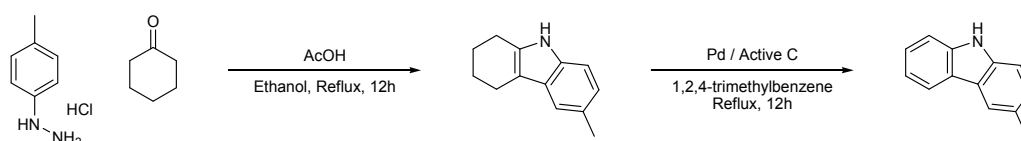


Figure 3.21: Synthesis of 3-methylcarbazole.

Secondly, the 3-methylcarbazole monomer has been formed by synthesis of the aryl hydrazone from 4-methylhydrazine hydrochloride and cyclohexanone followed by a ring closing Fischer-type indol reaction. According to a literature procedure,^[130] the tetrahydro carbazole intermediate was used without further purification and reduced with help of palladium on charcoal (Figure 3.21) to yield about 80 % of 3-methylcarbazole as white crystals.

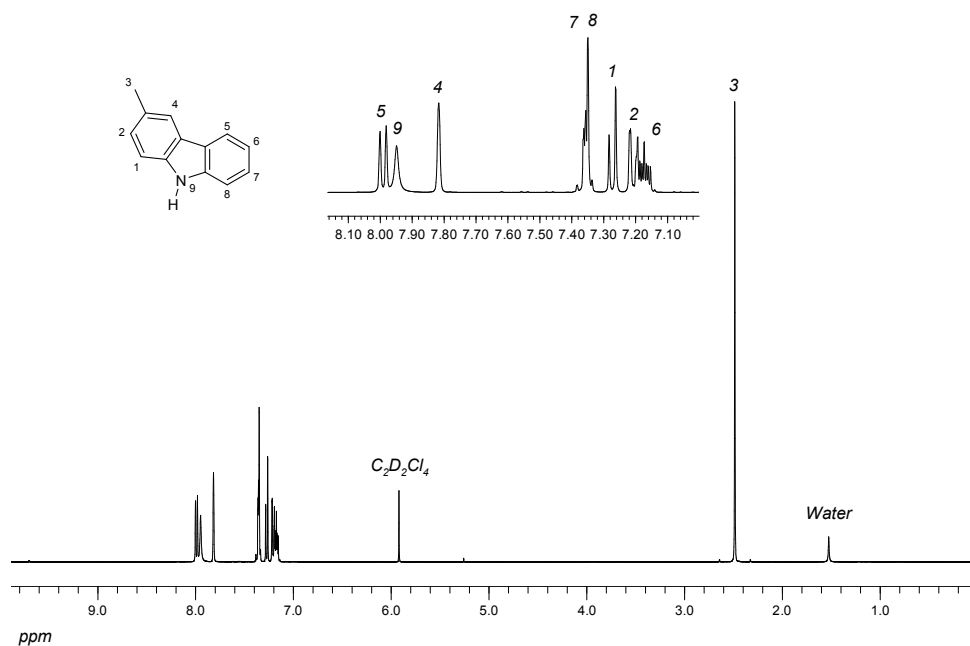


Figure 3.22: ^1H NMR of spectrum 3-methylcarbazole in $\text{C}_2\text{D}_2\text{Cl}_4$.

The structural integrity of 3-methylcarbazole was proved by MS and NMR studies. The ^1H NMR spectrum of the title compound is depicted in Figure 3.22. The singlet at $\delta = 2.43$ ppm can be attributed to the proton (3) of the methyl group. The ^1H - ^1H COSY long-range spectrum reveals a clear long range coupling between the protons (3) and the protons of the singlet at $\delta = 7.82$ ppm and the doublet at $\delta = 7.21$ ppm. Thus, the singlet at $\delta = 7.82$ ppm can logically be attributed to the proton (4) and the doublet at $\delta = 7.21$ ppm to the proton (2). The ^1H - ^1H COSY reveals also a coupling of the doublet at $\delta = 7.21$ ppm with the doublet at $\delta = 7.27$ ppm which can be associated to the proton (1). In the aromatic region, the remaining singlet at $\delta = 7.95$ ppm can be easily assigned to the proton (9) of the amine group. In the ^{13}C NMR spectrum, two very narrow peaks for tertiary carbon atoms can be observed at $\delta = 120.5$ ppm. The ^1H - ^{13}C COSY spectrum shows the coupling of these peaks with the singlet at $\delta = 7.82$ ppm as well as with the doublet at $\delta = 7.99$ ppm. It can be then deduced that one peak on the ^{13}C NMR spectrum corresponds to the carbon bearing the proton (4). Thus, the almost chemically equivalent peak corresponds to the carbon atom bearing the proton (5), which can be legitimately assigned to the doublet at $\delta = 7.99$ ppm. From the ^1H - ^1H COSY spectrum, the coupling between the protons (5) and (6), (6) and (7) as well as (7) and (8) can clearly be determined. The proton (6) can be associated to the multiplet at $\delta = 7.17$ ppm and the protons (7) and (8) to the multiplet (doublet+triplet) at $\delta = 7.35$ ppm. Beside the extensive NMR investigation, the ^{13}C NMR (dept135) allowed to recognize one peak for a primary

carbon atom in the aliphatic region as well as seven peaks for tertiary carbon atoms and five peaks for quaternary carbon atoms in the aromatic region, as expected. The structure was also confirmed by mass spectrometry with a molar peak at $180.8 \text{ g}\cdot\text{mol}^{-1}$. The 1,3-dicarbazolybenzene monomer **dCP1** has been synthesized by palladium-catalyzed Buchwald-Hartwig-type amination of 1,6-dibromo-5-*tert*-butylbenzene and 3-methylcarbazole (Figure 3.23). The catalyst system was composed of $\text{Pd}_2(\text{dba})_3$ as catalyst and biphenyl-2-di-*tert*-butylphosphine (JohnPhos) as ligand with $\text{NaO-}t\text{-Bu}$ as base. This system provided the best selectivity and yield (about 90 %) compared to other catalytic systems or other reactions procedures (e.g. Ullman-type amination).

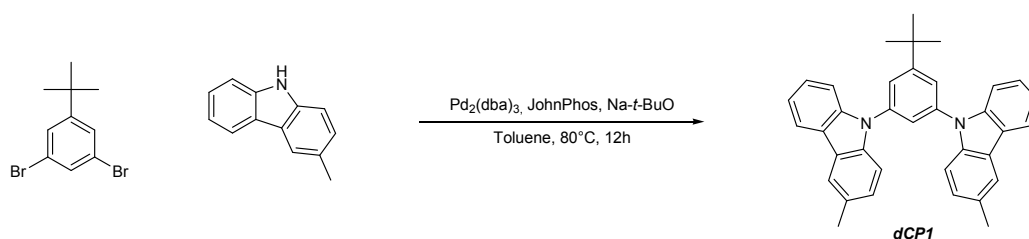


Figure 3.23: Synthesis of the 1,3-dicarbazolybenzene monomer **dCP1** by palladium-catalyzed Buchwald-Hartwig-type amination.

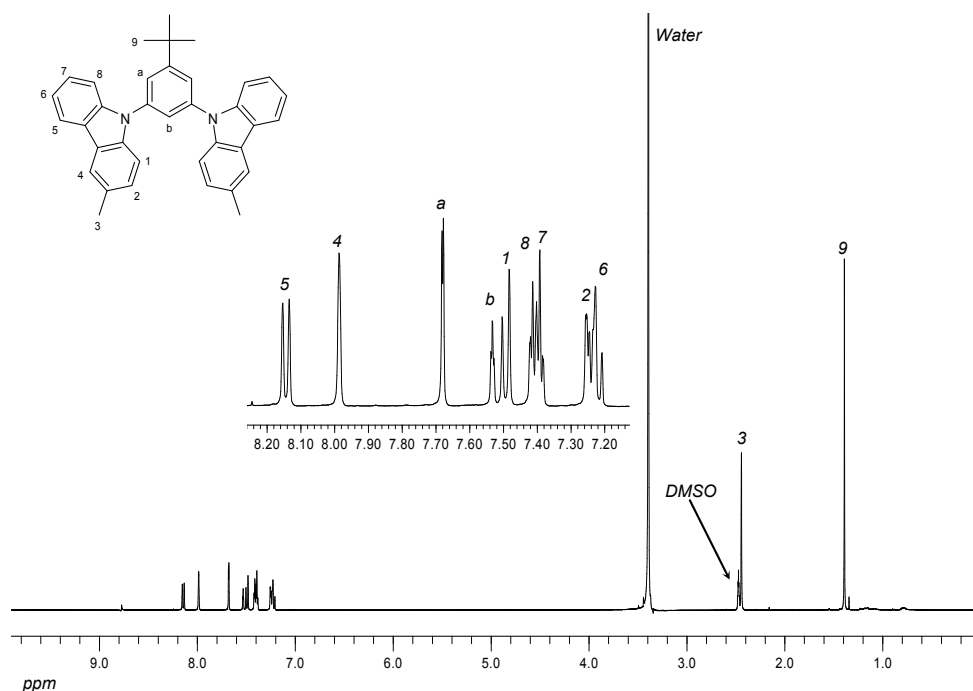


Figure 3.24: ^1H NMR spectrum of **dCP1** in DMSO-d_6 .

Structural identification was completed by mass spectrometry and NMR spectroscopy investigations. Figure 3.24 shows the ^1H NMR spectrum of the compound **dCP1** in DMSO-d_6 . In the aliphatic region, the two singlets at $\delta = 2.44$ ppm and at $\delta = 1.39$ ppm can be attributed to the protons (3) of the methyl groups and to the protons (9) of *tert*-butyl group respectively. The typical long range coupling constant $^4J = 1.7$ Hz allows to identify the protons of the metaphenylene bridge with a doublet for the protons (a) at $\delta = 7.68$ ppm and a triplet for the proton (b) at $\delta = 7.53$ ppm. The other peaks in this region can be associated with the protons of the 3-methylcarbazole unit, as described previously, with a doublet at $\delta = 8.14$ ppm for (5), a singlet at $\delta = 7.99$ ppm for (4), a doublet at $\delta = 7.49$ ppm for (1), a multiplet around $\delta = 7.40$ ppm (doublet+triplet) for (7) and (8), and finally another multiplet around $\delta = 7.22$ ppm (doublet+triplet) for (2) and (6). The postulate concerning the molecular structure was confirmed by mass spectrometry with a molar peak at $495.4 \text{ g}\cdot\text{mol}^{-1}$.

The **MdCP1** monomer unit has been finally generated by bromination of **dCP1** in the 6,6'-positions with NBS in acetonitrile at room temperature (Figure 3.25) with a conversion over 80 %.

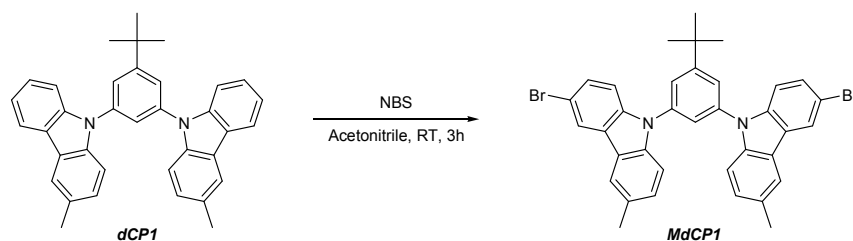


Figure 3.25: Synthesis of the **MdCP1** monomer.

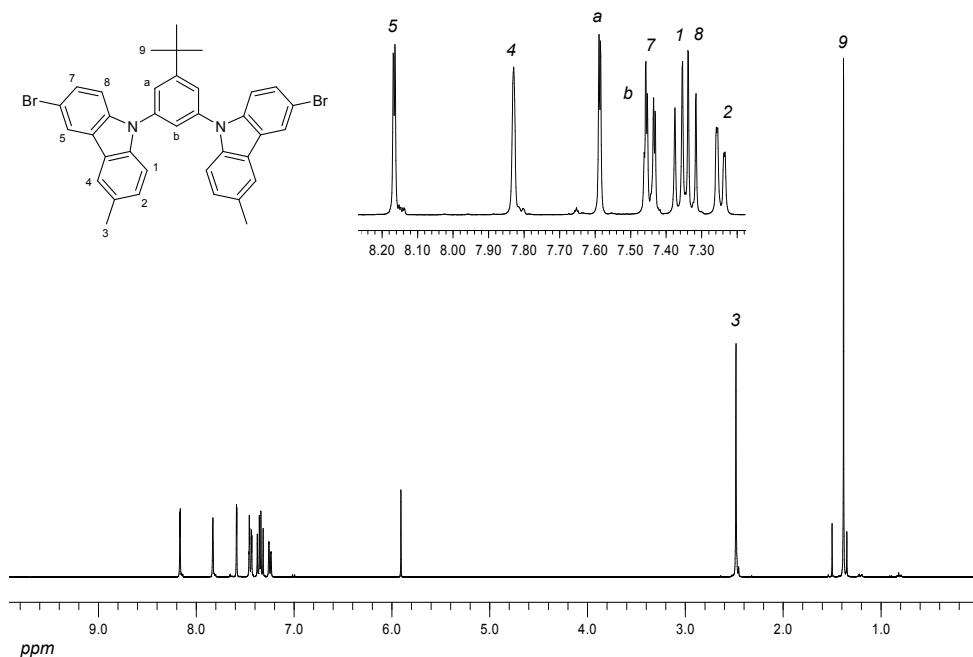


Figure 3.26: ^1H NMR spectrum of **MdCP1**.

In the ^1H NMR spectrum of the monomer **MdCP1** (Figure 3.26), the peak for the proton (5) at $\delta = 8.16$ ppm displays now a long range coupling ($^4J = 1.8$ Hz) with the protons (7) but no short range coupling. The signal associated to the proton (7) is now a doublet with a long range coupling constant $^4J = 1.8$ Hz and a short range coupling constant $^3J = 8.7$ Hz associated to a strong deshielding effect due to the neighboring bromine atom. Additionally, the multiplet around $\delta = 7.22$ ppm corresponding to the proton in the 6-position disappeared. A new doublet at 7.24 ppm is associated to the proton (2). In the aromatic region of ^{13}C NMR (dept135) spectrum, eight peaks of tertiary carbon atoms and eight peaks of quaternary carbon atoms of the monomer **MdCP1** can be determined. **MdCP1** presents one non-equivalent tertiary carbon atom less and one non-equivalent quaternary carbon atom more compared to the non-brominated precursor **dCP1**. Moreover, the peak for the quaternary carbon atom rises around $\delta = 115$ ppm which is

typical of a C-Br group. The MS investigation gave a further proof of the expected structure by exhibiting the molar peak at $648.3 \text{ g}\cdot\text{mol}^{-1}$.

The **PdCP1** polymer has been synthesized, like **PNPC8**, in a Yamamoto-type aryl-aryl coupling reaction^[126] of the monomeric compound **MdCP1** in THF with $\text{Ni}(\text{COD})_2$ as catalyst, COD and BPy as ligands under microwave irradiation during twelve minutes at 120°C (Figure 3.27). At the end of the reaction, an end-capping procedure with bromobenzene was applied to remove the bromine atoms left at the terminals of the polymer chains. After purification, the reaction yielded 80 % of the **PdCP1** polymer as a grey solid.

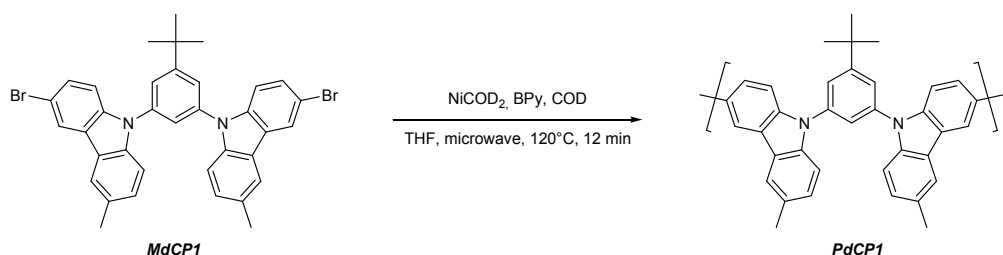


Figure 3.27: Synthesis of **PdCP1** polymer.

The **PdCP1** polymer was extracted with ethyl acetate to remove short chain oligomers to afford a polymer with $M_n = 2.5 \times 10^4 \text{ g}\cdot\text{mol}^{-1}$ and $PD = 2.1$. The ^1H NMR spectrum of the **PdCP1** polymer showed two singlets in the aliphatic region at $\delta = 1.53$ and 2.60 ppm, respectively, for the protons of the *tert*-butyl and methyl groups. In the aromatic region, four doublets at $\delta = 7.33$, 7.53 , 7.70 and 7.86 ppm, two singlets at $\delta = 8.08$ and 8.49 ppm as well as a multiplet at $\delta = 7.77$ ppm can be observed. This peak pattern is hereby similar to the one in the ^1H NMR spectrum of the **MdCP1** monomer. Moreover, in the ^{13}C NMR spectrum, as for the **MdCP1** monomer, eight peaks for tertiary carbon atoms and eight peaks for quaternary carbon atoms can be observed in the aromatic region. As expected, a DSC analysis of this polymer did not reveal any thermal transition such as recrystallization or melting, but also no clear glass transition.

3.2.2.2. Optical Properties and Energy Levels

The absorption and emission spectra of the **PdCP1** polymer display some similarity with those of the **PNPC8** polymer. As deduced from the molecular structure, the conjugation along the polymer main chain is reduced to two π -interacting carbazole units. The polymer absorbs light up to 390 nm . In chloroform solution as well as in solid state, the absorption spectrum displays two distinct peaks around 250 and 309 nm (maximum absorption λ_{max})

with a weak shoulder around 355 nm (Figure 3.28, Table 3.2). The carbazole-based polymer **PdCP1** exhibits a blue emission with a maximum centered at 414 nm in solution or 421 nm in the solid state. Here as well, the rather large Stokes shift (105 nm in solution and 112 nm in solid state) points for distinct structural differences between the ground and excited states. The absence of any shift between the absorption spectra in solution and in the film suggests the absence of any higher order in the solid state.

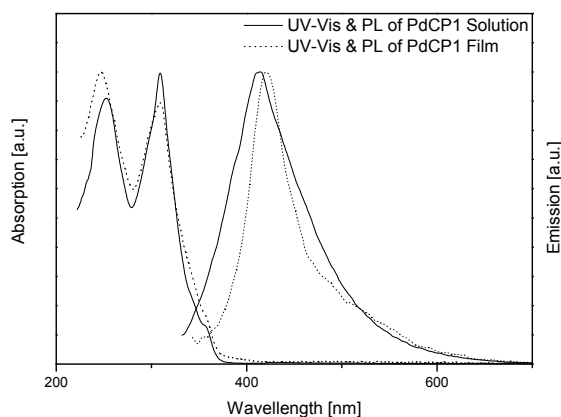


Figure 3.28: UV-Vis and PL spectra of **PdCP1** in chloroform solution and in the solid state.

PdCP1		
<i>Solution</i>	<i>Absorption [nm]</i>	252, 309 (355)
	<i>Emission [nm]</i>	414
<i>Film</i>	<i>Absorption [nm]</i>	247, 309 (358)
	<i>Emission [nm]</i>	421

Table 3.2: Absorption and emission data of **PdCP1** in chloroform solution and in solid state.

The band gap of this polymer, as determined by the onset position of its absorption bands in the solid state ($\lambda_g = 358$ nm), was about 3.8 eV. The HOMO level of the material was determined by UPS to be ca. 5.5 eV.

3.2.2.3. OFET Characteristics

As for the previous materials, the OFET characteristics (output and transfer) has been investigated for the same kind of devices presenting a bottom-gate/bottom-contact configuration with highly *n*-doped silicon as gate, a thermally grown SiO₂ dielectric layer as well as source and drain gold electrodes. The hole mobility has been measured from the saturation regime of the transfer characteristics for $V_D = -100$ V.

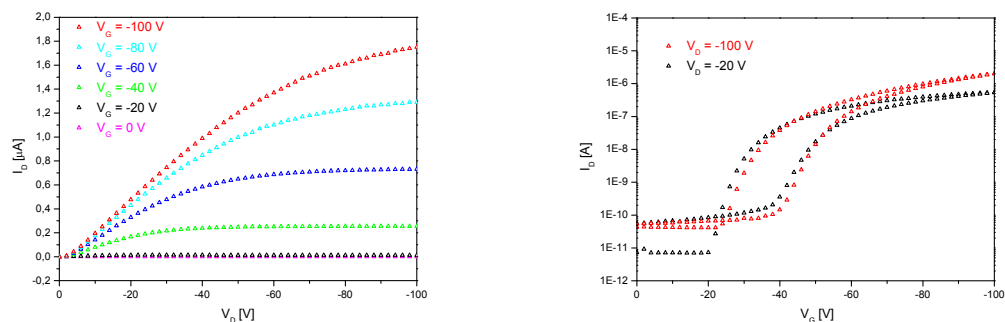
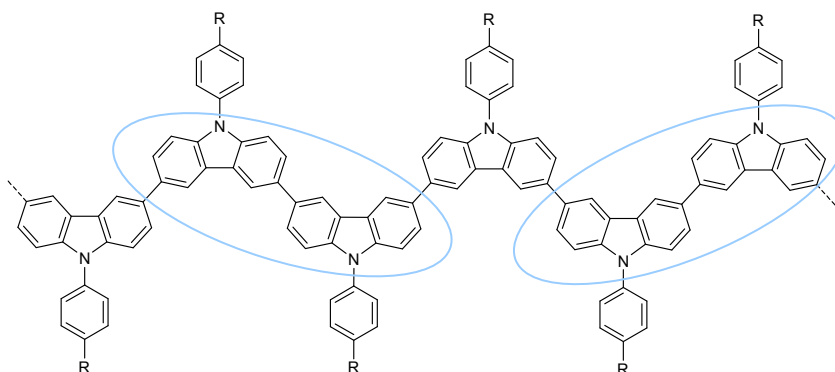


Figure 3.29: Output and transfer characteristics for OFETs based on **PdCP1**.

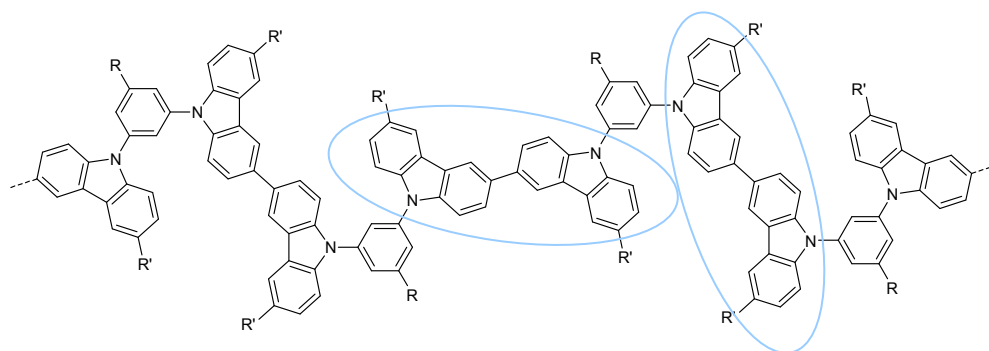
The device based on **PdCP1** exhibits a nice field-effect behaviour with a clear saturation regime in the output characteristics as plotted in Figure 3.29. On the other hand, the transfer characteristics displays a moderate turn-on voltage V_{on} around -20 V but a large hysteresis which could be explained by the presence of hole traps (defects or impurities; e.g. metal traps from the catalyst) or an oxidation in solution prior to processing. Also here, similar to **PNCP8**, only a quite moderate mobility with $\mu_{FET} = 7 \times 10^{-5} \text{ cm}^2 \cdot \text{V}^{-1} \cdot \text{s}^{-1}$ in the saturation regime for $V_G = -100 \text{ V}$ has been measured for this device. The on/off ratio was up to 10^4 .

3.3. Conclusion

During this work, two novel, soluble 3,6-carbazole-based, amorphous polymers have been developed for solution processed OFETs devices. In these two semiconducting materials, the hole conduction should occur via formation of radical cations along the backbone, with dimeric units being the most extended conjugated segment (Figure 3.30).



a) Most extended π -conjugated segment for **PNPC8**



b) Most extended π -conjugated segment for **PdCP1**

Figure 3.30: Most extended π -conjugated segments in a) **PNPC8** and b) **PdCP1**.

The measured HOMO levels were below -5.0 eV for the two materials indicating a good stability against air and oxygen. The band gap of 3.4 eV for **PNPC8** and 3.8 eV for **PdCP1** determined from the absorption spectra were in accordance with those of other carbazole-based polymers ($3-4$ eV) such as poly(9-alkylcarbazole-2,7-diyl)s or poly(9-alkylcarbazole-3,6-diyl)s. Moreover, the presence of the *meta*-substituted phenylene bridge between two carbazole dimers clearly reduces the planarity of the backbone, inducing a somewhat blue-shifted absorption both in solution and in the solid state as well as a higher band gap energy.

These two polymers exhibited a very similar field effect behaviour as well, with mobilities μ_{FET} of $6 \times 10^{-5} \text{ cm}^2 \cdot \text{V}^{-1} \cdot \text{s}^{-1}$ for **PNPC8** and $7 \times 10^{-5} \text{ cm}^2 \cdot \text{V}^{-1} \cdot \text{s}^{-1}$ for **PdCP1**. Even if a higher on/off ratio has been observed for **PNPC8** (10^5 against 10^4 for **PdCP1**) **PdCP1** seems to show more room for improvement via reduction of the strong hysteresis and presents a slightly smaller turn-on voltage. Optimization of the monomer and polymer synthesis and purification or of the processing conditions could lead to an improvement of the OFET parameters, e.g. by reducing the amount of defects or impurities which act as energy traps.

The **PdCP1** polymer has already been used by *Evonik Degussa Creavis-S2B Nanotronics*, Marl in partnership with the group of Prof. Hübler, *TU Chemnitz*, for an application in all-printed organic transistors.

4. Phenazine-Based Materials

4.1. Introduction

Electron-rich compounds are potentially useful materials in several electronic or magnetic devices. As developed previously, due to their electron donating π -electron system and reversible redox properties, oligomers and polymers based on nitrogen containing heterocycles seem to be attractive candidates. 5,10-Diaryl-5,10-dihydrophenazine-based compounds (Figure 4.1) can be considered as one promising class of such materials.

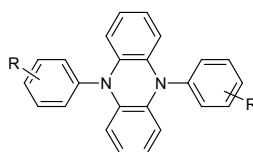


Figure 4.1: 5,10-Diaryl-5,10-dihydrophenazine compound.

Lots of procedures to synthesize 5,10-dialkyl-5,10-dihydrophenazine derivatives from 5,10-dihydrophenazine have been developed. These are mainly based on reduction/alkylation sequences,^[131] reduction/lithiation/alkylation sequences,^[132] or the use of Grignard reagents^[133] to afford the desired compounds in high yields. The synthesis of 5,10-diarylsubstituted 5,10-dihydrophenazines has been first achieved in a Ullmann-type copper-catalyzed coupling reaction of lithiated phenazine with aryl halides, as reported by Gilman and Dietrich in 1957, but required very harsh conditions (e.g. 210 °C during 12 hours to yield 16 % of 5,10-diphenyl-5,10-dihydrophenazine).^[131] Other methods involving electrochemical^[134] or aromatic nucleophilic^[135] cyclizations have also been reported. Nevertheless, the best synthetic method for the formation of symmetrically or asymmetrically substituted 5,10-diaryl-5,10-dihydrophenazines were reported by Okada and co-workers. This procedure based on the Buchwald-Hartwig-type palladium-catalyzed cross coupling reaction of 5,10-dihydrophenazine and an aryl halide using NaO-*t*-Bu as a base, P(*t*-Bu)₃ as a ligand and Pd(OAc)₂ as a catalyst in toluene allowed to afford the desired derivatives in good yields (65 to 85 %) depending on the substituents.^[136] Several of the compounds developed by Okada and co-workers were used in electroluminescent devices^[136] or for magnetic^[137] applications (Figure 4.2). EL device studies in particular showed good hole injecting properties for 5,10-diaryl-5,10-dihydrophenazines.

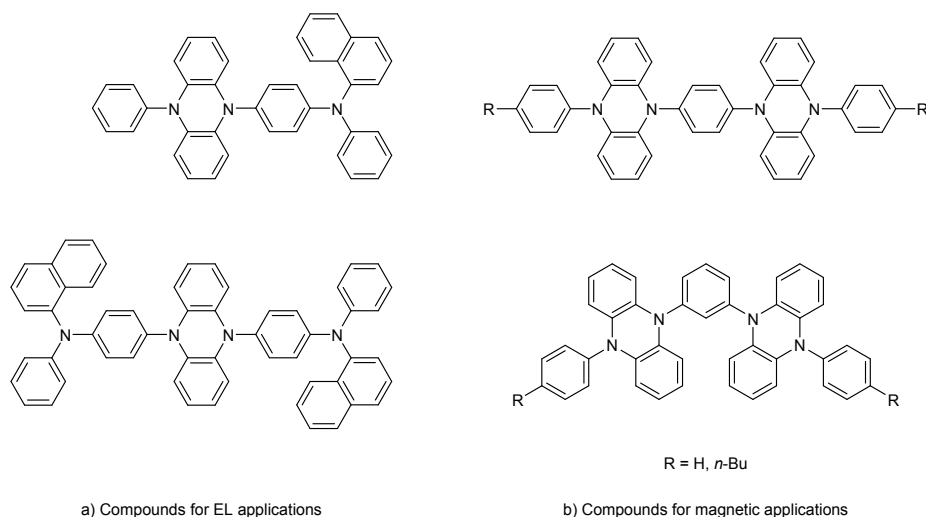


Figure 4.2: 5,10-Diaryl-5,10-dihydrophenazine-based compounds developed by Okada and co-workers for a) electroluminescent^[136] and b) magnetic applications.^[137]

Polymers containing photosensitive 5,10-dihydrophenazine units for laser ablation applications were also reported by Mikulla *et al.*^[138] They explored the influence of an incorporation of such units in polyamides on the resulting optical properties. The 5,10-bis(4-aminophenyl)-5,10-dihydrophenazine monomer used was prepared by *in-situ* silylation of phenazine to form 5,10-bis(trimethylsilyl)-5,10-dihydrophenazine followed by a reaction with 4-nitrobenzoyl chloride and catalytic hydrogenation. The final polyamides were then synthesized by polycondensation of the bisamino monomer with terephthaloyl chloride in *N*-methyl-2-pyrrolidone (Figure 4.3).

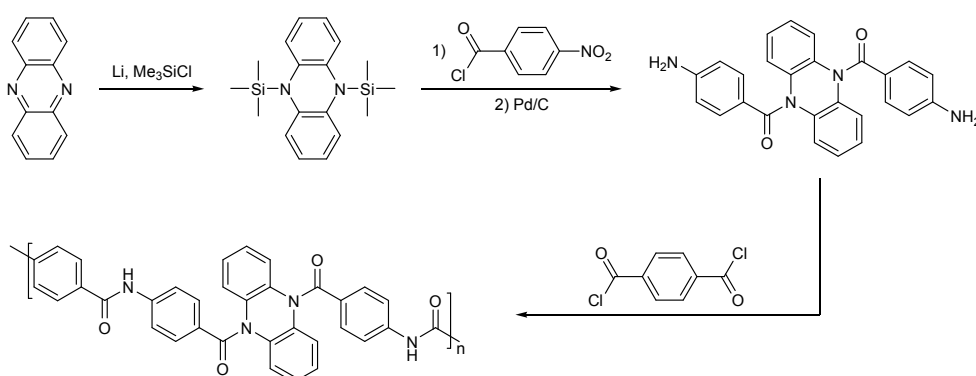


Figure 4.3: Preparation of a polyamide containing phenazine units according to Mikulla *et al.*^[138]

In this chapter, the synthesis and characterization of one model compound and several copolymers containing the 5,10-diaryl-5,10-dihydrophenazine unit are presented.

4.2. Model Compound

A 5,10-diphenyl-5,10-dihydrophenazine model with two octyl chain at both phenyl side groups (**d8PPz**) has been first synthesized and characterized within this study. The long alkyl chains were attached to increase the solubility and processability of the diphenyl phenazine compound.

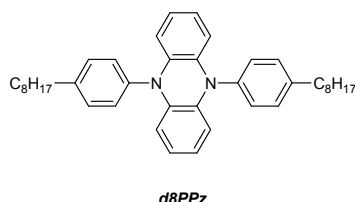


Figure 4.4: Diphenyl phenazine-based model compound (**d8PPz**).

4.2.1. Synthesis

For the synthesis of the model compound, phenazine was first reduced to 5,10-dihydrophenazine with sodium dithionite^[138] and arylated in a palladium-catalyzed Buchwald-Hartwig-type coupling reaction with the corresponding aryl halide (Figure 4.5).^[139]

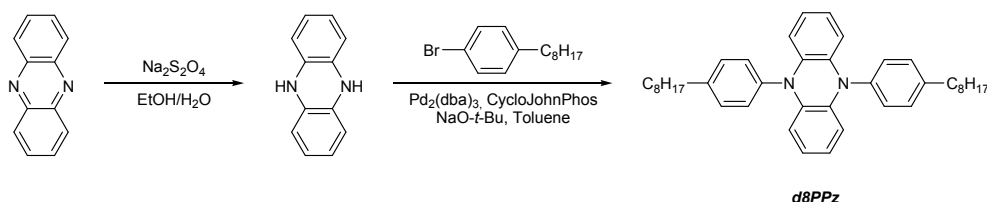


Figure 4.5: Synthesis of the model compound (**d8PPz**).

The catalytic system used for the amination reaction was based on Pd₂(dba)₃ and 2-(dicyclohexylphosphino)biphenyl (CycloJohnPhos) in toluene with NaO-*t*-Bu as a base. A screening procedure of several ligands and catalysts monitored by GC-MS allowed to determine the above mentioned system as the most efficient one concerning yield and selectivity. In this reaction, after purification 90 % of **d8PPz** could be isolated as orange crystals. Unfortunately, only a MS investigation was possible yielding a molar peak at 557.3 g·mol⁻¹. Despite the fact that **d8PPz** showed a good solubility in common deuterated solvents (e.g. CDCl₃, DMSO-d₆) its poor stability in solution against light and air did not allow the recording of NMR spectra.

4.2.2. Optical Properties and Stability Investigation

The absorption and emission spectra of the **d8PPz** model compound were measured by UV-Vis and photoluminescence (PL) spectroscopy, both in chloroform solution and in the solid state (thin film). A detailed UV-Vis study of **d8PPz** was carried out to investigate its stability in solution. As previously described, the HOMO energy level was estimated by UV photoelectron spectroscopy (UPS).

Figure 4.6 shows the UV-Vis and PL spectra of **d8PPz** in chloroform solution and in solid state (film).

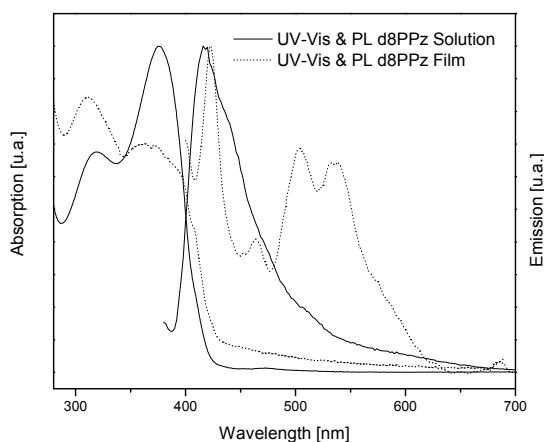


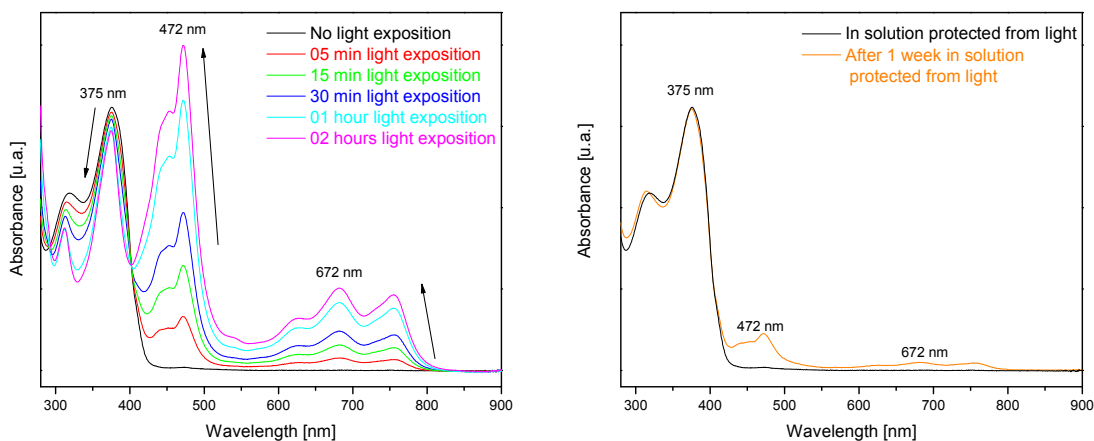
Figure 4.6: UV-Vis and PL spectra of **d8PPz** in chloroform solution and in solid state.

d8PPz		
Solution	Absorption [nm]	318, 375
	Emission [nm]	416
Film	Absorption [nm]	310, 367
	Emission [nm]	423, 464, 505, 537

Table 4.1: Absorption and emission data of **d8PPz** in chloroform solution and in solid state.

The model compound **d8PPz** in chloroform solution and in the solid state displays two UV-absorption maxima λ_{max} at approx. 320 and 375 nm (Figure 4.6, Table 4.1). In solution, it exhibits an unstructured blue emission peak centered at 416 nm. On the other hand, a handful of low energy emission peaks of unclear origin appear in the solid state (Figure 4.6, Table 4.1).

The stability of **d8PPz** against ambient conditions (air and light) in solution was investigated by absorption spectroscopy for several times of exposition.



a) In chloroform solution under light exposition. b) In chloroform solution protected from light.

Figure 4.7: Evolution of the UV-Vis spectra of **d8PPz** in chloroform solution a) under light exposition and b) protected from light.

The UV-Vis spectrum of **d8PPz** in chloroform solution displays a main peak at 375 nm and a smaller peak at ca. 320 nm (Figure 4.7, black curve). The generation of several lower energy peaks around 470 nm and in a range between 560 and 800 nm as well as a decrease of the main absorption peak at 375 nm can clearly be observed after a few minutes of exposition to sunlight. The exposition to light seems to be the critical factor regarding the stability. The triphenylamine derivatives, this phenomenon is probably due to a photooxidation of the compound and the occurrence of radical cationic species. This hypothesis could be corroborated by further investigations e.g. EPR analysis. The stability of **d8PPz** against light seems to be poor and probably insufficient for an application in solution-processed OFETs.

As determined from the onset position of its absorption band in the solid state ($\lambda_g = 428$ nm) **d8PPz** possesses a band gap energy around 3.2 eV. The HOMO level of the material was measured to be approx. 5.1 eV by UPS. The values for the energy levels are similar to the ones of the PTPA polymers.

4.2.3. OFET Characteristics

The OFET characteristics (output and transfer) have been investigated for devices in a bottom-gate/bottom-contact configuration with highly *n*-doped silicon as gate, thermally grown SiO₂ dielectric layer and source and drain gold electrodes. The mobility has been measured from the transfer characteristics for $V_D = -100$ V. The active layer has been spin-coated from chloroform solution onto the devices.

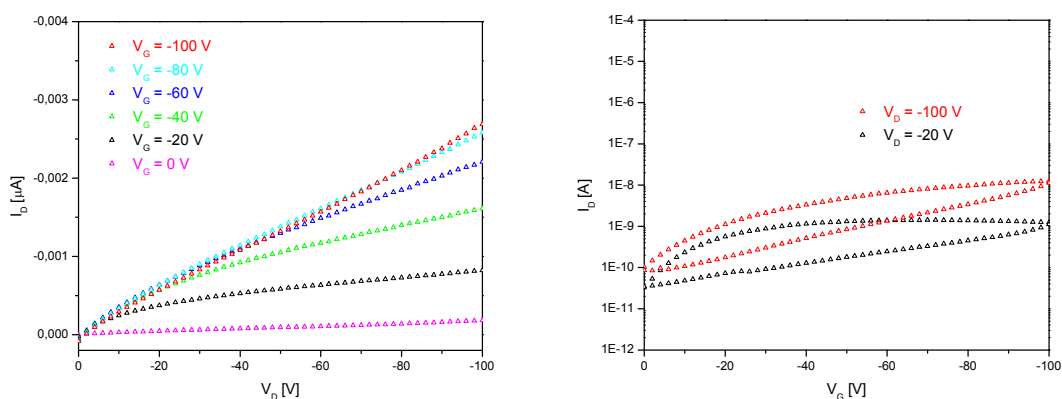


Figure 4.8: Output and transfer characteristics for OFETs based on **d8PPz**.

As depicted in Figure 4.8 the devices based on **d8PPz** showed only poor OFET behavior without a clear saturation region for high source-to-drain voltages V_D . The same conclusion can be deduced from the transfer characteristics where a poor OFET behavior can be observed. The extracted mobility for this device is logically very poor with a hole mobility $\mu_{FET} = 4 \times 10^{-7} \text{ cm}^2 \cdot \text{V}^{-1} \cdot \text{s}^{-1}$ at an on/off ratio of only approx. 10. These values are far below the ones observed for the other triphenylamine derivatives.^[136] OLEDs devices based on similar compounds have been all prepared by vacuum evaporation processes, avoiding the decomposition in solution.^[136]

4.3. Phenazine-Containing Polymers

Despite the low stability of the diphenyl phenazine model compound, several copolymers (PdPPzs) with comonomeric units such as carbazole or triphenylamine were synthesized and characterized (Figure 4.9).

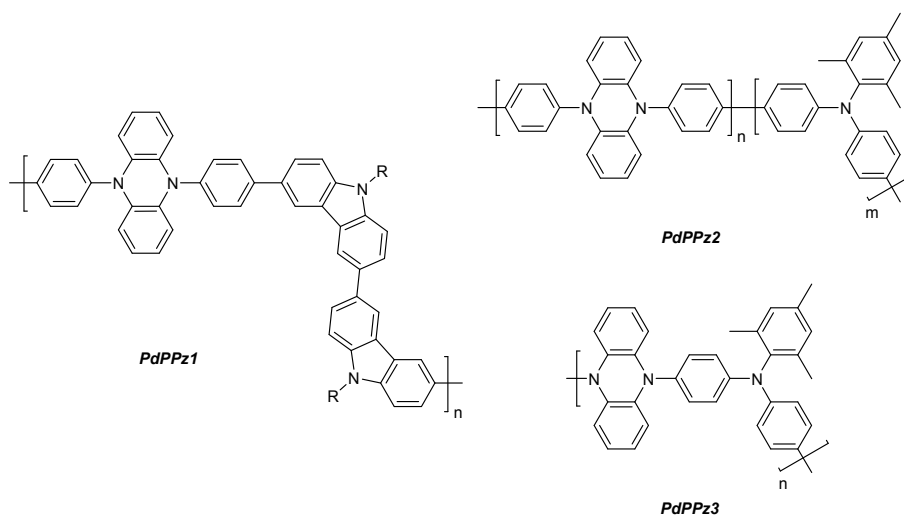


Figure 4.9: Phenazine containing copolymers.

4.3.1. Synthesis

A dibromo-functionalized diphenyl phenazine monomer (**MdPPz**) was synthesized similar to the model compound **d8PPz** by palladium-catalyzed Buchwald-Hartwig-type amination of an aryl halide and 5,10-dihydrophenazine as depicted in Figure 4.10.

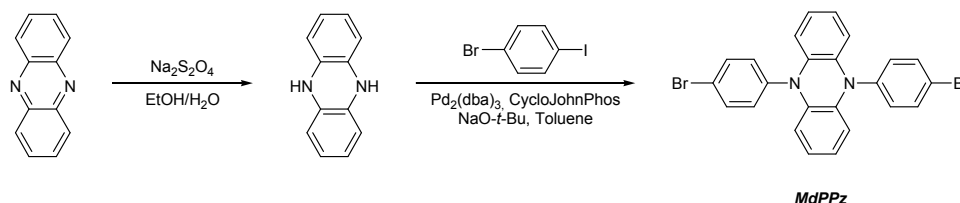


Figure 4.10: Synthesis of a bis(bromophenyl)phenazine monomer (**MdPPz**).

In this case, as for the TPA monomers, 1-bromo-4-iodobenzene was used as aryl halide due to the lower dissociation energy of the C-I bond compared to the C-Br bond allowing to afford dibromo-functionalized monomers within one step. This procedure yielded approx. 80 % of the **MdPPz** compound too, as yellow crystals after purification by recrystallization from toluene. No NMR spectroscopy investigation could be carried out for this compound due to its very poor solubility in all available deuterated solvents (e.g. CDCl_3 , $\text{C}_2\text{D}_2\text{Cl}_4$, $\text{DMSO}-d_6$). As for the model compound, characterization could only be done by mass spectrometry showing molar peak at $490.7 \text{ g}\cdot\text{mol}^{-1}$.

A first attempt was made to synthesize the corresponding homopolymer in a homocoupling reaction according to Yamamoto. Unfortunately, this procedure did not lead to any coupling product due to the very low solubility of the **MdPPz** monomer in the solvents commonly used for this kind of reaction (e.g. THF, toluene and DMF).

A first copolymer synthesized was an alternating copolymer of diphenyl phenazine and dicarbazole units (**PdPPz1**). This polymer was prepared by standard palladium-catalyzed Suzuki-Miyaura-type cross-coupling reaction of aryl halides and boronic ester compound. The dicarbazole bis(boronic ester) comonomer was prepared by oxidative dimerization of *N*-decylcarbazole followed by bromination and formation of the diboronic ester (Figure 4.11) to afford ca. 35 % (overall) of the pure comonomer as white crystals. The molecular integrity was shown by NMR spectroscopy and mass spectrometry (see Experimental Section).

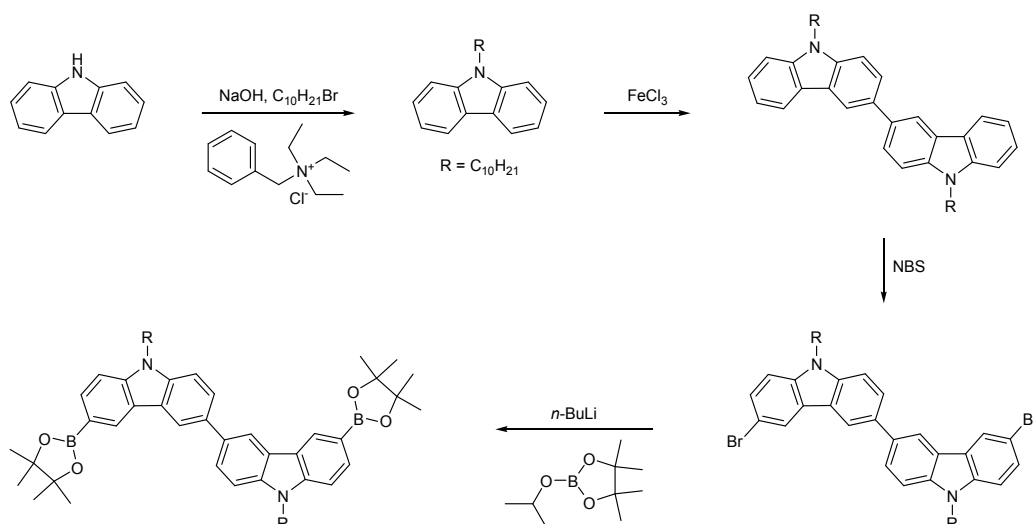


Figure 4.11: Synthesis of the dicarbazole bis(boronic ester) comonomer.

The Suzuki-Miyaura-type cross-coupling reaction has already been the focus of a wide range of publications^[140] and will not be described here any further. This reaction was carried out with tetrakis(triphenylphosphine)palladium(0) (Pd(PPh₃)₄) as catalyst, aqueous potassium carbonate as base in toluene with Aliquat 336 as phase-transfer catalyst (Figure 4.12)^[141] to afford more than 85 % of **PdPPz1**.

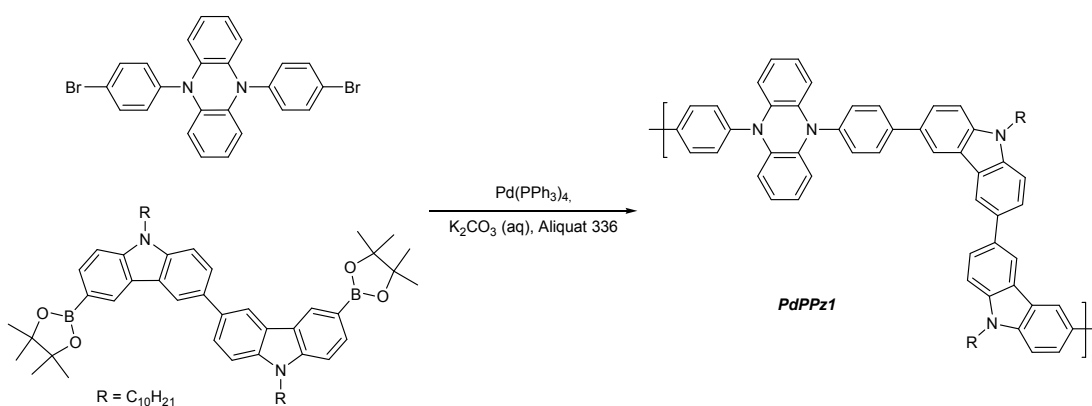


Figure 4.12: Synthesis of the copolymer **PdPPz1**.

After purification, the **PdPPz1** copolymer displayed a molecular weight $M_n = 2.1 \times 10^3 \text{ g} \cdot \text{mol}^{-1}$ with a polydispersity at $PD = 1.16$. Considering that the molecular weight of one repeat unit is around $1000 \text{ g} \cdot \text{mol}^{-1}$, the material produced was just a dimer. This low molecular weight can be explained by the poor solubility of the products in the reaction medium leading to a precipitation of oligomers.

The second copolymer prepared was a random copolymer with diphenyl phenazine and triphenylamine building blocks (**PdPPz2**). A mixture of 20 % **MdPPz** and 80 % of **MTPA3** was randomly polymerized in a Yamamoto-type homo-coupling procedure as shown in Figure 4.13, to yield ca. 55 % of **PdPPz2**.

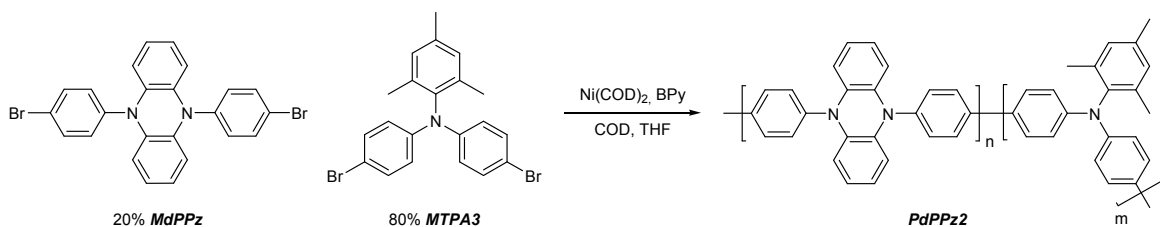


Figure 4.13: Synthesis of **PdPPz2**.

After purification and extraction, the random copolymer **PdPPz2** exhibited a molecular weight $M_n = 2.1 \times 10^4 \text{ g} \cdot \text{mol}^{-1}$ with a polydispersity $PD = 1.6$. The exact amount of incorporated diphenyl phenazine units into the polymer chain could not be exactly estimated by ^1H NMR investigation due to the fact that no characteristic for both monomeric units were available in the spectrum.

The third and last copolymer synthesized for this study was an alternating copolymer of phenazine and triphenylamine units (**PdPPz3**). In order to overcome the solubility problems, 5,10-dihydrophenazine was directly coupled with the triphenylamine units in a Buchwald-Hartwig-type amination, as depicted in Figure 4.14.

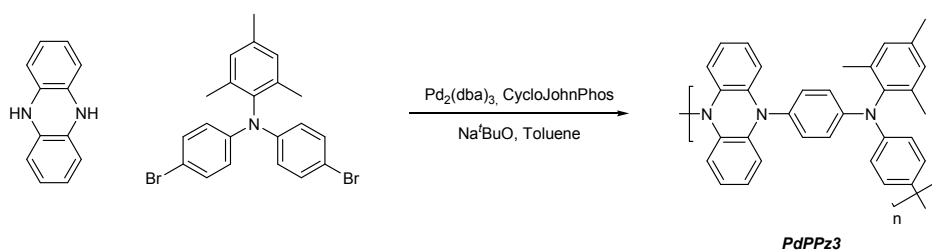


Figure 4.14: Synthesis of **PdPPz3**.

As shown by Hartwig and co-workers, polymers with high molecular weight can be obtained by direct amination of dihaloaryls and diamine with a suitable catalytic system based on a palladium catalyst and phosphine ligands. For this reaction, conditions as used for the model compound were applied and ca. 65 % of a polymer **PdPPz3** have been isolated. Beside CycloJohnPhos, the alternative $\text{P}(t\text{-Bu})_3$ proved to be also an effective phosphine ligand. The polymer exhibited a molecular weight $M_n = 6.7 \times 10^3 \text{ g} \cdot \text{mol}^{-1}$

with a polydispersity of $PD = 1.2$ after extraction with ethyl acetate to remove low molecular weight oligomers.

4.3.2. Optical Properties and OFET Investigation

Figure 4.15 shows the UV-Vis spectra of the three phenazine-containing copolymers (**PdPPz1**, **PdPPz2**, **PdPPz3**) in chloroform compared to the triphenylamine homopolymer **PTPA3**, the dibromomonomer **MTPA3** and the model compound **d8PPz**.

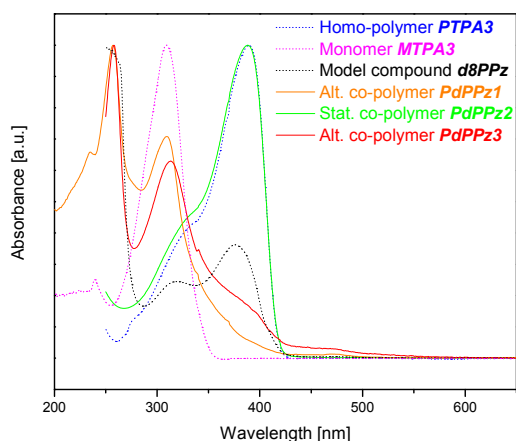


Figure 4.15: UV-Vis spectra of **PTPA3** (blue dotted curve), **MTPA3** (pink dotted curve), **d8PPz** (black dot curve), **PdPPz1** (orange curve), **PdPPz2** (green curve) and **PdPPz3** (red curve) in chloroform.

PdPz1 (Figure 4.15, orange curve) presents two distinct absorption maxima centered at 258 nm and at 308 nm, **PdPPz3** exhibits two peaks at 258 and 312 nm. Both polymers display absorption shoulders at ca. 375 nm. The shoulders correspond to the main chain diphenyl phenazine units (Figure 4.15, red and black curves). The random copolymer **PdPPz2** displays an unstructured absorption band centered at 388 nm similar to that of **PTPA3**. This may suggest that only few diphenyl phenazine units are incorporated into the backbone.

The optical band gaps of **PdPPz1** and **PdPPz2** were determined by the onset of the absorption bands to be 3.8 and 3.2 eV, respectively, and the HOMO levels to 4.90 eV and 5.02 eV respectively (UPS analysis).

A bottom-gate/bottom-contact-configured OFET device based on **PdPPz1** did not show any field-effect behavior under ambient conditions. On the other hand, devices based on the **PdPPz2** random copolymer showed good field effect behavior with clear saturation region, moderate turn-on voltage ($V_{on} = -10$ V) and small hysteresis (Figure 4.16).

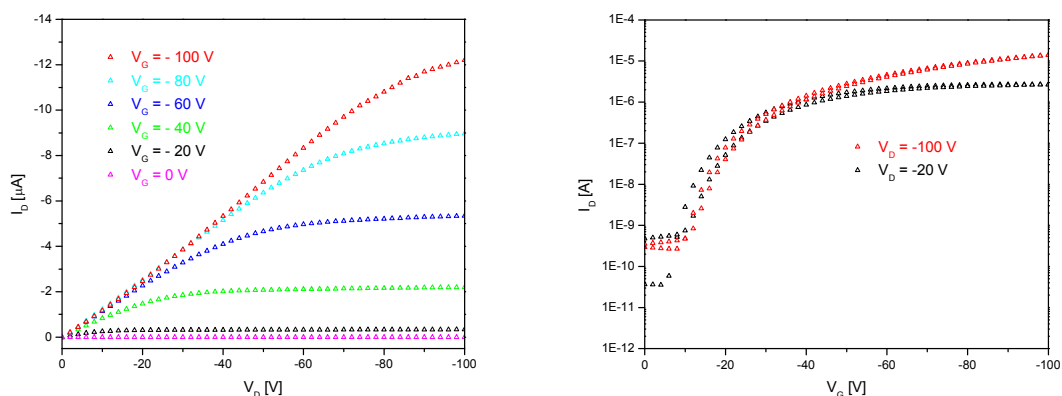


Figure 4.16: Output and transfer characteristics of **PdPPz2** based OFET devices.

The mobility measured in the saturation regime is $\mu_{FET} = 4 \times 10^{-4} \text{ cm}^2 \cdot \text{V}^{-1} \cdot \text{s}^{-1}$ with an on/off ratio up to 10^5 . These good results have to be contrasted by the fact that the amount of incorporated phenazine units is unclear.

The alternating copolymer **PdPPz3** have not been analyzed so far and thus, no results concerning the energy levels or OFET characteristics could be presented here.

4.3.3. Conclusion

Despite the encouraging results shown in other studies, the different phenazine-based derivatives of this study did not fulfill the expectations of being suitable materials for solution-processed OFETs. The **d8PPz** model compound showed a very weak stability in solution, especially in daylight. After a very short time (approx. 1 min), solutions of the material were already oxidized preventing a satisfying OFET performances.

Beside its very low molecular weight, a first alternating copolymer with diphenyl phenazine and dicarbazole units (**PdPPz1**) exhibited the similar stability problems in solution, probably also in the solid state (film). The devices based on this material did not even show any OFET behavior.

Concerning the random copolymer **PdPPz2** composed of diphenylphenazine and triphenylamine units, the characterization results indicate the incorporation of only a low amount of phenazine subunits. The OFET properties are mainly influenced by the polytriarylamine backbone with low influence of the phenazine moieties.

The last alternating copolymer produced (**PdPPz3**) showed a higher concentration of incorporated phenazine units. The Buchwald-Hartwig-type amination allowed to overcome the solubilization problem of the phenazine monomer and afforded a copolymer with reasonable molecular weight ($M_n > 5 \times 10^3 \text{ g} \cdot \text{mol}^{-1}$). Moreover, the higher amount of incorporated phenazine units in the polymer will allow to study the influence of this moiety

on the OFET properties. The **PdPPz3** polymer will now be investigated for its OFET properties. However, early UV-Vis investigation as well as difficulties to obtain well-resolved NMR spectra indicate stability problems as for the model compound **d8PPz**. In conclusion, despite the promising literature reports on phenazine-based materials as hole-conducting materials for optoelectronic applications, their poor stability make them unsuitable for a use in solution-processed OFETs.

5. Summary

In this thesis, it has been shown that triarylamine-based semiconducting polymers represent suitable candidates for solution-processed organic field-effect transistors. A couple of materials showed a clear field-effect when used as semiconducting layer in OFET devices. Moreover, a special focus of this work has been put on the stability against air which is one of the most crucial prerequisites. Thiophene-based polymers show serious restrictions in this direction.

In the polytriphenylamine series, **PTPA3** showed the most promising electronic properties regarding the stability as well as the OFET performance, with a hole mobility μ_{FET} around $10^{-3} \text{ cm}^2 \cdot \text{V}^{-1} \cdot \text{s}^{-1}$ and on/off ratio up to 10^6 . It has been determined that the stability of the polymers is directly related to the shielding effect induced by the *ortho*-substituents at the side chain phenyl group. However, the stability of the PTPA polymers could not further be improved due to restrictions in the chemical reactions that have been applied in the synthesis of the triphenylamine monomers. Monomers with increased shielding effect could not be prepared in the amination reaction (according to Buchwald-Hartwig or Ullmann) due to the high steric hindrance of the arylating reagents with larger *ortho*-substituents.

In the case of the polycarbazoles (**PNPC8** and **PdCP1**), OFET devices based on these polymers exhibited a promising OFET behavior comparable to the OFET properties (mobility and on/off ratio) of **PTPA3**.

At last, phenazine-containing polymers turned out to be unsuitable for air-stable, solution processed OFET devices. Their very poor stability in solution against light and air seems to exclude this class of compounds for OFET applications.

6. Outlook

6.1. New Polymers for OFETs

Concerning the polytriphenylamines PTPAs, further improvements via modification of the molecular structure seem possible. Nevertheless, **PTPA3** has already proved to be the most suited polymer for OFET applications so far. The use of larger aromatic main chain segments seems to decrease the solubility and processibility of the materials without any increase of the OFET performance including mobility and on/off ratio.

In partnership with the *Evonik Degussa Creavis*, new carbazole containing polymers will be developed and tested for OFET applications. Based on the **PdCP** structure (two carbazoles bridged by an aromatic group) similar compounds with different aromatic cores are under investigation. Through this, it will be possible to determine the influence of the core unit on the OFET properties. Possible core units are pyridine-2,6-diyl, 1,4-phenylene or more complex aromatic systems (e.g. benzophenone, fluorene) as depicted in Figure 6.1.

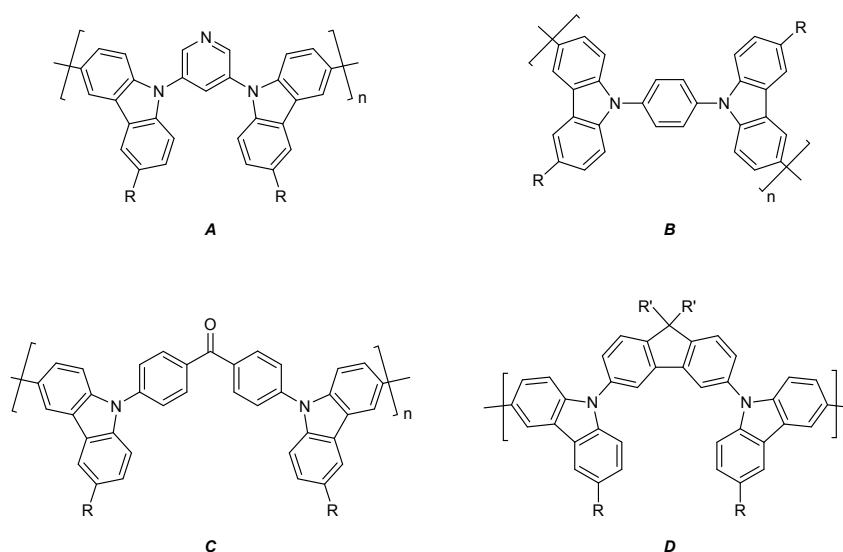


Figure 6.1: PdCP-type polymers with pyridine (**A**), *para*-phenylene (**B**), benzophenone (**C**) or fluorene (**D**) as core unit.

As for thiophene-based polymers, “fused” carbazole compounds such as indolocarbazoles could be also attractive for OFET applications (See Chapter 3).^[123,124] In this view, polymers like **E** or **F** are possible candidates for an use as semiconducting layer in OFET devices (Figure 6.2).

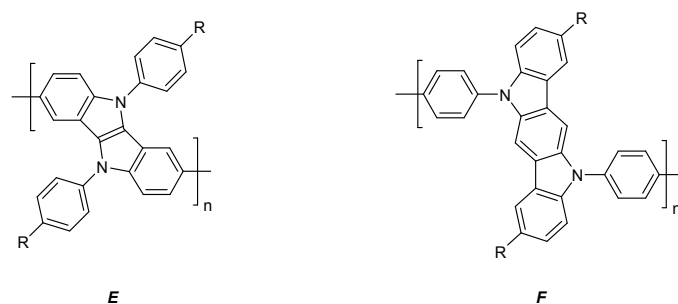


Figure 6.2: Fused carbazole-containing materials.

6.2. Triphenylamine-Based Polymers as Bio-Sensor and Dyes

During the last few years, sensor applications of conjugated polymers and oligomers appeared as a new research field. Several sensors have already been developed for metallic cations and anions, proteins or DNA based on small organic molecules or polymers.^[14, 142] In this view, triarylamine-based polymers containing heterocyclic side groups such as 4-pyridyl (Figure 6.3) should be of interest for the detection of acidic analytes e.g. in the gas or liquid phase.

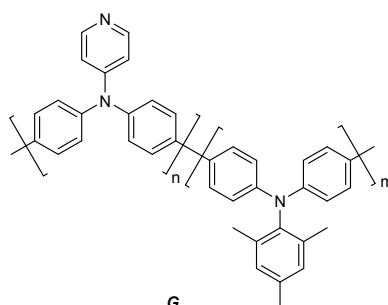


Figure 6.3: A 4-pyridyl-containing polytriphenylamine for potential sensor applications.

Dye-sensitized organic solar cells have also been the focus of intense research.^[143] However, only a few polymers containing triphenylmethane-type dyechromophores incorporated into the backbone of a semiconducting polymer have been described so far.^[144] Therefore, copolymers containing triphenylmethane dyes (TPMD) as depicted in Figure 6.4 could be an interesting target.

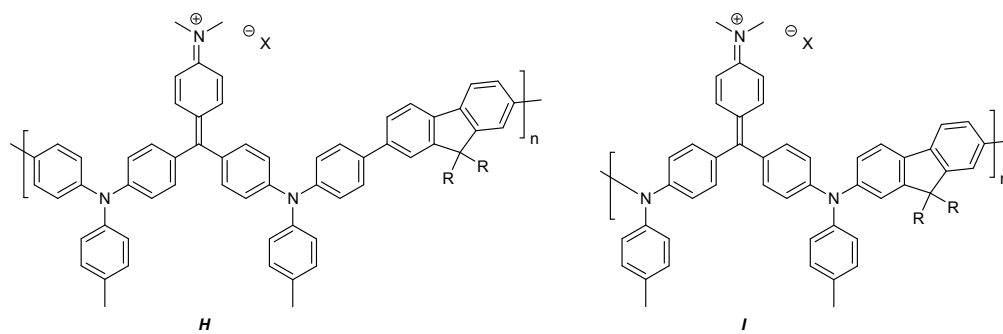


Figure 6.4: Dye-containing triphenylamine-based semiconducting polymers.

7. Experimental Section

7.1. General Methods

The ^1H and ^{13}C NMR spectra were recorded on a Bruker ARX 400 spectrometer. Low-resolution mass spectrometry (LR-MS) was carried out on a Varian MAT 311 A operating at 70 eV (electron impact) and reported as m/z . Elemental analyses were performed on a Vario EL II (CHNS) instrument. UV-Vis absorption spectra were recorded on a Jasco V 550 spectrophotometer. Fluorescence measurements were carried out on a Varian Cary Eclipse instrument.

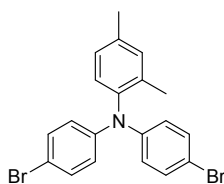
Unless otherwise indicated, all reagents were obtained from commercial suppliers and were used without further purification. All reactions were carried out under an argon atmosphere by use of standard and Schlenk techniques. The solvents were used as commercial p.a. quality.

7.2. Synthesis of Triphenylamine-Based Materials

7.2.1. General procedure for the synthesis of *N,N*-bis(4-bromophenyl)-arylanilines (MTPAs)

To a stirred solution of $\text{Pd}_2(\text{dba})_3$ (126 mg, 0.138 mmol), DPPF (230 mg, 0.414 mmol), 1-bromo-4-iodobenzene (13.07 g, 46 mmol) and $\text{NaO}-t\text{-Bu}$ (5.3 g, 55 mmol) in 30 ml of toluene a solution of freshly distilled aniline (22 mmol) in 10 ml of toluene was slowly added at 80 °C. The reaction mixture was stirred for 24 hours at 90 °C. At the end of the reaction, the mixture was diluted with hot ethyl acetate and mixed with celite. The non-soluble solids were filtered off and washed several times with hot ethyl acetate. The filtrate was washed with aqueous, saturated EDTA solution and water, the organic layer subsequently dried over MgSO_4 and all solvents removed under vacuum. The raw product was then purified by column chromatography with hexane as eluent and recrystallized from a methanol/2-propanol (1/3) mixture to afford the monomers as white crystals.

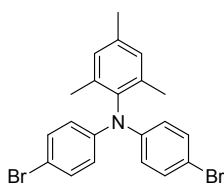
7.2.1.1. *N,N*-bis(4-bromophenyl)-2,4-dimethylaniline (**MTPA2**).



According to the general procedure, 2,4-dimethylaniline (2.67 g, 22 mmol) was used to obtain 5.88 g (62 %) of the title compound as white crystals.

^1H NMR (400 MHz, CDCl_3 , 32 °C): δ [ppm] = 7.29 (td, 4H, Ar-H, $^3J = 8.9$ Hz), 7.07 (s, 1H, Ar-H), 7.03 (d, 1H, Ar-H, $^3J = 8.1$ Hz), 6.97 (d, 1H, Ar-H, $^3J = 8.0$ Hz), 6.83 (td, 4H, Ar-H, $^3J = 9.0$ Hz), 2.35 (s, 3H, $-\text{CH}_3$), 2.00 (s, 3H, $-\text{CH}_3$). ^{13}C NMR (101 MHz, CDCl_3 , 32 °C): δ [ppm] = 146.2, 141.8, 136.5, 136.0, 132.6, 132.1, 129.2, 128.4, 122.8, 113.9, 21.0, 18.3. LR-MS (EI, 70 eV): $m/z = 430.6$ [M^+]. Anal. Calcd. for $\text{C}_{20}\text{H}_{17}\text{Br}_2\text{N}$: C 55.71 %, H 3.97 %, N 3.25 %. Found: C 55.88 %, H 3.92 %, N 3.33 %.

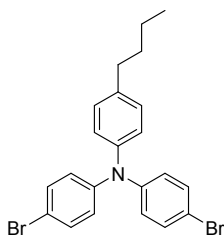
7.2.1.2. *N,N*-bis(4-bromophenyl)-2,4,6-trimethylaniline (**MTPA3**).



According to the general procedure, 2,4,6-trimethylaniline (2.97 g, 22 mmol) was used to give 3.7 g (38 %) of the title compound as white crystals.

^1H NMR (400 MHz, CDCl_3 , 32 °C): δ [ppm] = 7.27 (d, 4H, Ar-H, $^3J = 8.6$ Hz), 6.94 (s, 2H, Ar-H), 6.82 (d, 4H, Ar-H, $^3J = 8.9$ Hz), 2.32 (s, 3H, $-\text{CH}_3$), 1.98 (s, 6H, $-\text{CH}_3$). ^{13}C NMR (101 MHz, CDCl_3 , 32 °C): δ [ppm] = 144.8, 139.2, 137.4, 137.3, 132.1, 130.1, 121.1, 113.27, 21.0, 18.4. LR-MS (EI, 70 eV): $m/z = 446.6$ [M^+]. Anal. Calcd. for $\text{C}_{21}\text{H}_{19}\text{Br}_2\text{N}$: C 56.66 %, H 4.30 %, N 3.15 %. Found: C 56.64 %, H 4.28 %, N 3.19 %.

7.2.1.3. *N,N*-bis(4-bromophenyl)-4-butyylaniline (**MTPA4**)

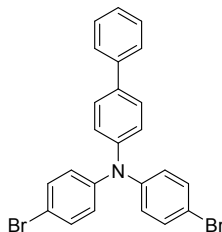


According to the general procedure, 4-butyylaniline (3.28 g, 22 mmol) was used to afford 6.36 g (63 %) of the title compound as white crystals.

^1H NMR (400 MHz, $\text{C}_2\text{D}_2\text{Cl}_4$, 32 °C): δ [ppm] = 7.25 (m, 4H, Ar-H), 7.01 (d, 2H, Ar-H, $^3J = 8.4$ Hz), 6.89 (d, 2H, Ar-H, $^3J = 8.3$ Hz), 6.85 (m, 4H, Ar-H), 2.49 (t, 2H, $-\alpha\text{CH}_2$, $^3J = 7.7$ Hz), 1.52 (m, 2H, $-\text{CH}_2-$), 1.29 (m, 2H, $-\text{CH}_2-$), 1.29 (t, 3H, $-\text{CH}_3$, $^3J = 7.3$ Hz). ^{13}C NMR (101 MHz, $\text{C}_2\text{D}_2\text{Cl}_4$, 32 °C): δ [ppm] = 146.9, 144.4, 139.2, 132.5, 129.8, 125.3,

125.2, 115.1, 35.3, 33.8, 22.7, 14.4. LR-MS (EI, 70 eV): $m/z = 459.6 [M^+]$. Anal. Calcd. for $C_{22}H_{21}Br_2N$: C 57.54 %, H 4.61 %, N 3.05 %. Found: C 57.81 %, H 4.53 %, N 3.14 %.

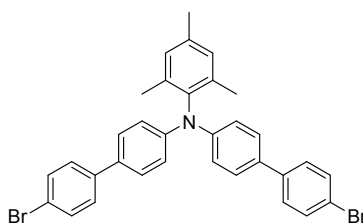
7.2.1.4. *N,N*-bis(4-bromophenyl)-4-phenylaniline (**MTPA5**)



According to the general procedure, 4-phenylaniline (3.72 g, 22 mmol) was used to give 5.48 g (52 %) of the title compound as white crystals.

1H NMR (400 MHz, $C_2D_2Cl_4$, 32 °C): δ [ppm] = 7.52 (d, 2H, Ar-H, $^3J = 7.5$ Hz), 7.44 (d, 2H, Ar-H, $^3J = 8.4$ Hz), 7.36 (t, 2H, Ar-H, $^3J = 7.5$ Hz), 7.30 (d, 4H, Ar-H, $^3J = 8.4$ Hz), 7.26 (t, 1H, Ar-H, $^3J = 7.5$ Hz), 7.05 (d, 2H, Ar-H, $^3J = 8.4$ Hz), 6.92 (d, 4H, Ar-H, $^3J = 8.4$ Hz). ^{13}C NMR (101 MHz, $C_2D_2Cl_4$, 32 °C): δ [ppm] = 146.6, 146.3, 140.4, 136.2, 132.7, 129.2, 128.3, 127.5, 126.9, 125.9, 124.7, 115.8. LR-MS (EI, 70 eV): $m/z = 479.6 [M^+]$. Anal. Calcd. for $C_{24}H_{17}Br_2N$: C 60.15 %, H 3.58 %, N 2.92 %. Found: C 60.30 %, H 3.51 %, N 2.99 %.

7.2.1.5. *N,N*-bis(4-bromo-1,1'-biphen-4'-yl)-2,4,6-trimethylaniline (**MTPA6**)



To a stirred solution of tris $Pd_2(dba)_3$ (126 mg, 0.138 mmol), DPPF (230 mg, 0.414 mmol), 1-bromo-4-iodobiphenyl (16.51 g, 46 mmol) and Na-*t*-BuO (5.3 g, 55 mmol) in 30 ml of toluene a solution of fresh distilled 2,4,6-trimethylaniline (2.97 g, 22 mmol) in 10 ml of toluene was slowly added at 80 °C. The reaction mixture was stirred for 24 hours at 90 °C. At the end of the reaction, the mixture was diluted with hot ethyl acetate and mixed with celite. The non-soluble solids were filtered off and washed several times with hot ethyl acetate. The filtrate was washed with aqueous, saturated EDTA solution and water, the organic layer subsequently dried over $MgSO_4$ and all solvents removed under vacuum. The raw product was then purified by column chromatography with hexane as eluent and

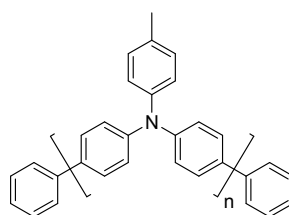
recrystallized from a methanol/2-propanol (1/3) mixture to afford 6.12 g (46 %) of the title compound as pale yellow crystals.

^1H NMR (400 MHz, CDCl_3 , 32 °C): δ [ppm] = 7.52 (d, 4H, Ar-H, $^3J = 8.7$ Hz), 7.42 (dd, 8H, Ar-H, $^3J = 8.6$ Hz), 7.07 (d, 4H, Ar-H, $^3J = 8.7$ Hz), 6.98 (s, 2H, Ar-H), 6.82 (d, 4H, Ar-H, $^3J = 8.9$ Hz), 2.35 (s, 3H, Ar- CH_3), 2.05 (s, 6H, Ar- CH_3). ^{13}C NMR (101 MHz, CDCl_3 , 32 °C): δ [ppm] = 145.5, 139.6, 137.6, 137.2, 132.3, 131.8, 130.1, 128.0, 127.5, 127.3, 120.7, 119.9, 21.1, 18.5. LR-MS (EI, 70 eV): $m/z = 597.6$ [M^+]. Anal. Calcd. for $\text{C}_{33}\text{H}_{27}\text{Br}_2\text{N}$: C 66.35 %, H 4.56 %, N 2.34 %. Found: C 66.87 %, H 4.42 %, N 2.59 %.

7.2.2. General procedure for the synthesis of triphenylamine-based polymers (PTPAs)

To a stirred solution of $\text{Ni}(\text{COD})_2$ (1.98 g, 7.2 mmol), BPy (1.124 g, 7.2 mmol) and COD (779 mg, 7.2 mmol) in 10 ml of DMF at 80 °C, a solution of the corresponding monomer (3 mmol) in 20 ml of toluene was slowly added under argon and protected from light. The reaction mixture was stirred at 90 °C for 48 hours. Afterwards, a solution of bromobenzene in toluene (3 ml, 1 M) was added and the reaction mixture stirred at this temperature for additional 24 hours. The mixture was then allowed to cool down to room temperature, diluted with 1000 ml of warm chloroform and filtered to remove the solid catalyst. The chloroform phase was washed several times with aqueous, saturated EDTA solution and water, concentrated and precipitated into 2000 ml of mixture of methanol/acetone/conc. aq. HCl (1/3/0.2, v/v/v). The greenish product was then filtered off, re-dissolved in chloroform and stirred overnight with 2 ml of aqueous hydrazine hydrate (80 %). The solvents were removed under vacuum, the polymer re-dissolved in small amount of chloroform and finally precipitated (as a highly concentrated solution) into 1000 ml of methanol to give a pale yellow solid. The raw polymer was extracted 24 hours in a soxhlet apparatus with ethyl acetate and additional 24 hours with chloroform. The chloroform fraction was concentrated and re-precipitated into methanol to obtain the target polymer as a pale yellow solid. In all cases, the chloroform fraction was used for the following characterization and OFET experiments.

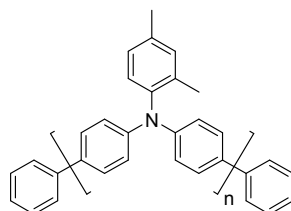
7.2.2.1. Poly(*N,N*-diphenyl-4-methylaniline) (PTPA1)



According to the general procedure, *N,N*-bis(4-bromophenyl)-4-methylaniline (1.251 g, 3 mmol) was polymerized to afford after extraction about 500 mg (approx. 65 %) of the title compound.

^1H NMR (400 MHz, CDCl_3 , 32 °C): δ [ppm] = 7.58 (d, Ar-H), 7.44 (m, Ar-H), 7.32 (d, Ar-H), 7.13 (d, Ar-H), 7.09 (m, Ar-H), 7.02 (d, Ar-H), 6.96 (d, Ar-H), 2.34 (s, $-\text{CH}_3$). ^{13}C NMR (101 MHz, CDCl_3 , 32 °C): δ [ppm] = 146.7, 145.0, 134.5, 132.1, 130.1, 130.0, 128.7, 127.2, 126.6, 125.1, 124.7, 123.7, 20.8. GPC Anal.: $M_n = 2\,500\text{ g}\cdot\text{mol}^{-1}$, $M_w = 5\,000\text{ g}\cdot\text{mol}^{-1}$, PD = 2.0. UV-Vis & PL (CHCl_3): $\lambda_{\text{max,ab}} = 373\text{ nm}$, $\lambda_{\text{max,em}} = 423\text{ nm}$. UV-Vis & PL (Film): $\lambda_{\text{max,ab}} = 375\text{ nm}$, $\lambda_{\text{max,em}} = 428\text{ nm}$.

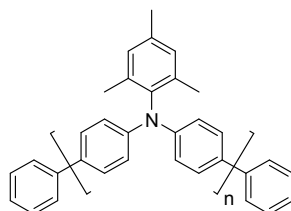
7.2.2.2. Poly(*N,N*-diphenyl-2,4-dimethylaniline) (**PTPA2**)



According to the general procedure, *N,N*-bis(4-bromophenyl)-2,4-dimethylaniline (1.293 g, 3 mmol) was polymerized to yield after extraction about 640 mg (approx. 75 %) of the title compound.

^1H NMR (400 MHz, CDCl_3 , 32 °C): δ [ppm] = 7.72 (d, Ar-H), 7.50 (d, Ar-H), 7.41 (m, Ar-H), 7.08 (d, Ar-H), 7.03 (d, Ar-H), 6.96 (m, Ar-H), 2.36 (s, $-\text{CH}_3$), 2.05 (s, $-\text{CH}_3$). ^{13}C NMR (101 MHz, CDCl_3 , 32 °C): δ [ppm] = 146.2, 142.5, 136.3, 135.9, 133.6, 132.4, 129.5, 128.1, 127.4, 127.3, 127.0, 121.5, 21.0, 18.4. GPC Anal.: $M_n = 4\,600\text{ g}\cdot\text{mol}^{-1}$, $M_w = 16\,600\text{ g}\cdot\text{mol}^{-1}$, PD = 3.6. UV-Vis & PL (CHCl_3): $\lambda_{\text{max,ab}} = 377\text{ nm}$, $\lambda_{\text{max,em}} = 418\text{ nm}$. UV-Vis & PL (Film): $\lambda_{\text{max,ab}} = 385\text{ nm}$, $\lambda_{\text{max,em}} = 422\text{ nm}$.

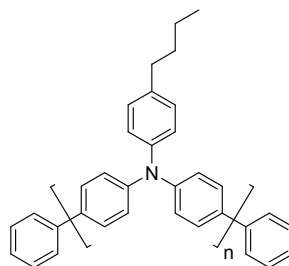
7.2.2.3. Poly(*N,N*-diphenyl-2,4,6-trimethylaniline) (**PTPA3**)



According to the general procedure, *N,N*-bis(4-bromophenyl)-2,4,6-trimethylaniline (1.336 g, 3 mmol) was polymerized to give after extraction about 750 mg (approx. 85 %) of the title compound.

^1H NMR (400 MHz, CDCl_3 , 32 °C): δ [ppm] = 7.72 (d, Ar-H), 7.65 (d, Ar-H), 7.50 (d, Ar-H), 7.46 (d, Ar-H), 7.43 (d, Ar-H), 7.36 (d, Ar-H), 7.08 (d, Ar-H), 7.04 (d, Ar-H), 6.97 (s, Ar-H), 2.36 (s, $-\text{CH}_3$), 2.05 (s, $-\text{CH}_3$). ^{13}C NMR (101 MHz, CDCl_3 , 32 °C): δ [ppm] = 144.7, 140.0, 137.7, 136.8, 133.0, 129.9, 128.8, 127.5, 127.4, 126.9, 126.7, 119.8, 21.0, 18.6. GPC Anal.: $M_n = 37\,600\text{ g}\cdot\text{mol}^{-1}$, $M_w = 68\,700\text{ g}\cdot\text{mol}^{-1}$, PD = 1.8. UV-Vis & PL (CHCl_3): $\lambda_{\text{max,ab}} = 389\text{ nm}$, $\lambda_{\text{max,em}} = 417\text{ nm}$. UV-Vis & PL (Film): $\lambda_{\text{max,ab}} = 390\text{ nm}$, $\lambda_{\text{max,em}} = 422\text{ nm}$.

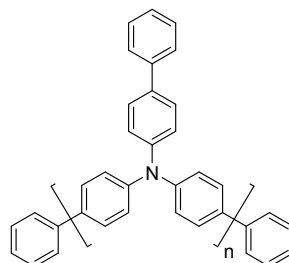
7.2.2.4. Poly(*N,N*-diphenyl-4-butylaniline) (**PTPA4**)



According to the general procedure, *N,N*-bis(4-bromophenyl)-4-butylaniline (1.378 g, 3 mmol) was polymerized to afford after extraction about 700 mg (approx. 80 %) of the title compound.

^1H NMR (400 MHz, $\text{C}_2\text{D}_2\text{Cl}_4$, 32 °C): δ [ppm] = 7.71 (m, Ar-H), 7.52 (m, Ar-H), 7.44 (d, Ar-H), 7.12 (d, Ar-H), 7.08 (m, Ar-H), 2.58 (m, $-\alpha\text{CH}_2$), 1.61 (m, $-\text{CH}_2-$), 1.38 (m, $-\text{CH}_2-$), 0.94 (m, $-\text{CH}_3$). ^{13}C NMR (101 MHz, CDCl_3 , 32 °C): δ [ppm] = 146.8, 145.1, 138.0, 134.6, 132.5, 130.8, 129.3, 128.8, 127.2, 124.9, 123.9, 123.8, 35.1, 33.6, 22.4, 14.0. GPC Anal.: $M_n = 8\,700\text{ g}\cdot\text{mol}^{-1}$, $M_w = 21\,400\text{ g}\cdot\text{mol}^{-1}$, PD = 2.5. UV-Vis & PL (CHCl_3): $\lambda_{\text{max,ab}} = 379\text{ nm}$, $\lambda_{\text{max,em}} = 423\text{ nm}$. UV-Vis & PL (Film): $\lambda_{\text{max,ab}} = 378\text{ nm}$, $\lambda_{\text{max,em}} = 428\text{ nm}$.

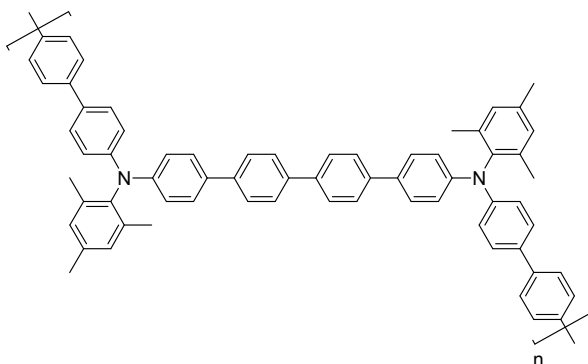
7.2.2.5. Poly(*N,N*-bis(phenyl)-4-phenylaniline-4,4'-yl) (**PTPA5**)



According to the general procedure, *N,N*-bis(4-bromophenyl)-4-phenylaniline (1.438 g, 3 mmol) was polymerized to give after extraction about 300 mg (approx. 30 %) of the title compound.

^1H NMR (400 MHz, CDCl_3 , 32 °C): δ [ppm] = 7.58 (m, Ar-H), 7.50 (m, Ar-H), 7.41 (m, Ar-H), 7.31 (m, Ar-H), 7.21 (m, Ar-H). ^{13}C NMR (101 MHz, CDCl_3 , 32 °C): δ [ppm] = 128.7, 127.9, 127.4, 127.3, 126.7, 124.5, 124.3. GPC Anal.: $M_n = 3\,200\text{ g}\cdot\text{mol}^{-1}$, $M_w = 4\,700\text{ g}\cdot\text{mol}^{-1}$, PD = 1.4. UV-Vis & PL (CHCl_3): $\lambda_{\text{max,ab}} = 370\text{ nm}$, $\lambda_{\text{max,em}} = 425\text{ nm}$. UV-Vis & PL (Film): $\lambda_{\text{max,ab}} = 378\text{ nm}$, $\lambda_{\text{max,em}} = 434\text{ nm}$, $\lambda_{\text{em}} = 460\text{ nm}$.

7.2.2.6. Poly[*N,N*-bis(1,1-biphenyl)-2,4,6-trimethylaniline] (**PTPA6**)

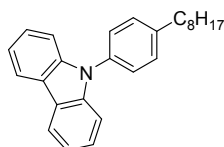


According to the general procedure, *N,N*-bis(4-bromo-1,1'-biphen-4'-yl)-2,4,6-trimethylaniline (1.792 g, 3 mmol) was polymerized to give after extraction about 1.1 g (approx. 85 %) of the title compound.

^1H NMR (400 MHz, $\text{C}_2\text{D}_2\text{Cl}_4$, 32 °C): δ [ppm] = 7.64 (m, Ar-H), 7.50 (d, Ar-H), 7.40 (m, Ar-H), 7.15 (m, Ar-H), 7.06 (d, Ar-H), 6.94 (s, Ar-H), 2.32 (s, $-\text{CH}_3$), 2.04 (s, $-\text{CH}_3$). ^{13}C NMR (101 MHz, CDCl_3 , 32 °C): δ [ppm] = 145.8, 139.8, 139.0, 137.9, 132.9, 130.8, 130.3, 128.0, 127.7, 127.4, 126.9, 120.6, 120.3, 21.3, 18.7. GPC Anal.: $M_n = 11\,200\text{ g}\cdot\text{mol}^{-1}$, $M_w = 19\,100\text{ g}\cdot\text{mol}^{-1}$, PD = 1.7. UV-Vis & PL (CHCl_3): $\lambda_{\text{max,ab}} = 382\text{ nm}$, $\lambda_{\text{max,em}} = 429\text{ nm}$. UV-Vis & PL (Film): $\lambda_{\text{max,ab}} = 385\text{ nm}$, $\lambda_{\text{max,em}} = 435\text{ nm}$, $\lambda_{\text{em}} = 454\text{ nm}$.

7.3. Synthesis of Carbazole-Based Monomers and Polymers

7.3.1. Synthesis of 9-(4-octylphenyl)carbazole (**NPC8**)

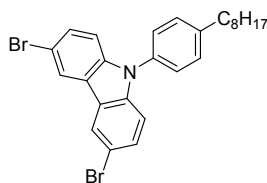


To 40 ml of ethylmagnesium bromide (40 mmol, 1 M in THF) a solution of carbazole (6.21 g, 37.1 mmol) in 20 ml of THF was added dropwise under nitrogen at room temperature. Then the THF of the reaction mixture was removed under vacuum and replaced by 20 ml of dry toluene. After addition of $\text{NiCl}_2(\text{PPh}_3)_2$ (972 mg, 1.49 mmol), PPh_3

(779 mg, 2.97 mmol) and 1-bromo-4-octylbenzene (8 g, 29.7 mmol) the reaction mixture was reacted at 100 °C for 8 hours, and then cooled down to room temperature, quenched with 40 ml water, and filtered through a pad of silica. The organic layer was separated, and the aqueous phase extracted with ether. The combined organic phases were dried over MgSO₄ and all solvents removed under vacuum. The residue was purified by column chromatography on silica gel with petroleum ether as eluent to afford 6.2 g (59 %) of the desired product.

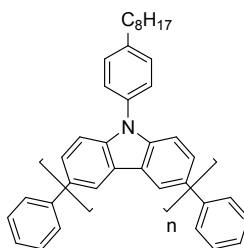
¹H NMR (400 MHz, C₂D₂Cl₄, 32 °C): δ [ppm] = 8.09 (d, 2H, Ar-H, ³J = 7.7 Hz), 7.43–7.32 (m, 8H, Ar-H), 7.24 (m, 2H, Ar-H), 2.68 (t, 2H, -αCH₂, ³J = 7.8 Hz), 1.67 (q, 2H, -CH₂-, ³J = 7.7 Hz), 1.42–1.19 (m, 10H, -CH₂-), 0.86 (t, 3H, -CH₃, ³J = 7.0 Hz). ¹³C NMR (101 MHz, C₂D₂Cl₄, 32 °C): δ [ppm] = 142.7, 141.2, 135.1, 130.1, 127.0, 126.3, 123.3, 120.5, 120.1, 110.3, 36.0, 32.2, 31.7, 29.8, 29.7, 29.6, 23.0, 14.6. LR-MS (EI, 70 eV): m/z = 354.8 [M⁺].

7.3.2. 3,6-Dibromo-9-(4-octylphenyl)carbazole (**MNPC8**)



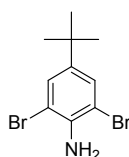
To a solution of 9-(4-octylphenyl)carbazole (4.03 g, 11.3 mmol) in 50 ml of DMF, a solution of *N*-bromosuccinimide (4.24 g, 23.8 mmol) in 35 ml of DMF was added dropwise under nitrogen at 0 °C. The reaction mixture was then allowed to warm up to room temperature, stirred for 3 hours and poured onto ice. The precipitate was filtered off and purified by recrystallization from hexane to afford 5.1 g (88 %) of the title compound as yellow crystals.

¹H NMR (400 MHz, C₂D₂Cl₄, 32 °C): δ [ppm] = 8.19 (d, 2H, Ar-H, ⁴J = 1.9 Hz), 7.49 (dd, 2H, Ar-H, ³J = 8.7 Hz, ⁴J = 1.9 Hz), 7.38 (m, 4H, Ar-H), 6.85 (d, 2H, Ar-H, ³J = 8.7 Hz), 2.73 (t, 2H, -αCH₂, ³J = 7.7 Hz), 1.72 (q, 2H, -CH₂-, ³J = 7.7 Hz), 1.36 (m, 10H, -CH₂-), 0.91 (t, 3H, -CH₃, ³J = 7.0 Hz). ¹³C NMR (101 MHz, C₂D₂Cl₄, 32 °C): δ [ppm] = 143.2, 140.1, 134.2, 130.0, 129.3, 126.8, 123.8, 123.1, 112.9, 111.6, 35.7, 31.9, 31.4, 29.5, 29.4, 29.3, 22.7, 14.1. LR-MS (EI, 70 eV): m/z = 512.5 [M⁺]. Anal. Calcd. for C₂₆H₂₇Br₂N: C 60.84 %, H 5.30 %, N 2.73 %. Found: C 61.03 %, H 5.25 %, N 2.81 %.

7.3.3. Poly[9-(4-octylphenyl)carbazole] (**PNPC8**)

A solution of 3,6-dibromo-9-(4-octylphenyl)carbazole (150 mg, 0.292 mmol), Ni(COD)₂ (177 mg, 0.643 mmol), BPy (110 mg, 0.701 mmol) and COD (76 mg, 0.701 mmol) in 2 ml of THF was irradiated with microwaves (300 W) at 120 °C for 12 min. A 1 M solution of bromobenzene (0.3 ml, 0.03 mmol) in toluene was then added and the reaction mixture stirred at 80 °C overnight. The reaction mixture was poured into 100 ml of chloroform and the non-soluble solids filtered off. The chloroform solution was washed with aqueous, saturated EDTA solution, water and stirred with 1 ml aqueous hydrazine hydrate (80 %) for 1 hour. Afterwards, the solvents were removed under vacuum. The grey solid was dissolved in a small amount of CHCl₃ and precipitated from a highly concentrated solution into 250 ml of methanol to afford 70 mg (68 %) of the target polymer as a grey solid.

¹H NMR (400 MHz, CDCl₃, 32 °C): δ [ppm] = 8.56 (s, Ar-H), 7.73 (d, Ar-H), 7.53–7.22 (m, Ar-H), 2.71 (m, -αCH₂), 1.71 (m, -CH₂-), 1.49-1.19 (m, -CH₂-), 0.89 (m, -CH₃). ¹³C NMR (101 MHz, CDCl₃, 32 °C): δ [ppm] = 142.0, 140.4, 134.1, 129.6, 127.3, 126.6, 125.6, 124.2, 118.7, 110.1, 35.7, 31.9, 31.5, 29.7, 29.5, 29.5, 29.3, 22.7, 14.1. GPC Anal.: M_n = 4 700 g·mol⁻¹, M_w = 6 100 g·mol⁻¹, PD = 1.3. UV-Vis & PL (CHCl₃): λ_{ab} = 259 nm, λ_{max,ab} = 313 nm, λ_{max,em} = 432 nm. UV-Vis & PL (Film): λ_{ab} = 259 nm, λ_{max,ab} = 322 nm, λ_{max,em} = 451 nm.

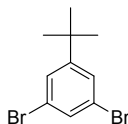
7.3.4. 2,6-Dibromo-4-*tert*-butylaniline

In a 250 ml flask 50 ml of a bromine solution (43 g, 270 mmol) in dichloromethane were added to a cold (0 °C), stirred solution of 4-*tert*-butylaniline (20 g, 134 mmol) in 100 ml of dichloromethane within 1 hour. The reaction mixture was then stirred for 2 more hours at 0 °C, allowed to warm up to room temperature and stirred for additional 12 hours. The white precipitate was filtered off and washed several times with dichloromethane to afford

32.5 g (79 %) of 2,6-dibromo-4-*tert*-butylaniline as white crystals. The product was used for the next step without further purification.

^1H NMR (400 MHz, $(\text{CD}_3)_2\text{SO}$, 32 °C): δ [ppm] = 7.37 (s, 2H, Ar-H), 5.37 (s, -NH₂), 1.20 (s, 9H, C-(CH₃)₃). ^{13}C NMR (101 MHz, $\text{C}_2\text{D}_2\text{Cl}_4$, 32 °C): δ [ppm] = 141.6, 140.3, 128.6, 107.8, 33.7, 30.9. LR-MS (EI, 70 eV): m/z = 306.2 [M^+].

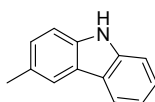
7.3.5. 3,5-Dibromo-1-*tert*-butylbenzene



Sodium nitrite (9 g, 130 mmol) in 9 ml of conc. sulphuric acid was added to a stirred solution of 2,6-dibromo-4-*tert*-butylaniline (19 g, 61 mmol) in 100 ml of ethanol and 34 ml of benzene, and the reaction mixture was refluxed for 3 hours. After addition of ether (200 ml) the organic layer was separated, washed with water, dried over Mg_2SO_4 and concentrated under vacuum. The oil obtained was then purified by column chromatography with hexane as eluent to give 9.3 g (52 %) of the desired product as colorless oil.

^1H NMR (400 MHz, $\text{C}_2\text{D}_2\text{Cl}_4$, 32 °C): δ [ppm] = 7.42 (m, 1H, Ar-H), 7.37 (m, 2H, Ar-H), 1.22 (s, 9H, -CH₃). ^{13}C NMR (101 MHz, $\text{C}_2\text{D}_2\text{Cl}_4$, 32 °C): δ [ppm] = 155.8, 131.4, 127.9, 123.0, 35.3, 31.3. LR-MS (EI, 70 eV): m/z = 293.0 [M^+].

7.3.6. 3-Methylcarbazole

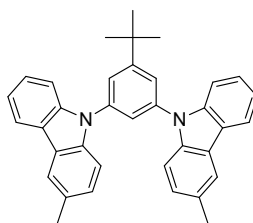


To a refluxed solution of *p*-tolylhydrazine hydrochloride (6.345 g, 40 mmol) and 5 ml of acetic acid in 150 ml of ethanol, a solution of cyclohexanone (4 ml, 60 mmol) in 50 ml of ethanol was added over 1 hour. The mixture was refluxed overnight and allowed to cool to room temperature. The solution was neutralized with aq. sodium carbonate until the carbon dioxide formation is finished and then cooled down to 0 °C. The formed solid was filtered off and washed several times with cold ethanol. In order to get the maximum of product, the filtrate was concentrated under vacuum, one more time cooled in the fridge. Finally all solids were filtered off. The beige product was mixed with 5 g palladium (5 %) on char coal in a 1,2,4-trimethylbenzene/water (1/3) mixture and refluxed overnight under argon and protected from light. The reaction mixture was diluted with hot CHCl_3 (150 ml),

the solids were filtered off and washed several times with hot CHCl_3 . The organic layer was separated and the solvents removed under vacuum. The product was then recrystallized several times from methanol to afford 5,89 g (82 %) of 3-methylcarbazole as white crystals.

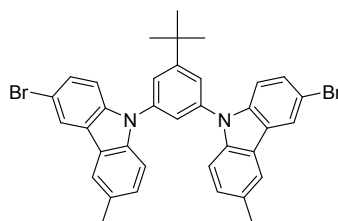
^1H NMR (400 MHz, CDCl_3 , 32 °C): δ [ppm] = 7.97 (d, 1H, $J = 8.0$ Hz, Ar-H), 7.94 (s, 1H, N-H), 7.80 (s, 1H, Ar-H), 7.33 (d, 2H, $J = 3.7$ Hz), 7.26 (d, 1H, $J = 8.2$ Hz), 7.17 (m, 2H), 2.47 (s, 3H). ^{13}C NMR (100 MHz, CDCl_3 , 32 °C): δ [ppm] = 140.0, 137.9, 129.1, 127.6, 126.1, 123.6, 123.3, 120.5 ($\times 2$), 119.6, 111.0, 110.7, 21.8. LR-MS (EI, 70 eV): $m/z = 180.8$ [M^+].

7.3.7. 1,3-Bis(6'-methylcarbazol-9'-yl)-5-*tert*-butylbenzene (**dCP**)



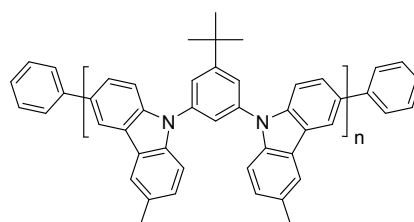
To a solution of $\text{Pd}_2(\text{dba})_3$ (22 mg, 24 μmol), 2-(di-*tert*-butylphosphino)biphenyl (14 mg, 48 μmol), 3-methylcarbazole (218 mg, 1.2 mmol) and $\text{NaO-}t\text{-Bu}$ (250 mg, 2.6 mmol) in 4 ml of toluene, a solution of 1,5-dibromo-5-*tert*-butylbenzene in 2 ml of toluene was added dropwise and the reaction mixture reacted at 100 °C for 3 hours. Afterwards, the mixture was allowed to cool down to room temperature, all solvents removed under vacuum and the raw product diluted with chloroform (20 ml). The chloroform phase was washed with aqueous, saturated EDTA solution and water, and finally dried over MgSO_4 . The crude product was then purified by column chromatography (hexane/dichloromethane/triethylamine, 1/9/0.5 %) and dried under high vacuum to afford 260 mg (90 %) of the title compound as a white solid.

^1H NMR (400 MHz, $(\text{CD}_3)_2\text{SO}$, 32 °C): δ [ppm] = 8.18 (d, 1H, Ar-H, $^3J = 7.7$ Hz), 7.99 (s, 2H, Ar-H), 7.69 (d, 2H, Ar-H, $^4J = 1.7$ Hz), 7.53 (t, 1H, $^4J = 1.7$ Hz), 7.49 (d, 2H, $^3J = 8.2$ Hz), 7.40 (m, 4H, Ar-H), 7.22 (m, 4H, Ar-H), 2.44 (s, 6H, $-\text{CH}_3$), 1.39 (s, 9H, $-(\text{CH}_3)_3$). ^{13}C NMR (101 MHz, $(\text{CD}_3)_2\text{SO}$, 32 °C): δ [ppm] = 153.6, 139.5, 137.7, 137.6, 128.2, 126.0, 124.6, 122.3, 122.1, 121.4, 120.5, 119.0, 118.6, 108.3, 108.4, 108.1, 34.0, 30.0, 20.0. LR-MS (EI, 70 eV): $m/z = 495.4$ [M^+].

7.3.8. 1,3-Bis(3'-bromo-6'-methylcarbazole-9'-yl)-5-*tert*-butylbenzene (**MdCP**)

To a stirred solution of 1,3-bis(6'-methylcarbazole-9'-yl)-5-*tert*-butylbenzene (493 mg, 1 mmol) in 10 ml of acetonitrile, NBS (445 mg, 2.5 mmol) was added in 10 portions under protection from light. The mixture was stirred for 3 hours at room temperature. At the end of the reaction, the mixture was poured into ice, the precipitate filtered off and washed with cold acetonitrile. The raw product was purified by column chromatography (hexane/dichloromethane, 9/1) to afford 597 mg (92 %) of the title compound as a white powder.

^1H NMR (400 MHz, $\text{C}_2\text{D}_2\text{Cl}_4$, 32 °C): δ [ppm] = 8.16 (d, 2H, Ar-H, $^4J = 1.8$ Hz), 7.83 (s, 2 H), 7.59 (d, 2H, Ar-H, $^4J = 1.7$ Hz), 7.46 (dd, 3H, Ar-H, $^3J = 8.8$ Hz, $^4J = 1.7$ Hz), 7.36 (d, 2H, Ar-H, $^3J = 8.4$ Hz), 7.33 (d, 2H, Ar-H, $^3J = 8.7$ Hz), 7.24 (d, 2H, Ar-H, $^3J = 8.4$ Hz), 2.48 (s, 6H, $-\text{CH}_3$), 1.38 (s, 9H, $-(\text{CH}_3)_3$). ^{13}C NMR (101 MHz, $\text{C}_2\text{D}_2\text{Cl}_4$, 32°C): δ [ppm] = 155.8, 139.7, 139.5, 138.8, 130.6, 129.0, 128.7, 125.3, 123.4, 123.2, 122.7, 121.6, 120.8, 113.0, 111.6, 110.1, 52.9, 35.6, 31.5, 21.7. LR-MS (EI, 70 eV): $m/z = 648.3$ [M^+]. Anal. Calcd. % for $\text{C}_{36}\text{H}_{30}\text{Br}_2\text{N}_2$: C 66.48 %, H 4.65 %, N 4.31 %. Found: C 66.68 %, H 4.77 %, N 4.10 %.

7.3.9. Poly[1,3-bis(3'-methylcarbazole-9'-yl)-5-*tert*-butylphenylene-6',6''-diyl] (**PdCP**)

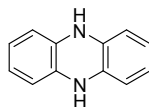
A solution of 1,3-bis(3'-bromo-6'-methylcarbazole-9'-yl)-5-*tert*-butylbenzene (150 mg, 0.231 mmol), $\text{Ni}(\text{COD})_2$ (140 mg, 0.507 mmol), BPy (86 mg, 0.553 mmol) and COD (60 mg, 0.553 mmol) in 2 ml of THF was irradiated with microwaves (300 W) at 120 °C for 12 min. A 0.1 M solution of bromobenzene in toluene (0.25 ml, 0.025 mmol) was then added and the reaction mixture stirred at 80 °C overnight. The reaction mixture was

poured into 100 ml of chloroform and the non-soluble solids filtered off. The chloroform solution was washed with aqueous, saturated EDTA solution, water and stirred with 1 ml of aqueous hydrazine hydrate (80 %) for 1 hour. Afterwards, the solvents were removed under vacuum. The grey solid was dissolved in a small amount of CHCl_3 and precipitated from a highly concentrated solution into 250 ml of methanol to afford 91 mg (80 %) of the target polymer as a grey solid.

^1H NMR (400 MHz, CDCl_3 , 32 °C): δ [ppm] = 8.48 (s, Ar-H), 8.08 (s, Ar-H), 7.84 (d, Ar-H), 7.78 (m, Ar-H), 7.70 (d, Ar-H), 7.52 (m, Ar-H), 7.33 (d, Ar-H), 2.60 (s, $-\text{CH}_3$), 1.53 (s, $-(\text{CH}_3)_3$). ^{13}C NMR (101 MHz, CDCl_3 , 32 °C): δ [ppm] = 140.0, 139.5, 139.2, 134.4, 129.7, 127.6, 125.88, 124.1, 124.0, 122.6, 121.6, 120.5, 118.9, 110.0, 109.7, 35.4, 31.4, 21.4. GPC Anal.: $M_n = 25\,000\text{ g}\cdot\text{mol}^{-1}$, $M_w = 57\,000\text{ g}\cdot\text{mol}^{-1}$, PD = 2.3. UV-Vis & PL (CHCl_3): $\lambda_{\text{max,ab}} = 252\text{ nm}$, $\lambda_{\text{ab}} = 309\text{ nm}$, $\lambda_{\text{ab}} = 355\text{ nm}$, $\lambda_{\text{max,em}} = 414\text{ nm}$. UV-Vis & PL (Film): $\lambda_{\text{max,ab}} = 247\text{ nm}$, $\lambda_{\text{ab}} = 309\text{ nm}$, $\lambda_{\text{ab}} = 358\text{ nm}$, $\lambda_{\text{max,em}} = 421\text{ nm}$.

7.4. Synthesis of the Phenazine-Based Materials

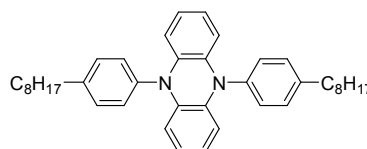
7.4.1. 5,10-Dihydrophenazine



To a solution of phenazine (10 g, 55.5 mmol) dissolved in 300 ml of boiling ethanol under argon, a solution of sodium dithionite (19.3 g, 110.1 mmol) in 300 ml of water was added over one hour. The reaction mixture was then stirred for 2.5 hours at room temperature. The precipitate was filtered off and dried under vacuum overnight to afford 9.8 g (97 %) of a slightly greenish product.

^1H NMR (400 MHz, $(\text{CD}_3)_2\text{SO}$, 32 °C): δ [ppm] = 7.25 (s, 2H, N-H), 6.26 (m, 4H, Ar-H), 6.01 (m, 4H, Ar-H). ^{13}C NMR (101 MHz, $(\text{CD}_3)_2\text{SO}$, 32 °C): δ [ppm] = 133.7, 120.2, 111.3. LR-MS (EI, V): $m/z = 180.2$ [M^+].

7.4.2. 5,10-Bis(4-octylphenyl)-5,10-dihydrophenazine (**d8PPz**)

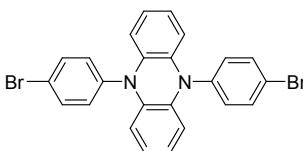


To a solution of $\text{Pd}_2(\text{dba})_3$ (9.2 mg, 10 μmol), 2-(dicyclohexylphosphino)biphenyl (10.5 mg, 30 μmol), 1-octyl-4-bromophenyl (80 mg, 3 mmol) and $\text{NaO}-t\text{-Bu}$ (346 mg, 3.6 mmol) in

3 ml of toluene, a solution of 5,10-dihydrophenazine (182 mg, 1 mmol) in 2 ml of toluene was slowly added at 80 °C. The reaction mixture was stirred for 24 hours at 90 °C under protection from light. The mixture was then allowed to cool down to room temperature, diluted with hot chloroform and mixed with celite. The non-soluble solids were filtered off and washed several times with hot chloroform. The chloroform filtrates were washed with saturated, aqueous EDTA solution and water. The organic layer was subsequently dried over MgSO₄ and all solvents removed under vacuum. The raw product was then purified by flash chromatography using chloroform as an eluent and further recrystallized from toluene to afford 528 mg (94 %) of the title compound as orange crystals.

¹H NMR (400 MHz, 32 °C): decomposition during the recording of the spectra. ¹³C NMR (101 MHz, 32 °C): decomposition during the recording of the spectra. LR-MS (EI, 70 eV): m/z = 557.3 [M⁺].

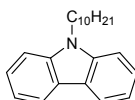
7.4.3. 5,10-Bis(4-bromophenyl)-5,10-dihydrophenazine (**MdPPz**)



To a solution of Pd₂(dba)₃ (27.5 mg, 30 μmol), 2-(dicyclohexylphosphino)biphenyl (31.5 mg, 90 μmol), 1-Bromo-4-iodobenzene (2.55 g, 9 mmol) and NaO-*t*-Bu (1.038 g, 10.8 mmol) in 10 ml of toluene, a solution of 5,10-dihydrophenazine (546 mg, 3 mmol) in 5 ml of toluene was slowly added at 80 °C. The reaction mixture was stirred for 24 hours at 90 °C under protection from light. The mixture was then allowed to cool down to room temperature, diluted with hot chloroform and mixed with celite. The non-soluble solids were filtered off and extracted several times with hot chloroform. The chloroform filtrates were washed with saturated, aqueous EDTA solution and water. The organic layer was subsequently dried over MgSO₄ and all solvents removed under vacuum. The raw product was then purified by recrystallization from toluene to afford 3.41 g (77 %) of the title compound as yellow crystals.

¹H NMR (400 MHz, 32 °C): decomposition during the recording of the spectra. ¹³C NMR (101 MHz, 32 °C): decomposition during the recording of the spectra. LR-MS (EI, 70 eV): m/z = 490.7 [M⁺].

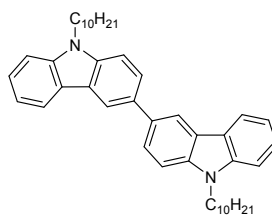
7.4.4. 9-Decylcarbazole



To a stirred solution of carbazole (10 g, 60 mmol) and benzyltriethylammoniumchloride (400 mg, 3 %mol) in 50 ml of toluene at room temperature, 1-bromodecane (14 g, 70 mmol) was added dropwise and the mixture refluxed overnight. Afterwards, the reaction mixture was washed with water, dried over MgSO_4 and concentrated. The crude was purified by column chromatographie (hexane/triethylamine, 98/2) to afford 16.3 g (88 %) of the title compound as a colorless oil.

^1H NMR (400 MHz, CDCl_3 , 32 °C): δ [ppm] = 8.06 (d, 2H, Ar-H, $^3J = 7.7$ Hz), 7.44 (t, 2H, Ar-H, $^3J = 8.1$ Hz), 7.38 (d, 2H, Ar-H, $^3J = 7.8$ Hz), 4.23 (t, 2H, $-\alpha\text{CH}_2$, $^3J = 7.3$ Hz), 1.82 (q, 2H, $-\text{CH}_2-$, $^3J = 7.3$ Hz), 1.40-1.18 (m, 14H, $-\text{CH}_2-$), 0.85 (t, 3H, $-\text{CH}_3$, $^3J = 7.0$ Hz). ^{13}C NMR (101 MHz, CDCl_3 , 32 °C): δ [ppm] = 140.4, 126.0, 122.9, 120.6, 119.1, 109.1, 43.4, 32.2, 29.85, 29.7, 29.6, 29.3, 27.6, 23.0, 14.5. LR-MS (EI, 70 eV): $m/z = 307.2$ [M^+].

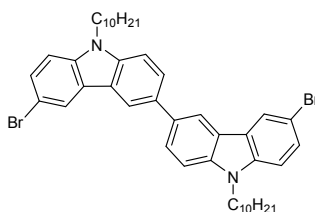
7.4.5. 9,9'-Didecyl-3,3'-bicarbazole



A solution of 9-decylcarbazole (10 g, 32.5 mmol) and iron(III) chloride (10.5 g, 65 mmol) in 150 ml of chloroform was stirred overnight at room temperature. The reaction was quenched with water, the organic layer separated, washed with water and dried over MgSO_4 . After removal of the solvents, the raw product was purified by column chromatography (hexane/dichloromethane/triethylamine, 80/19/1) and recrystallized from a dichloromethane/hexane mixture to yield 81 % (16.1 g) of the carbazole dimer as white crystals.

^1H NMR (400 MHz, CDCl_3 , 32 °C): δ [ppm] = 8.42 (d, 2H, Ar-H, $^4J = 1.5$ Hz), 8.20 (d, 2H, Ar-H, $^3J = 7.7$ Hz), 7.84 (dd, 2H, Ar-H, $^3J = 8.4$ Hz, $^4J = 1.7$ Hz), 7.49 (m, 4H, Ar-H), 7.44 (d, 2H, Ar-H, $^3J = 8.0$ Hz), 7.27 (t, 2H, Ar-H, $^3J = 6.9$ Hz), 4.35 (t, 4H, $-\alpha\text{CH}_2$, $^3J = 7.2$ Hz), 1.93 (q, 4H, $-\text{CH}_2-$, $^3J = 7.2$ Hz), 1.48-1.22 (m, 28H, $-\text{CH}_2-$), 0.90 (t, 6H, $-\text{CH}_3$, $^3J = 7.0$ Hz). ^{13}C NMR (101 MHz, CDCl_3 , 32 °C): δ [ppm] = 140.9, 139.6, 133.4, 125.6, 125.5, 123.4, 123.1, 120.4, 118.9, 118.7, 108.9, 108.8, 43.2, 31.9, 29.5 ($\times 2$), 29.4, 29.3, 29.0, 27.3, 22.7, 14.1. LR-MS (EI, 70 eV): $m/z = 610.9$ [M^+].

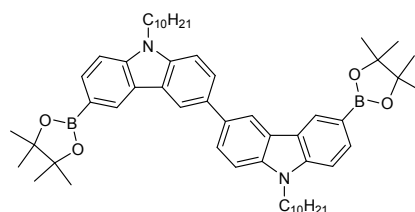
7.4.6. 6,6'-Dibromo-9,9'-didecyl-3,3'-bicarbazole



To a stirred solution of 9,9'-didecyl-3,3'-bicarbazole (6 g, 9.8 mmol) in 200 ml of THF at 0 °C, NBS (3.5 g, 19.6 mmol) was added in small portions. The mixture was allowed to warm up to room temperature and stirred overnight. The THF was then removed under vacuum, the mixture diluted with diethyl ether and washed several times with water. The organic layer was dried over MgSO₄ and concentrated. The raw product was purified by column chromatography (hexane/dichloromethane, 95/5) and recrystallized from an hexane/dichloromethane mixture to afford 4.8 g (64 %) of the title compound as white crystals.

¹H NMR (400 MHz, C₂D₂Cl₄, 32 °C): ppm] = 8.26 (d, 2H, Ar-H, ⁴J = 1.5 Hz), 8.22 (d, 2H, Ar-H, ⁴J = 1.8 Hz), 7.78 (dd, 2H, Ar-H, ³J = 8.5 Hz, ⁴J = 1.6 Hz), 7.50 (dd, 2H, Ar-H, ³J = 8.7 Hz, ⁴J = 1.9 Hz), 7.44 (d, 2H, Ar-H, ³J = 8.6 Hz), 7.25 (d, 2H, Ar-H, ³J = 8.7 Hz), 4.23 (t, 4H, -αCH₂, ³J = 7.2 Hz), 1.82 (q, 4H, -CH₂-, ³J = 7.2 Hz), 1.37-1.13 (m, 28H, -CH₂-), 0.81 (t, 6H, -CH₃, ³J = 7.0 Hz). LR-MS (EI, 70 eV): m/z = 768.7 [M⁺].

7.4.7. 9,9'-Didecyl-6,6'-bis(4,4,5,5-tetramethyl-1,3,2-dioxaborolan-2-yl)-3,3'-bicarbazole

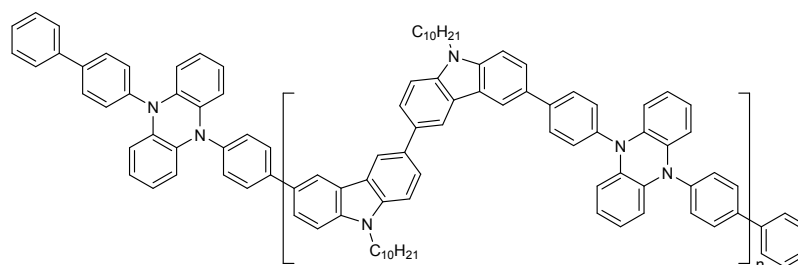


To a stirred solution of 6,6'-dibromo-9,9'-didecyl-3,3'-bicarbazole (4.6 g, 6 mmol) in 100 ml of THF under argon at -78 °C, a 1.6 N solution of *n*-BuLi in hexane (10 ml, 16 mmol) was added dropwise and the mixture stirred for 1.5 hours. Afterwards, 2-isopropoxy-4,4,5,5-tetramethyl-1,3,2-dioxaborolane (3.5 g, 19 mmol) was added dropwise, the mixture allowed to warm up to room temperature and stirred overnight. The THF was then removed under vacuum, the mixture diluted with diethyl ether and washed several times with water. The organic layer was dried over MgSO₄ and

concentrated. The raw product was purified by recrystallization from a hexane/diethyl ether mixture to yield 3.7 g (71 %) of the desired product as white crystals.

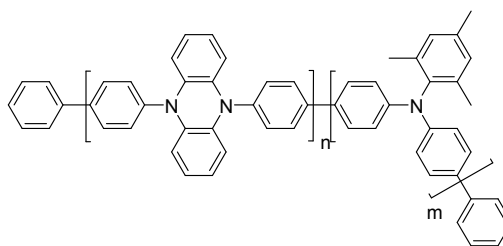
^1H NMR (400 MHz, CDCl_3 , 32 °C): δ [ppm] = 8.72 (s, 2H, Ar-H), 8.50 (s, 2H, Ar-H), 7.95 (d, 2H, Ar-H, $^3J = 8.2$ Hz), 7.85 (d, 2H, Ar-H, $^3J = 8.5$ Hz), 7.50 (d, 2H, Ar-H, $^3J = 8.4$ Hz), 7.42 (d, 2H, Ar-H, $^3J = 8.3$ Hz), 4.35 (t, 4H, $-\alpha\text{CH}_2$, $^3J = 7.0$ Hz), 1.92 (m, 4H, $-\text{CH}_2-$), 1.43 (m, 24H, $-\text{CH}_3$), 1.26 (m, 28H, $-\text{CH}_2-$), 0.89 (t, 6H, $-\text{CH}_3$, $^3J = 7.0$ Hz). ^{13}C NMR (101 MHz, CDCl_3 , 32 °C): δ [ppm] = 140.9, 139.6, 133.4, 128.3, 127.2, 125.6, 125.5, 123.4, 123.1, 120.4, 118.9, 108.9, 43.2, 31.9, 29.5 ($\times 2$), 29.4, 29.3, 29.0, 27.3, 22.7, 14.1. LR-MS (EI, 70 eV): $m/z = 862.1$ [M^+].

7.4.8. Alternating Copolymer **dPPz**/Bis-*N*-decylcarbazol (**PdPPz1**)



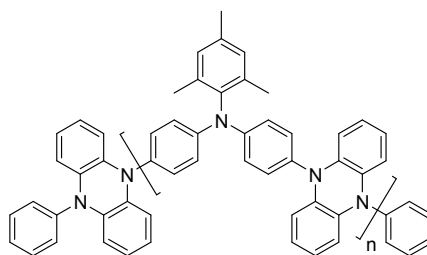
A 25 ml Schlenk tube containing a mixture of **MdPPz** (147.7 mg, 0.3 mmol) and 9,9'-Didecyl-6,6'-bis(4,4,5,5-tetramethyl-1,3,2-dioxaborolan-2-yl)-3,3'-bicarbazole (259.5 mg, 0.3 mmol), 1 drop of Aliquat 336, aqueous saturated K_2CO_3 (3 ml, 6 mmol) and 2 mol% of tetrakis(triphenylphosphine)palladium(0) catalyst (7 mg, 6 μmol) in 5 ml of toluene was stirred at 55 °C for 48 hours under argon and protected from light. The polymer formed was end-capped by addition of a mixture of 7 mg phenylboronic acid and some fresh catalyst in 1 ml of toluene and stirred at 55 °C for 24 more hours. The reaction mixture was then stopped with the addition of aq. 2 w% NaCN and stirred for several hours. This procedure was then repeated one more time with fresh aq. NaCN. The organic layer was separated, dried over MgSO_4 and the solvent removed. The polymer was precipitated from a highly concentrated chloroform solution into 100 ml of methanol to afford 248 mg (88 %) of the target polymer as an orange solid.

^1H NMR (400 MHz, 32 °C): decomposition during the recording of the spectra. ^{13}C NMR (101 MHz, 32 °C): decomposition during the recording of the spectra. GPC Anal.: $M_n = 2\ 100\ \text{g}\cdot\text{mol}^{-1}$, $M_w = 2\ 400\ \text{g}\cdot\text{mol}^{-1}$, $D = 1.16$. UV-Vis & PL (CHCl_3): $\lambda_{\text{max,ab}} = 358\ \text{nm}$, $\lambda_{\text{ab}} = 308\ \text{nm}$.

7.4.9. Random Copolymer **dPPz(20%)/TPA3 (PdPPz2)**

To a stirred mixture of $\text{Ni}(\text{COD})_2$ (999 mg, 3.6 mmol), BPy (562 mg, 3.6 mmol) and COD (389 mg, 3.6 mmol) in 5 ml of DMF at 80 °C, a solution of 5,10-bis(4-bromophenyl)-5,10-dihydrophenazine **MdPPz** (148 mg, 0.2 mmol) and *N,N*-bis(4-bromophenyl)-2,4,6-methylaniline **MTPA3** (534 mg, 1.2 mmol) in 10 ml of toluene was added. The resulting mixture was stirred at 80 °C for 48 hours under protection from light. Afterwards, a 0.1 M solution of bromobenzene in toluene (1.5 ml, 0.15 mmol) was added and the mixture stirred for additional 24 hours. The mixture was then allowed to cool down to room temperature, dissolved in warm CHCl_3 and filtered to remove the solid catalyst. The chloroform phase was washed several times with saturated, aqueous EDTA solution and water, and stirred overnight with 2 ml of aqueous hydrazine hydrate (80 %). The solvents were then removed under vacuum, the polymer re-dissolved in a small amount of chloroform and finally precipitated from a highly concentrated solution into 750 ml of methanol to give a pale yellow solid. The raw polymer was extracted 24 hours with dichloromethane, and then 24 hours with chloroform. The chloroform extract was concentrated and re-precipitated one more time into 150 ml of methanol to give 289 mg (56 %) of the polymer as beige solid.

^1H NMR (400 MHz, CDCl_3 , 32 °C): δ [ppm] = 7.41 (d, Ar-H), 7.03 (d, Ar-H), 6.96 (s, Ar-H), 2.36 (s, $-\text{CH}_3$), 2.05 (s, $-\text{CH}_3$). ^{13}C NMR (101 MHz, CDCl_3 , 32 °C): δ [ppm] = 144.7, 140.0, 137.7, 136.8, 133.0, 129.9, 126.9, 119.8, 21.0, 18.6. GPC Anal.: $M_n = 21\,000\text{ g}\cdot\text{mol}^{-1}$, $M_w = 33\,600\text{ g}\cdot\text{mol}^{-1}$, $D = 1.6$. UV-Vis & PL (CHCl_3): $\lambda_{\text{max,ab}} = 388\text{ nm}$, $\lambda_{\text{max,em}} = 417\text{ nm}$. UV-Vis & PL (Film): $\lambda_{\text{max,ab}} = 389\text{ nm}$, $\lambda_{\text{max,em}} = 421\text{ nm}$.

7.4.10. Alternating Copolymer Phenazine **TPA3 (PdPPz3)**

To a mixture of 5,10-dihydrophenazine (182 mg, 1 mmol), *N,N*-bis(4-bromophenyl)-2,4,6-methylaniline **MTPA3** (445 mg, 1 mmol) and NaO-*t*-Bu (269 mg, 2.8 mmol) in 18 ml of toluene, a solution of Pd₂(dba)₃ (18 mg, 0.02 mmol) in 2 ml of toluene and P(*t*-Bu)₃ as 1 M toluene solution (0.4 ml, 0.04 mmol) were added under argon. The reaction mixture was stirred at 90 °C for 48 hours. For end-capping, bromobenzene as 0.1 M solution in toluene (1 ml, 0.1 mmol) was added and the mixture stirred for additional 8 hours. The mixture was then allowed to cool down to room temperature, diluted with hot chloroform and filtered to remove most of the catalyst. The organic phase was washed several times with saturated, aqueous EDTA solution and water, and stirred overnight with 2 ml of aqueous hydrazine hydrate (80 %). The solvents were then removed under vacuum, the polymer dissolved in a small amount of chloroform (2 ml) and finally re-precipitated from a highly concentrated solution into 150 ml of methanol to give a pale orange, solid product. The raw polymer was extracted 24 hours with dichloromethane, and then 24 hours with chloroform. The chloroform extract was concentrated and precipitated into 400 ml of methanol to give 298 mg (64 %) of the target polymer as a pale orange solid.

¹H NMR (400 MHz, 32 °C): decomposition during the recording of the spectra.
¹³C NMR (101 MHz, 32 °C): decomposition during the recording of the spectra.
GPC Anal.: M_n = 6 700 g·mol⁻¹, M_w = 7 700 g·mol⁻¹, D = 1.15. UV-Vis & PL (CHCl₃):
λ_{max,ab} = 258 nm, λ_{ab} = 312 nm, λ_{ab,sh} = 375 nm, λ_{ab,sh} = 475 nm.

References and Notes

- [1] P. Lahrude, C. Becq, *Rev. Hist. Pharm.* **2003**, *51*, 68.
- [2] C. Goodyear, *Gum-Elastic Vol. 1*, Published privately, New Heaven **1855**.
- [3] L.H. Baekeland, *Chemiker Zeitung* **1909**, *33*, 317.
- [4] R.A. Gortner, *Colloids in chemistry, J. Educ. Chem.* **1934**, *29*, 279.
- [5] H. Staudinger, *Ber. Deut. Chem. Ges.* **1920**, *53*, 1073.
- [6] a) H. Shirakawa, E.J. Louis, A.G. MacDiarmid, C.K. Chiang, A.J. Heeger, *J. Chem. Soc. Chem. Comm.* **1977**, 579 ; b) C.K. Chiang, C.R. Fischer, Y.W. Park, A.J. Heeger, H. Shirakawa, E.J. Louis, S.C. Gau, A.G. MacDiarmid, *Phys. Rev. Lett.* **1977**, *39*, 1098 ; c) C.K. Chiang, M.A. Druy, S.C. Gau, A.J. Heeger, E.J. Louis, A.G. MacDiarmid, Y.W. Park, H. Shirakawa, *J. Am. Chem. Soc.* **1978**, *100*, 1013.
- [7] U. Scherf, "Oligo- and Polyarylenes, Oligo- and Polyarylenevinylenes" in: *Topics in Current Chemistry* **1999**, *201*.
- [8] U. Scherf, E.J.W. List, *Adv. Mater.* **2002**, *14*, 477.
- [9] D. Fichou, *Handbook of Oligo- and Polythiophenes*, Wiley-VCH, Weinheim **1999**.
- [10] D.S. Weiss, M. Abkowitz, "Organic Photoconductors" in: *Springer Handbook of Electronic and Photonic Materials*, Ed. S. Kasap, P. Capper, Springer, New York, **2006**, 953.
- [11] K. Müllen, U. Scherf, *Organic Light-Emitting Devices*, Wiley-VCH, Weinheim **2006**.
- [12] a) C.D. Dimitrakopoulos, P.R.L. Malenfant, *Adv. Mater.* **2002**, *14*, 99 ; b) A. Facchetti, M.H. Yoon, T.J. Marks, *Adv. Mater.* **2005**, *17*, 1705.
- [13] S. Günes, H. Neugebauer, N.S. Sariciftci, *Chem. Rev.* **2007**, *107*, 1324.
- [14] S.W. Thomas III, G.D. Joly, T.M. Swager, *Chem. Rev.* **2007**, *107*, 1339.
- [15] H. Rost, *Kunststoffe* **2005**, *10*, 209.
- [16] S. Allard, M. Forster, B. Souharce, H. Thiem, U. Scherf, *Angew. Chem.* **2008**, in press.
- [17] a) J. Paloheimo, H. Strubb, P. Yli-Lathi, P. Kuivalainen, *Synth. Met.* **1991**, *41*, 563 ; b) C.D. Dimitrakopoulos, D.J. Mascaro, *IBM J. Res. & Dev.* **2001**, *45*, 11.
- [18] M. Thelakkat, *Macromol. Mater. Eng.* **2002**, *287*, 442.
- [19] a) J. Veres, S.D. Ogier, S.W. Leeming, B. Brown, D.C. Cupertino, *Mat. Res. Soc. Symp. Proc.* **2002**, *708*, BB8.7.1 ; b) L.A. Majewski, M. Grell, S.D. Ogier, J. Veres, *Org. Elect.* **2003**, *4*, 27 ; c) J. Veres, S.D. Ogier, S.W. Leeming, D.C. Cupertino, S.M. Khaffaf, *Adv. Funct. Mater.* **2003**, *13*, 199 ; d) J. Veres, S.D. Ogier, G. Lloyd, D. de Leeuw, *Chem. Mater.* **2004**, *16*, 4543.
- [20] a) M. Stolka, J.F. Yanus, D.M. Pai, *J. Phys. Chem.* **1984**, *88*, 4707 ; b) P.M. Borsenberger, D.S. Weiss, *Organic Photoreceptors for Imaging Systems*, Marcel Dekker, New York **1993**.
- [21] a) E.T. Seo, R.F. Nelson, J.M. Fritsch, L.S. Marcoux, D.W. Leedy, R.N. Adams, *J. Am. Chem. Soc.* **1966**, *88*, 3498 ; b) R.F. Nelson, R.N. Adams, *J. Am. Chem. Soc.* **1968**, *90*, 3925.
- [22] T. Sumiyoshi, *Chem. Lett.* **1995**, *24*, 645.

- [23] P.M. Borsenberger, L. Pautmeier, H. Bässler, *J. Chem Phys.* **1991**, *94*, 5447.
- [24] a) Y. Shirota, *J. Mater. Chem.* **2000**, *10*, 1 ; b) W. Ishikawa, H. Inada, H. Nakano, Y. Shirota, *Chem. Lett.* **1991**, 1731 ; c) Y. Shirota, T. Kobata, N. Noma, *Chem. Lett.* **1989**, 1145 ; d) H. Inada, Y. Shirota, *J. Mater. Chem.* **1993**, *3*, 319 ; e) M. Thelakkat, H.W. Schmidt, *Adv. Mater.* **1998**, *10*, 219.
- [25] M. Thelakkat, H.W. Schmidt, *Adv. Mater.* **1998**, *10*, 219.
- [26] M. Thelakkat, C. Schmitz, C. Hohle, P. Strohhriegl, H.W. Schmidt, U. Hofmann, S. Schloter, D. Haarer, *Phys. Chem. Chem. Phys.* **1999**, *1*, 1693.
- [27] W. Ishikawa, K. Noguchi, Y. Kuwabara, Y. Shirota, *Adv. Mater.* **1993**, *5*, 559.
- [28] M. Thelakkat, A. Bacher, R. Fink, F. Haubner, H.W. Schmidt, *Macromol. Symp.* **1997**, *125*, 157.
- [29] a) H. Zhao, C. Tanjutco, S. Thayumanavan, *Tetrahedron Lett.* **2001**, *42*, 4421 ; b) J. Louie, J.F. Hartwig, *Tetrahedron Lett.* **1995**, *36*, 3609 ; c) J.F. Hartwig, *Synlett* **1997**, 329 ; d) A.S. Guram, R. A. Rennels, S.L. Buchwald, *Angew. Chem. Int. Ed.* **1995**, *34*, 1348 ; e) J.P. Wolfe, S.L. Buchwald, *J. Org. Chem.* **1996**, *61*, 1133.
- [30] P. Strohhriegl, G. Jesberger, J. Heinze, T. Moll, *Makromol. Chem.* **1992**, *193*, 909.
- [31] O. Neunhoeffer, P. Heitmann, *Ber. Dtsch. Chem. Ges.* **1961**, *94*, 2511.
- [32] S. Tokito, H. Tanaka, K. Noda, A. Okada, Y. Taga, *Appl. Phys. Lett.* **1997**, *70*, 1929.
- [33] a) K. Katsuma, Y. Shirota, *Adv. Mater.* **1998**, *10*, 223 ; b) J. Louie, J.F. Hartwig, *J. Am. Chem. Soc.* **1997**, *119*, 11695.
- [34] S. Tanaka, T. Iso, Y. Doke, *Chem. Commun.* **1997**, 2063.
- [35] F. Wang, M.S. Wilson, R.D. Rauh, P. Schottland, J.R. Reynolds, *Macromolecules* **1999**, *32*, 4272.
- [36] M. Stolka, D.M. Pai, D.S. Renfer, J.F. Yanus, *J. Polym. Sci., Part A: Polym. Chem.* **1983**, *21*, 969.
- [37] a) H.H. Park, K. Ogino, H. Sato, *Polym. Adv. Technol.* **2000**, *11*, 349 ; b) K. Ogino, T. Nomura, T. Shichi, S.H. Park, H. Sato, T. Aoyama, T. Wada, *Chem. Mater.* **1997**, *9*, 2768.
- [38] M. Tamada, H. Koshikawa, T. Suwa, T. Yoshioka, H. Usui, H. Sato, *Polymer* **2000**, *41*, 5661.
- [39] E. Bellmann, S.E. Shaheen, R.H. Grubbs, S.R. Marder, B. Kippelen, N. Peyghambarian, *Chem. Mater.* **1999**, *11*, 399.
- [40] E. Bacher, M. Bayerl, P. Rudati, C.D. Müller, K. Meerholz, O. Nuyken, *Macromolecules* **2005**, *38*, 1640.
- [41] M. Thelakkat, J. Hagen, D. Haarer, H.W. Schmidt, *Synth. Met.* **1999**, *102*, 1125.
- [42] C. Schmitz, M. Thelakkat, H.W. Schmidt, *Adv. Mater.* **1999**, *11*, 821.
- [43] J. Louie, J.F. Hartwig, *Tetrahedron Lett.* **1995**, *36*, 3609.
- [44] A.S. Guram, R.A. Rennels, S.L. Buchwald, *Angew. Chem. Int. Ed.* **1995**, *34*, 1348.
- [45] F.E. Goodson, S.I. Hauck, J.F. Hartwig, *J. Am. Chem. Soc.* **1999**, *121*, 7527.
- [46] a) D.U. Kim, T. Tsutsui, S. Saito, *Chem. Lett.* **1995**, 587 ; b) D.U. Kim, T. Tsutsui, *J. Appl. Phys.* **1996**, *80*, 4785 ; c) S. Pfeiffer, H. Rost, H.H. Hörhold, *Macromol. Chem. Phys.* **1999**,

- 200, 2471 ; d) D. Hertel, H. Bässler, U. Scherf, H.H. Hörhold, *J. Chem. Phys.* **1999**, *110*, 9214 ; e) M. Zheng, F. Bai, Y. Li, G. Yu, D. Zhu, *J. Polym. Sci., Part A: Polym. Chem.* **1999**, *37*, 2587 ; f) Y. Liu, M.S. Liu, X.C. Li, A.K.Y. Jen, *Chem. Mater.* **1998**, *10*, 3301 ; g) X.C. Li, Y. Liu, M.S. Liu, A.K.Y. Jen, *Chem. Mater.* **1999**, *11*, 1568.
- [47] a) M. Redecker, D.D.C. Bradley, M. Inbasekaran, W.W. Wu, E.P. Woo, *Adv. Mater.* **1999**, *11*, 241 ; b) A.W. Grice, D.D.C. Bradley, M.T. Bernius, M. Inbasekaran, W.W. Wu, E.P. Woo *Appl. Phys. Lett.* **1998**, *73*, 629 ; c) M.T. Bernius, M. Inbasekaran, W.W. Wu, E.P. Woo, L. Wujkowski, *J. Mater. Sci.: Mater. Electron.* **2000**, *11*, 111.
- [48] J. Kido, G. Harada, K. Nagai, *Chem. Lett.* **1996**, 161.
- [49] a) L.S. Tan, K.R. Sreenivasan, S.J. Bai, *J. Polym. Sci., Part A: Polym. Chem.* **1997**, *35*, 1909 ; b) L.S. Tan, K.R. Sreenivasan, S.J. Bai, R.J. Spry, *J. Polym. Sci., Part A: Polym. Chem.* **1998**, *36*, 713 ; c) K.H. Park, M.A. Kakimoto, Y. Imai, *J. Polym. Sci., Part A: Polym. Chem.* **1998**, *36*, 1987.
- [50] a) Y. Liu, H. Ma, A.K.Y. Jen, *Chem. Commun.* **1998**, 2747 ; b) Y. Liu, H. Ma, A.K.Y. Jen, *Chem. Mater.* **1999**, *11*, 27.
- [51] a) C. Kvarnström, A. Petr, P. Damlin, T. Lindfors, A. Ivaska, L. Dunsch, *J. Solid State Electrochem.* **2002**, *6*, 505 ; b) A. Petr, C. Kvarnström, L. Dunsch, A. Ivaska, *Synth. Met.* **2000**, *108*, 245.
- [52] C. Lambert, G. Nöll, *Synth. Met.* **2003**, *139*, 57.
- [53] A quasiparticle refers to a particle-like entity arising in certain systems of interacting particles. It can be thought of as a single particle moving through the system, surrounded by a cloud of other particles that are being pushed out of the way or dragged along by its motion, so that the entire entity moves along somewhat like a free particle.
- [54] E.M. Conwell, *Transport in Conducting Polymers* in: "Handbook of Organic Conductive Molecules and Polymers Volume 4, Conductive Polymers: Transport, Photophysics and Applications", Ed. H.S. Nalwa, John Wiley & Sons, Chichester **1997**, 1.
- [55] A. Kraft, *ChemPhysChem* **2001**, *2*, 163.
- [56] a) M. Pope, C.E. Swenberg, *Electronic processes in organic crystals and polymers*, Oxford University Press **1999** ; b) C. Kittel, *Introduction to solid state physics, 8th Edition*, Wiley-VCH, Weinheim **2005**.
- [57] a) T. Holstein, *Ann. Phys.* **1959**, *8*, 325 ; b) T. Holstein, *Ann. Phys.* **1959**, *8*, 343 ; c) W. Warta, N. Karl, *Phys. Rev. B* **1985**, *32*, 1172.
- [58] a) P.G. Le Comber, W.E. Spear, *Phys. Rev. Lett.* **1970**, *25*, 509 ; b) M. Shur, *Physics of Semiconductor Devices*, Prentice-Hall, Englewood Cliffs, New Jersey **1990**.
- [59] a) G. Horowitz, M.E. Hajlaoui, R. Hajlaoui, *J. Appl. Phys.* **2000**, *87*, 4456 ; b) G. Horowitz, M.E. Hajlaoui, *Adv. Mater.* **2000**, *12*, 1046 ; c) G. Horowitz, *Adv. Funct. Mater.* **2003**, *13*, 53.
- [60] A. Miller, E. Abrahams, *Phys. Rev.* **1960**, *120*, 745.
- [61] H. Bässler, *Phys. Stat. Sol. B* **1993**, *175*, 15.
- [62] M.C.J.M. Vissenberg, M. Matters, *Phys. Rev. B* **1998**, *57*, 1296.

- [63] D. Monroe, *Phys. Rev. Lett.* **1985**, *54*, 146.
- [64] a) G. Horowitz, *Semiconducting Polymers*, Wiley-VCH, Weinheim, **2000** ; b) Y. Sun, Y. Liu, D. Zhu, *J. Mater. Chem.* **2005**, *15*, 53.
- [65] G. Horowitz, R. Hajlaoui, H. Bouchriha, R. Bourguiga, M.E. Hajlaoui, *Adv. Mater.* **1998**, *10*, 923.
- [66] G. Horowitz, M.E. Hajlaoui, R. Hajlaoui, *J. Appl. Phys.* **2000**, *87*, 4456.
- [67] J. Buckingham, *Dictionary of Natural Products*, Vol. 1, University Press, Cambridge, MA, **1994**.
- [68] R.O. Loutfy, C.K. Hsiao, P.M. Kazmaier, *Photogr. Sci. Eng.* **1983**, *27*, 5.
- [69] G. D'Aprano, M. Leclerc, G. Zotti, G. Schiavon, *Chem. Mater.* **1995**, *7*, 33.
- [70] a) S. Jungermann, N. Riegel, D. Müller, K. Meerholz, O. Nuyken, *Macromolecules* **2006**, *39*, 8911 ; b) P. Zacharias, M.C. Gather, M. Rojahn, O. Nuyken, K. Meerholz, *Angew. Chem. Int. Ed.* **2007**, *46*, 4388.
- [71] a) A. Cravino, S. Roquet, P. Leriche, O. Alévêque, P. Frère, J. Roncali, *Chem. Commun.* **2006**, 1416 ; b) C.S. Karthikeyan, H. Wietasch, M. Thelakkat, *Adv. Mater.* **2007**, *19*, 1091.
- [72] a) G.W. Gribble, P.D. Lord, J. Skotnicki, S.E. Dietz, J.T. Eaton, J.L. Johnson, *J. Am. Chem. Soc.* **1974**, *96*, 7812 ; b) P. Marchini, G. Liso, A. Reho, *J. Org. Chem.* **1975**, *40*, 3453 ; c) C.F. Lane, *Synthesis* **1975**, 135.
- [73] F. Ullmann, J. Bielecki, *J. Chem. Ber.* **1901**, *34*, 2174.
- [74] S.V. Ley, A.W. Thomas, *Angew. Chem. Int. Ed.* **2003**, *42*, 5400.
- [75] a) M. Kosugi, M. Kameyama, T. Migita, *Chem. Lett.* **1983**, 927 ; b) M. Kosugi, M. Kameyama, H. Sano, T. Migita *Nippon Kagaku Kaishi* **1985**, 3, 547.
- [76] a) J.K. Stille, *Angew. Chem. Int. Ed.* **1986**, *25*, 508 ; b) J.K. Stille, *Pure Appl. Chem.* **1985**, *57*, 1771 ; c) A. Suzuki, *Pure Appl. Chem.* **1994**, *66*, 213 ; d) A. Suzuki, *Pure Appl. Chem.* **1985**, *57*, 1749 ; e) N. Miyaura, A. Suzuki, *Chem. Rev.* **1995**, *95*, 2457 ; f) E. Negishi, *Acc. Chem. Res.* **1982**, *15*, 340 ; g) T. Hayashi, Y. Hagihara, Y. Katsuro, M. Kumada, *Bull. Chem. Soc. Jpn.* **1983**, *56*, 363 ; h) T.N. Mitchell, *Synthesis* **1992**, 803.
- [77] G. Mann, J.F. Hartwig, *J. Am. Chem. Soc.* **1996**, *118*, 13109.
- [78] J.F. Hartwig, S. Richards, D. Baranano, F. Paul, *J. Am. Chem. Soc.* **1996**, *118*, 3626.
- [79] A.R. Muci, S.L. Buchwald, "Practical Palladium Catalysts for C-N and C-O Bond Formation" in: *Topics in Current Chemistry*, 209, Ed. N. Miyaura, Springer-Verlag: Berlin, **2001**, 131.
- [80] J.P. Wolfe, R.A. Rennels, S.L. Buchwald, *Tetrahedron Lett.*, **1994**, *52*, 7525.
- [81] J.F. Hartwig, *Angew. Chem. Int. Ed.* **1998**, *37*, 2046.
- [82] M. Nishiyama, T. Yamamoto, Y. Koie, *Tetrahedron Lett.* **1998**, *39*, 317.
- [83] A.F. Littke, C. Dai, G.C. Fu, *J. Am. Chem. Soc.* **2000**, *122*, 4020.
- [84] C.C. Mauger, G.A. Mignani, *Aldrichimica Acta* **2006**, *39*, 17.
- [85] a) J.F. Fauvarque, F. Pflüger, *J. Organomet. Chem.* **1981**, *208*, 419 ; b) C. Amatore, F. Pflüger, *Organometallics* **1990**, *9*, 2276.

- [86] a) J.F. Hartwig, F. Paul, *J. Am. Chem. Soc.* **1995**, *117*, 5373 ; b) F. Barios-Landeros, *J. Am. Chem. Soc.* **2005**, *127*, 6944.
- [87] L.M. Alcazar-Roman, J.F. Hartwig, A.L. Rheingold, L.M. Liable-Sand, I.A. Guzei, *J. Am. Chem. Soc.* **1995**, *122*, 4618.
- [88] J.F. Hartwig, *Synlett*, **2006**, *9*, 1283.
- [89] a) J.P. Stambuli, M. Bühl, J.F. Hartwig, *J. Am. Chem. Soc.* **2002**, *124*, 9386 ; b) J.P. Stambuli, C.D. Incarvito, M. Bühl, J.F. Hartwig, *J. Am. Chem. Soc.* **2004**, *126*, 1184.
- [90] B.H. Yang, S.L. Buchwald, *J. Organomet. Chem.* **1999**, *576*, 125.
- [91] J.P. Wolfe, S. Wagaw, S.L. Buchwald, *J. Am. Chem. Soc.* **1996**, *118*, 7215.
- [92] M.S. Driver, J.F. Hartwig, *J. Am. Chem. Soc.* **1997**, *119*, 8232.
- [93] a) J.F. Hartwig, *J. Am. Chem. Soc.* **1996**, *118*, 7010 ; b) J.F. Hartwig, *J. Am. Chem. Soc.* **2001**, *123*, 7220.
- [94] J.F. Hartwig, S. Richards, D. Barañano, F. Paul, *J. Am. Chem. Soc.* **1996**, *118*, 3626.
- [95] J. Louie, J.F. Hartwig, *J. Am. Chem. Soc.* **1997**, *119*, 11695.
- [96] F. Diederich, P.J. Stang, *Metal-Catalysed Cross Coupling Reactions*, Wiley-VCH, Weinheim **1998**.
- [97] a) J. Hassan, M. Sévignon, C. Gozzi, E. Schulz, M. Lemaire, *Chem. Rev.* **2002**, *102*, 1359 ; b) J.P. Corbet, G. Mignani, *Chem. Rev.* **2006**, *106*, 2651.
- [98] M.F. Semmelhack, P.M. Helquist, L.D. Jones, L. Keller, L. Mendelsohn, L.S. Ryono, J.G. Smith, R.G. Stauffer, *J. Am. Chem. Soc.* **1981**, *103*, 6460.
- [99] a) T. Yamamoto, T. Ito, K. Kubota, *Chem. Lett.* **1988**, 153 ; b) T. Yamamoto, *Prog. Polym. Sci.* **1992**, *17*, 1153; c) T. Yamamoto, *J. Synth. Org. Chem. Jpn.* **1995**, 53.
- [100] a) Q.B. Pei, Y. Yang, *J. Am. Chem. Soc.* **1996**, *118*, 7416 ; b) S.C. Chang, Y. Yang, Q.B. Pei, *Appl. Phys. Lett.* **1999**, *74*, 2081.
- [101] A. Falcou, J. Schweiger, A. Ritter, Patent *DE 10241814 A1*, **2004**.
- [102] M. Troupel, Y. Rollin, S. Sibille, J. Perichon, J.F. Fauvarque, *J. Organomet. Chem.* **1980**, *202*, 435.
- [103] T. Yamamoto, *Macromol. Rapid Commun.* **2002**, *23*, 583.
- [104] J.V. Allen, J. Fergus, S.W. Leeming, J.D. Morgan, M. Thomas, Patent *WO 9932537 A1*, **1999**.
- [105] T.A. Carlson, *Photoelectron and Auger Spectroscopy*, Plenum Press, London **1975**.
- [106] I.G. Hill, A. Kahn, *J. Appl. Phys.* **1999**, *86*, 4515.
- [107] a) A. Zen, J. Pflaum, S. Hirschmann, W. Zhuang, F. Jaiser, U. Asawapirom, R. P. Rabe, U. Scherf, D. Neher, *Adv. Funct. Mater.* **2004**, *14*, 757 ; b) R. J. Kline, M. D. McGehee, E.N. Kadnikova, J. Liu, J. M. J. Frechet, M. F. Toney, *Macromolecules.* **2005**, *38*, 3312 ; c) R. J. Kline, M. D. McGehee, E.N. Kadnikova, J. Liu, J. M. J. Frechet, *Adv. Mater.* **2003**, *15*, 1519 ; d) J. Chang, B. Sun, D. W. Breiby, M. M. Nielsen, T. I. Solling, M. Giles, I. McCulloch, H. Sirringhaus, *Chem. Mater.* **2004**, *16*, 4772 ; e) A. Zen, M. Saphiannikova, D. Neher, J. Grenzer, S. Grigorian, U. Pietsch, U. Asawapirom, U. Scherf, *Macromolecules* **2006**, *39*,

- 2162 ; f) A. Zen, D. Neher, K. Silmy, A. Holländer, U. Asawapirom, U. Scherf, *Jpn. J. Appl. Phys., Part 1* **2005**, *15*, 3721.
- [108] a) H. Kempa, K. Reuter, M. Bartzsch, U. Hahn, A.C. Huebler, D. Zielke, M. Forster, U. Scherf, *Proc. IEEE Polytronic Conference* **2005** ; b) D. Zielke, A. C. Hübler, U. Hahn, N. Brandt, M. Bartzsch, U. Fügmann, T. Fischer, J. Veres, S.D. Ogier, *Appl. Phys. Lett.* **2005**, *87*, 123805.
- [109] J.F. Morin, M. Leclerc, D. Adès, A. Siove, *Macromol. Rapid Commun.* **2005**, *26*, 761.
- [110] a) J.V. Grazulevicius, P. Stroehriegl, J. Pielichowski, K. Pielichowski, *Prog. Polym. Sci.* **2003**, *28*, 1297 ; b) J.H. Pearson, M. Stolka, in: *Polymer Monographs, Vol. 6*, Ed. M.B. Huglin, Gordon and Breach, New York **1981** ; c) M. Stolka, *Encyclopaedia of Polymer Science and Engineering, Vol. 11*, Wiley, New York **1988** ; d) H. Narmann, P. Stroehriegl, *Handbook of Polymer Synthesis*, M. Dekker, New York **1992** ; e) P.M. Borsenberger, D. Weiss, *Organic Photoreceptors for Xerography*, M. Dekker, New York **1998**.
- [111] a) A. Desbene-Monvernay, P.C. Lacaze, J.E. Dubois, *J. Electroanal. Chem.* **1981**, *129*, 229 ; b) G. Mengoli, M.M. Musiani, B. Schreck, S. Zeccin, *J. Electroanal. Chem.* **1988**, *246*, 73 ; c) S. Cattarin, G. Mengoli, M.M. Musiani, B. Schreck, *J. Electroanal. Chem.* **1988**, *246*, 87 ; d) J.F. Ambrose, R.F. Nelson, *J. Electrochem. Soc. Electrochem. Sci.* **1967**, *115*, *11*, 1159 ; e) J.F. Ambrose, L.L. Carpenter, R.F. Nelson, *J. Electrochem. Soc. Electrochem. Sci. Techn.* **1975**, *122*, *7*, 876.
- [112] P. Marrec, C. Dano, N. Gueguen-Simonet, J. Simonet, *Synth. Met.* **1997**, *89*, 171.
- [113] a) S.H. Tucker, *J. Chem. Soc.* **1927**, 1214 ; b) P. Bersford, D.H. Iles, L.J. Kricka, A. Ledwith, *J. Chem. Soc., Perkin. Trans.* **1974**, *1*, 276.
- [114] A. Siove, D. Adès, *Polymer* **2004**, *45*, 4045.
- [115] a) A. Siove, D. Adès, C. Chevrot, G. Froyer, *Makromol. Chem.* **1989**, *190*, 1361 ; b) A. Siove, D. Adès, E. Ngbilo, C. Chevrot, *Synth. Met.* **1990**, *38*, 331 ; c) G. Helary, C. Chevrot, G. Sauvet, A. Siove, *Polym. Bull.* **1991**, *26*, 131 ; d) A. Aboukassim, K. Faïd, A. Siove, *Macromol. Chem.* **1993**, *194*, 29.
- [116] a) S.T. Wellinghoff, Z. Deng, J.F. Reed, J. Racchini, *Polym. Prepr.* **1984**, *25*, 238 ; b) S.A. Jenekhe, S.T. Wellinghoff, J.F. Reed, *Mol. Cryst. Liq. Cryst.* **1984**, *105*, 175.
- [117] a) U. Geissler, M. L. Hallensleben, A. Rienecker, N. Rohde, *Polym. Adv. Technol.* **1997**, *8*, 87 ; b) A. Iraqi, I. Wataru, *Synth. Met.* **2001**, *119*, 159 ; c) A. Iraqi, I. Wataru, *J. Polym. Sci., Part A: Polym. Chem.* **2004**, *42*, 6041.
- [118] Z.B. Zhang, M. Fujiki, H.Z. Tang, M. Motonaga, K. Torimistu, *Macromolecules* **2002**, *35*, 1988.
- [119] J. Ostrauskaite, P. Stroehriegl, *Macromol. Chem. Phys.* **2003**, *204*, 1713.
- [120] M. Belletête, M. Bédard, M. Leclerc, M. Durocher, *J. Mol. Struct.* **2004**, *679*, 9.
- [121] a) A. Iraqi, I. Wataru, *Chem. Mater.* **2004**, *16*, 442 ; b) J.F. Morin, S. Beaupré, M. Leclerc, I. Lévesque, M. D'lorio, *Appl. Phys. Lett.* **2002**, *80*, 34 ; c) J. Li, F. Dierschke, J. Wu, A.C. Grimdale, K. Müllen, *J. Mater. Chem.* **2006**, *16*, 96.

- [122] a) J.F. Morin, M. Leclerc, *Macromolecules* **2001**, *34*, 4680 ; b) F. Dierschke, A.C. Grimsdale, K. Müllen, *Synthesis* **2003**, *16*, 2470.
- [123] a) N. Blouin, A. Michaud, S. Wakim, P.L.T. Boudreault, M. Leclerc, B. Vercelli, S. Zecchin, G. Zotti, *Macromol. Chem. Phys.* **2006**, *207*, 166 ; b) Y. Li, Y. Wu, B.S. Ong, *Macromolecules* **2006**, *39*, 6521.
- [124] a) S. Patil, U. Scherf, A. Kadashchuk, *Adv. Funct. Mater.* **2003**, *13*, 609 ; b) F. Dierschke, A.C. Grimsdale, K. Müllen, *Macromol. Chem. Phys.* **2004**, *205*, 1147.
- [125] C. Chen, L.M. Yang, *Org. Lett.* **2005**, *7*, 2209.
- [126] K.R. Carter, *Macromolecules* **2002**, *35*, 6757.
- [127] a) C.O. Kappe, *Angew. Chem. Int. Ed.* **2004**, *43*, 6250 ; b) B.S. Nehls, T. Farrell U. Scherf, *Adv. Funct. Mater.* **2004**, *14*, 253 ; c) F. Galbrecht, T.W. Bünnagel, U. Scherf, T. Farrell, *Macromol. Rapid Commun.* **2007**, *28*, 387.
- [128] A. Iraqi, T.G. Simmance, H. Yi, M. Stevenson, D.G. Lidzey, *Chem. Mater.* **2006**, *18*, 5789.
- [129] D.B. Romero, M. Schaer, M. Leclerc, D. Adès, A. Siove, L. Zuppiroli, *Synth. Met.* **1996**, *80*, 271.
- [130] M. Kuroki, Y. Tsunashima, *J. Heterocycl. Chem.* **1981**, *18*, 709.
- [131] H. Gilman, J.J. Dietrich, *J. Am. Chem. Soc.* **1957**, *79*, 6178.
- [132] a) A. Sugimoto, T. Kotani, J. Tsujimoto, S. Yoneda, *J. Heterocycl. Chem.* **1989**, *36*, 435 ; b) A. Sugimoto, T. Yoshino, Y. Tsujimoto, R. Watanabe, K. Mizuno, K. Uehara, *J. Heterocycl. Chem.* **1999**, *36*, 1057.
- [133] G.F. Bettinetti, S. Maffei, S. Pietra, *Synthesis* **1976**, 748.
- [134] a) G. Cauquis, D. Serve, *Tetrahedron Lett.* **1973**, *14*, 2695 ; b) D. Serve, *Bull. Soc. Chim. Fr.* **1976**, 1567.
- [135] S. Rádl, *Chem. Listy* **2001**, *95*, 540.
- [136] T. Okamoto, E. Terada, M. Kozaki, M. Uchida, S. Kikukawa, K. Okada *Org. Lett.* **2003**, *5*, 373.
- [137] E. Terada, T. Okamoto, M. Kozaki, M.E. Masaki, D. Shiomi, K.Sato, T. Takui, K. Okada, *J. Org. Chem.* **2005**, *70*, 10073.
- [138] M. Mikulla, R. Mülhaupt, *Macromol. Chem. Phys.* **1998**, *199*, 795.
- [139] A. Tanatani, M.J. Mio, J.S. Moore, *J. Am. Chem. Soc.* **2001**, *123*, 1792.
- [140] a) M. Rehahn, A.D. Schlüter, G. Wegner, W.J. Feast, *Polymer* **1989**, *30*, 1060 ; b) A.D. Schlüter, *J. Polym. Sci., Part A: Polym. Chem.* **2001**, *39*, 1533 ; c) T.I. Wallow, B. M. Novak, *J. Am. Chem. Soc.* **1991**, *113*, 7411 ; d) S.K. Weber, U. Scherf, *Org. Lett.* **2006**, *8*, 4039.
- [141] K. Brunner, A. Van Dijken, H.F. Boerner, B.M.W. Langeveld, N.M.M. Kiggen, J.J.A.M. Bastiaansen, M.M. De Kok-Van Breemen, Patent *WO 2004055129 A1*, **2004**.
- [142] a) B. Liu, G.C. Bazan, *Proc. Natl. Acad. Sci.* **2005**, *102*, 589 ; b) K. Ding, F.E. Alemдарoglu, M. Börsch, R. Berger, A. Herrmann, *Angew. Chem. Int. Ed.* **2007**, *119*, 1191.
- [143] J.E. Kroeze, N. Hirata, L. Schmidt-Mende, C. Orizu, S.D. Ogier, K. Carr, M. Grätzel, J.R. Durrant, *Adv. Funct. Mater.* **2006**, *16*, 1832.

- [144] a) S.F. Beach, J.D. Hepworth, P. Jones, D. Mason, J. Sawyer, G. Hallas, M.M. Mitchell, *J. Chem. Soc. Perkin Trans. II*, **1989**, 1087 ; b) H. Mayr, T. Bug, M.F. Gotta, N. Hering, B. Irrgang, B. Janker, B. Kempf, R. Loos, A.R. Ofial, G. Remennikov, H. Schimmel, *J. Am. Chem. Soc.* **2001**, *123*, 9500 ; c) D. Bartholome, E. Klemm, *Macromolecules* **2006**, *39*, 5646.

Acknowledgement

I would like to express my gratitude to all those who gave me the possibility to complete this thesis. They will recognize themselves even if I do not name them.

My thanks are due firstly to my advisor, Ullrich Scherf who entrusted me in the field of synthetic chemistry and offered me the possibility to prove myself and emerge as a fully capable scientist. His broad scientific knowledge as well as the constant consideration and the great latitude I was given helped me all along this thesis.

I would also like to thank Emil J.W. List and his co-workers from the *TU Graz*, Austria as well as Heiko Thiem from *Evonik Degussa Creavis* for all the OFET measurements and investigations, the numerous constructive discussions and the friendly relationship.

My special thanks go to my friends and former colleagues from the Scherf group for their fairness, their helpfulness and the nice time spent together.

I would also like to thank all my family and friends who accompanied me along my education in France and in Germany.

Finally, I would like to thank my parents and my brother for their love and support in easy and hard times, as well as Anja for her encouragement and affection.

Curriculum Vitae

Benjamin Souharce

Geboren am 17 August 1979

Im Bordeaux, Frankreich



Seit Nov. 2007

Labor- und Projektleiter

F&E, HS-SBR & Kolloidchemie
PolymerLatex GmbH, Marl (D)

Mai 2004 - Okt. 2007

Promotion in Makromolekularer Chemie

Bergische Universität, Wuppertal (D)
Thema: "Triphenylamine and Carbazole-Based Hole Transporting
Polymers and their Applications in Organic Field-Effect
Transistor"
Doktorvater: Prof. Dr. Ullrich Scherf

März 2003 - Sept. 2003

DESS-Arbeit (Master-Arbeit, mit Auszeichnung)

Gerhard Mercator Universität, Duisburg (D)
Thema: "Synthesis and Characterization of a Liquid Crystalline Semi-
Rigid Polyester"
Betreuer: Dr. Michael Hess

Okt. 2002 - Okt. 2003

DESS in Materialwissenschaft (Master)

Université de Rouen (F)
Analysemethode für Materialien mit Schwerpunkt Polymere

Mai 2002

Praktikum in Mikroelektronik

"Atelier Interuniversitaire de MicroElectronique" (AIME)
Toulouse (F)
Thema: "Darstellung und Charakterisierung von MOS-type gedruckte
Schaltungen"

Sept. 2001 - Juni 2002

Maitrise in Materialwissenschaft

Université Paul Sabatier, Toulouse (F)

Juni 2001 - Aug. 2001

Labortechniker

"Centre Inter universitaire de Recherche et d'Ingénierie des

- Matériaux" (CIRIMAT), CNRS, Toulouse (F)
Korrosion und Materialienschutz Abteilung
Thema: "Messungen von elektrochemischer-Impedanz auf
Aluminiumlegierungen"
- Sept. 2000 - Juni 2001* **License in Physikalischer Chemie**
Université Paul Sabatier, Toulouse (F)
- März 2000 - Juli 2000* **Labortechniker**
"Centre Inter universitaire de Recherche et d'Ingénierie des
Matériaux" (CIRIMAT), CNRS, Toulouse (F)
Mechanics/Oxidation/Microstructures Abteilung
Thema: "Einrichtung einer Prüfanlage für zyklische Oxydation von
Aluminiumoxide unter kontrollierter Atmosphäre"
- Sept. 1998 - Juli 2000* **DUT Mesures Physiques**
Université Paul Sabatier, IUT A, Toulouse (F)
Analytische und Physikalische Chemie
- Sept. 1997 - Mai 1998* Hochschule "Ecole Nationale Supérieure d'Ingénieur" (ENI)
Tarbes (F)
Maschinenbau, Elektrotechnik, Ingenieurwesen
- Juni 1997* **Baccalauréat in Naturwissenschaft**, Toulouse (F)
Schwerpunkt Chemie und Physik
- Sept. 1994 - Juni 1997* Lycée Polyvalent Rive Gauche, Toulouse, France